An interpretation of the polarized crystal spectra of mixed metal trimethylammoniumchlorometallate salts
by Martha Jean Lindbeck

A thesis submitted in partial fulfillment of the requirements for the degree of DOCTOR OF PHILOSOPHY in Chemistry
Montana State University


Abstract:
Crystals fitting the formula (formula not captured in OCR)where M and M' represent the divalent ions of the first row transition metals Mn, Fe, Co, Ni and Cu have been found to be striking examples of pleochroism.

Because these highly colored crystals possess orthorhombic symmetry, their unit cell axes are easily oriented with respect to the electric vector in polarized light. Through observations of the polarized crystal spectra coupled with group theoretical calculations, energy level diagrams have been constructed for the various ions in (formula not captured in OCR) symmetry. In order to explain all the observed peaks transition moment integrals for both electric and magnetic dipole transitions had to be considered. In addition to the spectral work cell parameters for the previously unpublished pure Fe and Ni analogs have been determined using a Supper precession camera. Analyses of the mixed crystals for individual metal content established the relative ease with which these ions were incorporated into the lattice site.

# AN INTERPRETATION OF THE POLARIZED CRYSTAL SPECTRA OF MIXED METAL TRIMETHYLAMMONIUMCHLOROMETALLATE SALTS

by

MARTHA JEAN LINDBECK

A thesis submitted in partial fulfillment
of the requirements for the degree

of

DOCTOR OF PHILOSOPHY

in

Chemistry

MONTANA STATE UNIVERSITY
Bozeman, Montana

March, 1983

APPROVAL

of a thesis submitted by

Martha Jean Lindbeck

This thesis has been read by each member of the thesis committee and has been found to be satisfactory regarding content, English usage, format, citations, bibliographic style, and consistency, and is ready for submission to the College of Graduate Studies.

28 Feb 83
Date

Kenneth Emerson
Chairperson, Graduate Committee

Approved for the Major Department

28 Feb. 1983
Date

Edwin H Abbott
Head, Major Department

Approved for the College of Graduate Studies

3-1-83
Date

Michael P. Malone
Graduate Dean

# STATEMENT OF PERMISSION TO USE

In presenting this thesis in partial fulfillment of the requirements for a doctoral degree at Montana State University, I agree that the Library shall make it available to borrowers under the rules of the Library. I further agree that copying of this thesis is allowable only for scholarly purposes, consistent with "fair use" as prescribed in the U.S. Copyright Law. Requests for extensive copying or reproduction of this thesis should be referred to University Microfilms International, 300 North Zeeb Road, Ann Arbor, Michigan 48106, to whom I have granted "the exclusive right to reproduce and distribute copies of the dissertation in and from microfilm and the right to reproduce and distribute by abstract in any format."

Signature Martha J. Lindbeck

Date 23 Feb 1983

# TABLE OF CONTENTS

# LIST OF TABLES

# LIST OF FIGURES

## ABSTRACT

Crystals fitting the formula $[(CH_3)_3NH]M_xM'_{1-x}Cl_3 \cdot 2H_2O$ where M and M' represent the divalent ions of the first row transition metals Mn, Fe, Co, Ni and Cu have been found to be striking examples of pleochroism. Because these highly colored crystals possess orthorhombic symmetry, their unit cell axes are easily oriented with respect to the electric vector in polarized light. Through observations of the polarized crystal spectra coupled with group theoretical calculations, energy level diagrams have been constructed for the various ions in $D_{2h}$ symmetry. In order to explain all the observed peaks transition moment integrals for both electric and magnetic dipole transitions had to be considered. In addition to the spectral work cell parameters for the previously unpublished pure Fe and Ni analogs have been determined using a Supper precession camera. Analyses of the mixed crystals for individual metal content established the relative ease with which these ions were incorporated into the lattice site.

# INTRODUCTION

The history of alkylammonium chlorometallates, as it appears in the scientific literature, dates as far back as 1908 at which time Groth (1) published his work on the copper(II) salt $[(CH_3)_3NH]CuCl_3 \cdot 2H_2O$. This is one member, although a hydrated one, of a series of compounds represented by the general formula:

$$Am_nMX_{n+2}$$

where Am = an ammonium salt

M = a metal

X = a halogen

n = an integer such that $1 \leq n \leq 4$

In 1933 Remy and Laves (2) prepared a large number of these salts using various alkylamine hydrochlorides and copper(II) chloride as starting materials. For the most part their work, like Groth's, was preparative and descriptive. Except for the preceding papers, there is a dearth of literature concerning this series until the 1960's. Research interest in these salts was renewed at this time for a number of reasons. Instrumental technology had caught up with theory in the areas of magnetics and spectroscopy, and the structures of these compounds became the focus of increased interest. Good crystals of these salts were easily prepared, and thus the series provided a convenient source of material for testing existing theories.

In recent years there has been considerable interest in compounds which contain metals with unpaired d electrons and which are composed of linear chains and layers held together primarily by hydrogen bonding and van der Waals forces. Some of these serve as excellent experimental

models of one- and two-dimensional magnetic systems; low temperature heat capacity and susceptibility data have been obtained on such compounds and fitted to various theoretical models.

As experimental data accumulated on this series, it was discovered that some members displayed a property known as thermochromism. In 1968 Day (3) published a paper in which he defined thermochromism as "the reversible change in color of a compound when it is heated or cooled" and went on to review the existing literature on such compounds. Thermochromism can be classified as either continuous or discontinuous. In the former the color change is gradual and is due to the temperature dependence of the line widths of the absorption bands. In discontinuous thermochromism, which is more interesting chemically, there is a sharp color change corresponding to some characteristic temperature. This is due to a change in coordination geometry or ligand connectivity which results in an energy shift of the visible absorption bands. Remy and Laves (3) had noted that some of their copper(II) salts were thermochromic, but beginning in 1964, Willett was among the first to explore the underlying causes of these observed color changes. In 1974 he published a paper (4) in which he described two members of the following series which were excellent examples of discontinuous thermochromism:

$$Am_2CuCl_4$$

where Am = $(CH_3)_2CHNH_3^+$ or IPA

= $(C_2H_5)_2NH_2^+$ or DEA

Crystals of both of these salts are green at room temperature and upon heating undergo an abrupt color change to yellow; the $DEA_2CuCl_4$ changes at 43°C and the $IPA_2CuCl_4$ changes at 56°C. Differential thermal

analysis data and near IR spectra above and below the transition temperature suggest a change in coordination geometry of the $CuCl_4^=$ species. Comparison of these spectra with those of known structures indicated a square planar geometry for the low temperature structure and a flattened tetrahedral geometry for the high temperature structure. This work has recently been extended to the $IPACuCl_3$ salt (5) which changes from brown to orange at 51°C. The corresponding structural shift is from bibridged linear chains of the dimer $Cu_2Cl_6^=$ to tribridged chains of $(CuCl_3)_n^{n-}$. In conjunction with the interest in the magnetics of these systems, EPR and susceptibility data were collected along with the structural information.

Interest in the geometry, structure and related properties of the salts in this particular series led to the synthesis of a wide variety of crystals. In the course of these investigations some similar compounds were discovered which had a slightly different stoichiometry than the one previously cited. One such class of compounds which received attention is characterized by the formula:

$$TMA_3M_2Cl_7$$

where TMA = trimethylammonium, $(CH_3)_3NH^+$

Members of this series for which M = Mn and Cu have been prepared and studied (6,7). In this structure the divalent metal ions exist in two different environments; one is characterized by chains of face-sharing $MCl_6$ octahedra, the other by discrete $MCl_4^=$ tetrahedra. This structural arrangement is illustrated in Figure 1.

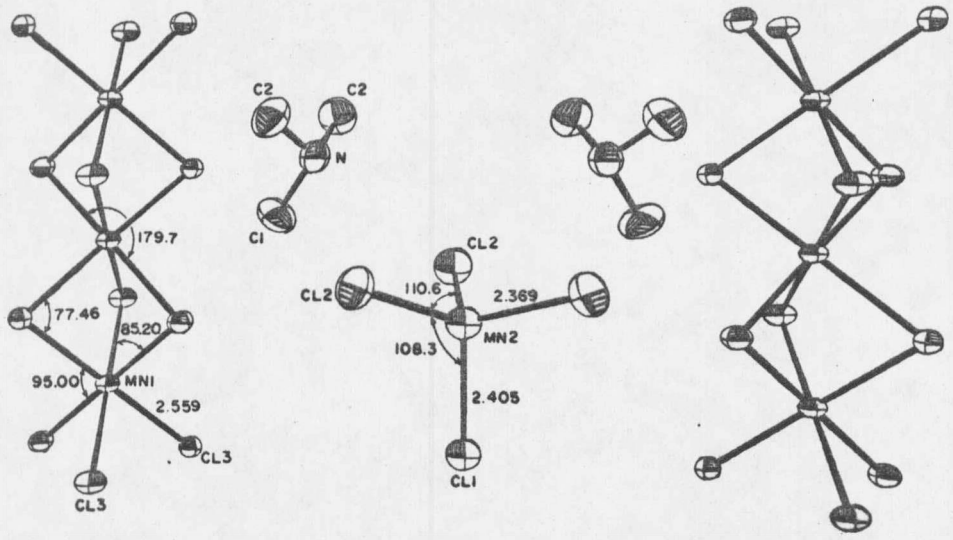


Figure 1 The Two Metal Sites in $TMA_3M_2Cl_7$

The existence of two different sites in such a system leads quite logically to an attempt to grow salts with a different metal in each of the sites. Mn(II) and Cu(II) will readily adopt either coordination, but other first row transition metals are not so flexible. For example, Co(II) and Zn(II) prefer the tetrahedral geometry in $MCl_4^=$ whereas cations such as Ni(II) and Cd(II) form the octahedral chains more readily. Clay, et. al., (7) attempted to grow the mixed metal salt with the formula $TMA_3CoCuCl_7$ where Co(II) was expected to occupy the tetrahedral site. Continuous solid solutions were obtained rather than a single product with the desired stoichiometry. Other than this paper, nothing further appears in the literature in reference to mixed metal

salts of this particular series.

The existence of two differently coordinated metal sites within a single structure is a rather unusual occurrence. The question arises as to whether, under the appropriate conditions, various metals could be forced to assume their preferred geometries in such a system. This research began as an effort to prepare such crystals with the stoichiometry $TMA_3MM'Cl_7$ where trimethylamine hydrochloride and the six possible pairs from the divalent chlorides of Mn, Co, Ni and Cu were used as starting material. When attempts to grow these mixed metal salts from stoichiometric amounts in anhydrous solutions of methanol and ethanol proved unsuccessful, the syntheses were performed in aqueous solution. Qualitative analyses of the crystals obtained from the latter procedure indicated that both metals were present in each pair. However, quantitative analyses along with precession photographs of the Mn-Co analog subsequently showed it to be isomorphic with the compound $TMAMnCl_3 \cdot 2H_2O$. A mixed metal product had indeed been prepared, but not one with the desired two-site structure.

The crystals which had been grown had the same stoichiometry as the Cu(II) salt studied by Groth in 1908 (1); these are the hydrated members of the series first prepared and studied by Remy and Laves (2). A literature search revealed that for this hydrated series crystals containing Mn, Co and Cu had been studied in detail, again in connection with their structural and magnetic properties. Historically, the Cu salt was prepared first; its crystal structure was the first to be elucidated and there is the most information on this compound in the literature (8). Heat capacity and susceptibility measurements have also

been made on both the Cu and Co analogs (8,9); only structural work has been done on the Mn member of this series (10). Of these three salts, the Mn and Co analogs are isomorphic; they are orthorhombic and belong to the Pnma space group. The Cu analog is monoclinic as Groth originally reported, and its space group is $P2_1/c$. Cell dimensions and the space group for these compounds are reported in Table I.

Table I

Cell Dimensions and Space Group for $TMAMCl_3 \cdot 2H_2O$ Salts

| | a(Å) | b (Å) | c (Å) | Group |
|---|---|---|---|---|
| $TMAMnCl_3 \cdot 2H_2O$ | 16.779(3) | 7.434(1) | 8.227(1) | Pnma |
| $TMACoCl_3 \cdot 2H_2O$ | 16.671(3) | 7.273(1) | 8.113(2) | Pnma |
| $TMACuCl_3 \cdot 2H_2O$ | 7.479(10) | 7.864(11) | 16.730(23) | $P2_1/c$ |

The names of these salts are indicative of their structure; for example, the manganese analog is named trimethylammonium catena-di-μ-chlorodiaquomanganese(II) chloride. Its structure is composed of infinite chains of edge-sharing $MnCl_4(H_2O)_2$ octahedra which run parallel to the b axis with bridging Cl atoms and O atoms in the trans positions. The chains are hydrogen bonded along the c axis through the free $Cl^-$ anions; the trimethylammonium cations lie between the planes of hydrogen bonded chains. The cobalt structure is completely analogous to this; the only differences occur in the cell dimensions due to the slightly smaller crystal ionic radius of the divalent cobalt.

Figure 2 on the following page is a view along the a axis of the unit cell of the $TMAMnCl_3 \cdot 2H_2O$ salt. The chains lie along the b

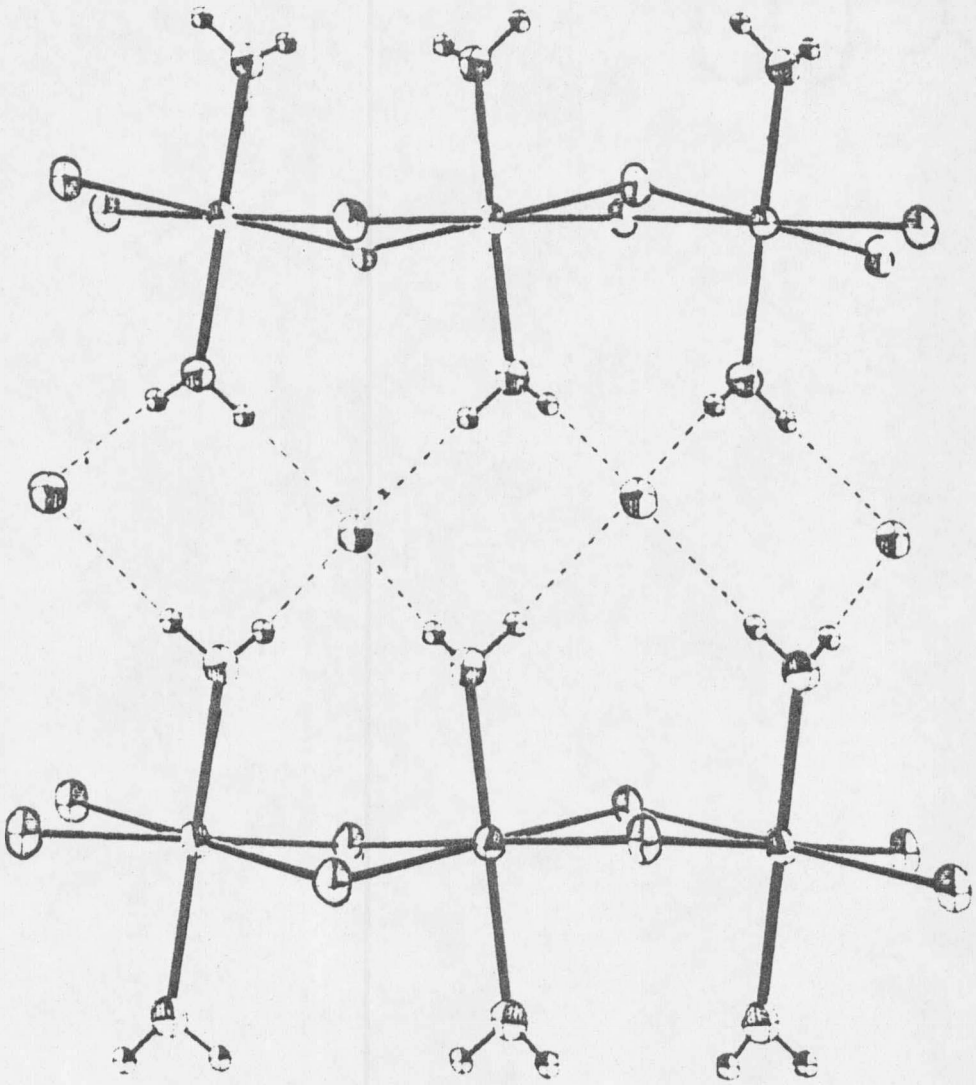

Figure 2 Unit Cell of $TMAMnCl_3 \cdot 2H_2O$ in the b-c Plane

crystallographic axis and are hydrogen bonded in the c direction.

In the copper(II) salt distortion of the $CuCl_4(H_2O)_2$ octahedra results in a slightly different packing arrangement which is sufficient to force this analog of the series into a different space group. By conventional choice of axes in the monoclinic $P2_1/c$ group, the chains now run parallel to a rather than b as in the orthorhombic cell. However, the bonding patterns remain the same. Two of the coordinated Cl atoms are found at a slightly greater distance from the central Cu atom than are the remaining four atoms of the coordination sphere. Although one angle is now distorted from 90°, the chains remain edge-shared with hydrogen bonding and van der Waals forces still in effect.

All of the work done on the trimethylammonium chlorometallate series has been with these three pure metal compounds. A look at the periodic table raises the question, can the pattern be completed? That is to say, can the Fe(II), Ni(II) and Zn(II) analogs be prepared, and will they adopt one of the above structures? Table II lists the metal atoms of interest along with their electron configurations and crystal ionic radii. The values of the radii are those reported by Shannon and Prewitt (11).

Synthesis of the series $TMAM_xM'_{1-x}Cl_3 \cdot 2H_2O$, although inadvertent, yielded some intriguing observations on the chemical and optical properties of the pairs as compared to the pure metal end members. Since the mixed metal crystals in this series were easily grown, it was deemed worthwhile to pursue the hydrated single-site metal pair system in some detail.

There are several aspects of this series which merit attention.

Table II

Information on Metals of Interest for the Series $TMAM_xM'_{1-x}Cl_3 \cdot 2H_2O$

| Metal | a | b | c |
|---|---|---|---|
| Mn(II) | $3d^5$ | 0.82 | Pnma |
| Fe(II) | $3d^6$ | 0.78 | Pnma* |
| Co(II) | $3d^7$ | 0.74 | Pnma |
| Ni(II) | $3d^8$ | 0.70 | Pnma* |
| Cu(II) | $3d^9$ | 0.73 | $P2_1/c$ |
| Zn(II) | $3d^{10}$ | 0.75 | ? |
| Cd(II) | $4d^{10}$ | 0.95 | ? |

column a outer shell configuration

column b crystal ionic radii (Å) for high spin six coordinate complex

column c space group, asterisk signifies compound not reported in the literature

Composition and structure are two of the areas which were investigated in this work. These properties are of particular interest in the Cu containing crystals since the pure Cu analog has a different structure than the other members of the series. Examination of the Cu subseries to ascertain whether these compounds crystallize as the monoclinic $P2_1/c$, orthorhombic Pnma or perhaps some new structure was one of the goals of this research. Crystals of the Fe and Ni members of this series were also synthesized and their structures determined to see if they followed the existing trend indicated by the Mn and Co salts.

These compounds also exhibit a phenomenon known as dichroism, a property of crystals which is discussed at length in a later section. Briefly, they display two different colors depending on their spatial orientation. This dichroism is not to be confused with the discontinuous thermochromism mentioned earlier. The color change observed in the latter usually involves a structural shift and is temperature dependent while the colors in the former are a result of the optical properties of the crystal and are both visible at room temperature. The presence of two metals seems to enhance this effect, as the mixed metal salts are much more strongly dichroic than are the pure metal end members of this series.

For dichroism to be observable in this chlorometallate series, absorption bands must be present in the visible region of the electromagnetic spectrum. In conjunction with the optical properties manifested by these crystals, spectral data were collected in both polarized and unpolarized light in order to gain a greater understanding of what governing factors control the colors displayed by the various mixed metal salts. The question as to whether metal-metal interactions could occur in the mixed metal compounds, thus giving rise to the striking dichroism of these crystals, was addressed and a careful comparison of the relative intensities and locations of absorption bands in various members of the series was made.

# EXPERIMENTAL METHODS

## SYNTHESES

Crystals of salts fitting the formula $TMAM_xM'_{1-x}Cl_3 \cdot 2H_2O$ were grown for eight of the ten possible combinations of the first row transition elements from Mn to Cu, inclusive. The pure end members, $x = 0$, were prepared by dissolving equimolar quantities of the divalent metal chlorides and trimethylamine hydrochloride in a minimal amount of water and allowing the aqueous solution to slowly evaporate. The crystals which contained metal pairs were prepared by mixing varying mole fractions from $\chi = 0.2$ to $\chi = 0.8$ of the metal(II) chlorides with a stoichiometric amount of the TMA solution and again merely letting the solution evaporate slowly.

It is characteristic of the mixed metal series that the crystals do not grow with the same stoichiometry as that of the original solution. If a crystal such as $TMAMn_{0.5}Cu_{0.5}Cl_3 \cdot 2H_2O$ is desired, the starting solution must have a $\chi_{Mn,soln} = 0.65$ in order to produce a solid with $\chi_{Mn,xtal} = 0.50$. The mole fraction found in the crystal *vs* that found in the starting solution will be tabulated for the individual series and discussed in a later section.

Petri dishes of various sizes and surface areas were utilized; practice with the rate of evaporation eventually led to the optimum methods of obtaining crystals of the desired size and quality. Even after much practice, though, there oftentimes seemed to be as much luck as skill involved in the process.

As these salts are extremely soluble in water, the solutions were sometimes quite viscous before crystals began to grow. This solubility

made it impossible to obtain crystals of this series containing only Zn which has a filled 3d subshell or calcium with an empty 3d subshell. Attempts to grow the pure Cd analog yielded the anhydrous salt $TMACdCl_3$.

Addition of excess chloride in the form of concentrated HCl to the solutions of the pure Co and Co-Ni mixtures resulted in the formation of larger crystals in these systems in a shorter period of time. This same effect was noted as a general rule for the other salts as well.

No special precautions were taken in the syntheses of the Mn, Co, Ni or Cu containing salts, but in the case of the Fe(II) salt and any mixture in the subseries containing this metal, air oxidation proved to be a problem. Solutions of iron(II) chloride were prepared from the hydrate, the anhydrous salt and from iron wire dissolved in concentrated HCl. Because iron(II) is not very stable in air, there is the possibility that some iron(III) is present in solutions made from the iron(II) salts. For this reason the most reliable syntheses of the Fe subseries were those done using the solutions of Fe(II) prepared from the iron wire. In order to obtain good quality crystals of the pure Fe analog and its mixed metal subseries, the starting solutions were placed in a vacuum desiccator containing concentrated $H_2SO_4$ as the desiccant and an inert nitrogen atmosphere. A successful synthesis of the Fe-Cu mixed salt with the proper stoichiometry was never accomplished, presumably because of the high probability of a redox reaction occurring between these two metals when both are present in the +2 oxidation state. The Fe-Co analog was also not prepared. The crystals containing iron were collected and stored under a nitrogen atmosphere.

Upon exposure to air the pure Fe end member began to show signs of deterioration in about a week, undergoing a color change from very pale yellow/green to amber and beginning to look wet.

## ANALYSES

Once suitable crystals of varying mole fraction had been prepared, the next step undertaken involved determination of the actual stoichiometry. Qualitative analyses of each batch indicated that both metals were present; quantitative measurements were then necessary to determine whether the mole fractions found in the crystal showed any relationship to that in the solution from which it was grown. Because only a limited amount of these crystals was available, under five grams in most cases, all samples were weighed on an M5 microbalance and all titrations were performed with a 1.0- or 2.5-ml microburet.

The chloride content was determined by Fajan's method (12), i.e. titration of $Cl^-$ with $AgNO_3$ using dichlorofluorescein, $DCF^-$, as the indicator. The AgCl precipitate exists as a white colloid and adsorption of the indicator anion, $DCF^-$, at the endpoint causes a color change in the precipitate from white to pink. In dilute solutions the AgCl will coagulate as well as change color. The $DCF^-$ in solution is yellow-green and this may somewhat mask the white colloidal AgCl prior to the endpoint. In order to keep the suspension highly dispersed, and thus the color change more visible, dextrin is sometimes added. If the analysis is done at the micro level, this work indicated that the $AgNO_3$ titrant should be standardized with and without the dextrin present to make certain that this reagent does not interfere.

The chloride analyses were used to characterize the pure metal salts and to establish that their stoichiometry and that of the mixed metal salts as well were indeed correct. Table III lists the %Cl found and compares these values to those calculated for the pure

compounds of the series $TMAM_xM'_{1-x}Cl_3 \cdot 2H_2O$. In the early stages of this work characterization of the mixed metal compounds by their chloride content was considered, since these analyses can be performed with a relative precision of two or three parts per thousand, ppt. However, it was subsequently determined that this system is actually a solid solution whose composition can be controlled only within a certain range. The growth of any one batch of crystals with a given stoichiometry has an inherent error of as much as 50 ppt relative in its metal composition. The magnitude of this variation within the crystals grown from one synthesis makes it impossible to utilize the small changes which occur in the %Cl determination to calculate an accurate weighted average of the two metals present. Since the mole fraction of the metals present in these crystals was of particular interest, other analytical techniques had to be considered.

Table III

Chloride and Metal Content of the Series $TMAMCl_3 \cdot 2H_2O$

| M | %Cl Found | %Cl Calculated | %M Found | %M Calculated | Molar Ratio |
|---|---|---|---|---|---|
| Mn | 41.50 | 41.32 | 21.46 | 21.34 | 2.997 |
| Fe | —— | 41.17 | —— | 21.62 | —— |
| Co | —— | 40.68 | —— | 22.54 | —— |
| Ni | 40.21 | 40.72 | 21.77 | 22.48 | 3.059 |
| Cu | 40.53 | 39.98 | 24.41 | 23.89 | 2.976 |

Included in Table III are the molar ratios of chloride to metal for each of the pure compounds analyzed. These values are quite close to the expected value of 3.000 which indicates that the crystals were actually the desired structure and stoichiometry. The chloride content was not determined for the Fe and Co members of this series since X-ray data showed these crystals to also be the orthorhombic Pnma structure.

Because of the wide range of mole fractions involved in any one metal pair subseries, methods of analyses had to be developed not only to determine the metals in question, but also to determine them in the presence of one another in a single sample. It is possible to determine all of the metals used in this series, Mn, Fe, Co, Ni and Zn, as well as Cu, complexometrically utilizing EDTA as the titrant (13). EDTA is an extremely versatile reagent, forming stable, soluble stoichiometric complexes with most metal ions, including all of those listed above. This very versatility, which makes EDTA such a valuable titrant, becomes a problem when selectivity is desired; in all pairs in question the metals will interfere with one another and conditions and reagents must be very carefully selected in order to obtain reliable data on individual metal content. By judicious utilization of masking agents, back titrations and redox reactions, various techniques were patched together making it possible to titrate both metals in one sample for any of the pairs which did not contain Fe(II). Before describing the procedures used in the mixed metal analyses, the simpler methods of titrating a single metal ion as in the pure salts will be discussed.

Cu may be determined by forming the ammine complex and titrating with EDTA using murexide as the indicator (13-16). The EDTA was

standardized against both Cu and Zn solutions prepared by dissolving the respective metal in acid. Welcher (13) recommends a saturated solution of the murexide, but Elbeih (14) uses a powdered mixture of the indicator and NaCl. Previous work in this lab (15) suggests that the latter method produces a more satisfactory endpoint. Elbeih reports good results when titrating 25-100 μg of metal, but found that for samples containing less than 25 μg the endpoint became indistinct.

The copper content can also be determined iodometrically using $Na_2S_2O_3$ as the titrant (17). Standardizations done using either Cu ribbon or $K_2Cr_2O_7$ did not give reliable results at the micro level; therefore, $KIO_3$ was ultimately chosen as the primary standard to determine the concentration of the titrant. The Cu containing crystals were dissolved in doubly distilled water, buffered with $NH_4HF_2$ and titrated to the starch endpoint. To prevent the endpoint from drifting due to the adsorption of free $I_2$ on the $Cu_2I_2$ precipitate, KSCN was added after the starch. Titrations of the pure Cu salt without KSCN gave the same results, but required more time.

In comparative titrations both the complexometric and the iodometric methods yielded the same results; to avoid interference problems the latter method was chosen for the Cu analyses of the mixed metal salts, since it is specific for the Cu(II) ion.

Samples containing only Ni were titrated with EDTA by the same procedure described above for Cu (13,14).

The Co titrations performed with EDTA also utilized the murexide indicator prepared in solid form as described above. Welcher (13) provides a fairly detailed procedure for this titration; additional

information appears in Houk's thesis previously cited (15). The pH must be controlled very carefully in this titration in order to obtain the correct color change at the endpoint. The easiest way to do this was to add acetic acid or ammonium hydroxide as needed to maintain a yellow color prior to the endpoint; after the endpoint the solution remains purple regardless of the amount of acid or base added. The Co titration may also be performed as a back titration using Eriochrome Black T (EBT) as the indicator at a pH of 10 (18).

The Mn determination in the pure salt was done following the procedure outlined by Welcher (13) except that the ZnO and KCN were not added as there were no other metals present to interfere. Ascorbic acid or hydroxylamine hydrochloride must be added to prevent the oxidation of Mn(II). The system is buffered at pH = 10; the indicator in this titration is again EBT in the solid form. The Mn(II) ion may thus be titrated directly or an excess of EDTA may be added and a back titration performed with a standard Zn solution.

The same basic methods used to titrate the pure metal compounds were utilized in the mixed salt analyses with some modifications to prevent any interferences. In the Cu containing subseries the Mn-Cu, Co-Cu and Ni-Cu pairs were first analyzed for Cu iodometrically. After the Cu content was determined, the Co-Cu and Ni-Cu pairs were titrated with EDTA for total metal content following the procedure described for the pure Cu salt. In the Mn-Cu subseries the Mn was subsequently titrated as in the pure salt except that KCN was added to form the $Cu(CN)_2^-$ complex, thus preventing the Cu ion from interfering.

In the Mn-Co and Mn-Ni subseries total metal was found first, KCN

was added to mask the Co and Ni respectively, and the liberated EDTA was titrated with a standard metal solution.

The method described by Welcher (13) for determination of both Co and Ni simultaneously proved impossible to duplicate. A spectrophotometric method described by Kratochvil and Harris was utilized to find the mole fractions of these two metals in the Co-Ni subseries (20).

From the titration data the relative solubilities of the metals in this series can be determined. For example, in the Cu containing subseries, the Cu ion occupies the metal site of the crystal most readily. In this particular subseries the Cu may be regarded as the solvent; Mn, Co and Ni are doped into the Cu salt. Mole fraction data indicate that the Mn(II) ion is the most soluble and the Ni(II) is the least soluble of the three solute ions. The Ni analog was the most difficult of the pure compounds in the entire series for which to grow crystals and this trend is reflected in the low solubility of the Ni(II) ion in the mixed metal compounds as well. In a solution containing equimolar amounts of the two metals such that $\chi_{Cu,soln} = 0.50$, the crystals which form will have $\chi_{Cu,xtal} = 0.74$ for the Mn-Cu salt, 0.96 for the Co-Cu salt and 0.99 for the Ni-Cu salt. The relationship between $\chi_{soln}$ and $\chi_{xtal}$ for the Cu containing subseries is presented in Table IV; a graphic presentation will be utilized in the discussion of these results in a later section.

Table V lists the corresponding mole fraction data for the Mn containing subseries. The Cu is more readily incorporated into the crystal structure than Mn as was observed in the preceding system; Co displays a greater solubility than Ni in this series as well.

Table IV Mole Fractions in Cu Containing Salts

| | Cu-Mn Subseries | Cu-Co Subseries | Cu-Ni Subseries |
|---|---|---|---|
| $X_{Cu,\ soln}$ | $X_{Cu,\ xtal}$ | $X_{Cu,\ xtal}$ | $X_{Cu,\ xtal}$ |
| 0.2000 | 0.1887(25) | 0.4057(50) | 0.6814(14) |
| 0.2500 | 0.2825(19) | 0.6398(12) | 0.8489(12) |
| 0.3333 | 0.5188(44) | 0.8330(14) | 1 |
| 0.5000 | 0.7500(14) | 0.9574(11) | 1 |
| 0.6667 | 0.9198(17) | 0.9640(24) | 1 |
| 0.7500 | 0.9830 (2) | 0.9825(24) | 1 |
| 0.8000 | 0.9785 (2) | 1 | 1 |

Table V Mole Fractions in Mn Containing Salts

| | Mn-Cu Subseries | Mn-Co Subseries | Mn-Ni Subseries |
|---|---|---|---|
| $X_{Mn,\ soln}$ | $X_{Mn,\ xtal}$ | $X_{Mn,\ xtal}$ | $X_{Mn,\ xtal}$ |
| 0.2000 | 0.0215(89) | 0.3973(29) | 0.7567(14) |
| 0.2500 | 0.0170(138) | 0.5181(10) | 0.7745 (2) |
| 0.3333 | 0.0802(190) | 0.6310 (3) | 0.8704 (6) |
| 0.5000 | 0.2500(43) | 0.7694 (2) | 0.9440 (3) |
| 0.6667 | 0.4812(48) | 0.8713 (5) | 0.9746 (1) |
| 0.7500 | 0.7175 (8) | 0.8321 (4) | 0.9608 (4) |
| 0.8000 | 0.8112 (6) | 0.9386 (5) | 0.9757 (1) |

There is also a change in structure in the Cu containing subseries which serves to complicate this system. The remaining pairs of all the subseries retain the orthorhombic structure regardless of metal composition and in all cases Ni displays the least tendency to be incorporated into the crystal site.

## MORPHOLOGY AND STRUCTURE

Before discussing the collection of X-ray data, the shape or habit that these crystals adopt will be described. Taken in conjunction with the observed dichroism, the habit can provide information as to the location of the principal axes in a crystal. This facilitates the mounting and orientation of individual crystals prior to taking precession photographs.

If no effort is made to control their size, stoichiometric preparations of the compounds in this series yield small acicular crystals with the needle axis parallel to the chain direction. Typically, these crystals are two millimeters or less in length and about the thickness of a hair. Slow growth will sometimes produce a lath-like habit with dimensions roughly 0.5 x 1.0 x 2-3 mm. This lath is an external expression of the unit cell and is bounded by (100) and (001); most of the structural work with the precession camera was done on crystals with this habit. The needle axis of the lath lies along the b crystallographic axis and corresponds to the chain direction of the $MCl_4(H_2O)_2$ octahedra. In terms of chemical bonding and cleavage, this external morphology is a logical outgrowth of the unit cell of the crystal. The c crystallographic axis is shorter than the a axis and the growth pattern of the laths will sometimes reflect this; however, there is no particular preference for a crystal to develop along the c axis rather than along a. The chain axis coincides with the needle axis of all crystals except those in the structure transition region.

Very large crystals 10-15 mm in length and several mm on a side

which are grown from solutions containing an excess of $Cl^-$ develop random faces; even the needle axis may be difficult to locate in such habits. Figure 3 shows some of the typical habits for this series.

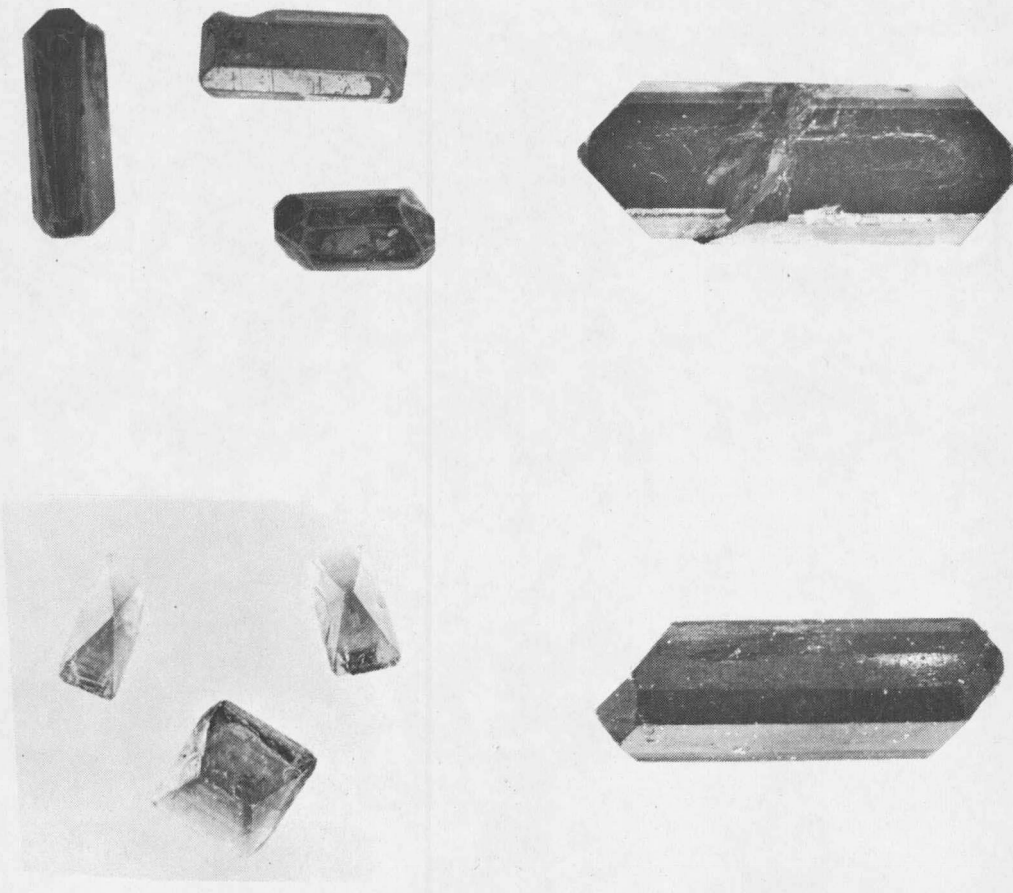

Figure 3 Some Habits Displayed by the Series $TMAM_xM'_{1-x}Cl_3 \cdot 2H_2O$

Growth in odd habits was especially common for mixed metal crystals which contained Cu. In these subseries a structural change from the orthorhombic Pnma to the monoclinic $P2_1/c$ must occur at some particular mole fraction. In the transition region crystals bounded by (101), (10$\bar{1}$), (110) and (1$\bar{1}$0) are the typical habit observed; this is shown in Figure 3c. In such cases it was extremely difficult to locate the principal axes and to orient the crystal for X-ray work solely by morphology. After mounting, the principal direction in such crystals was found more or less by trial and error.

Normally, the crystal was mounted with the needle axis coincident with the axis of the goniometer head and a principal direction located on the basis of a reflected face. Crystals with the orthorhombic structure were found to display two colors depending on orientation; the a-b and b-c planes could be found by color if the habit of the crystal did not happen to contain (100) or (001) planes which could be located easily. This made it possible to orient crystals of any habit in the orthorhombic structure with a minimum of effort.

In the Mn-Cu, Co-Cu and Ni-Cu salts the habit in Figure 3c predominates when $\chi_{Cu,xtal}$ approaches 0.75-0.80. The longest dimension in these crystals is along the a axis which corresponds to the chain direction in the monoclinic cell. However, these crystals retain the orthorhombic structure; a full set of precession photographs was required to demonstrate that these mixtures were indeed crystallizing in the Pnma space group. At $\chi_{Cu,xtal} \geq 0.80$ the Cu containing salts will crystallize in the monoclinic structure.

The X-ray data were collected on a Supper precession camera and

Mo Kα radiation with $\lambda$ = 0.70926 Å was utilized. The zero, first and second levels of the pure Mn and pure Cu salts were taken shooting into the a-b and b-c planes of lath-shaped crystals. These crystals were subsequently remounted and the zero, first and second levels of the a-c plane were obtained as well. This provided a complete set of precession photographs for both the orthorhombic Pnma and monoclinic $P2_1/c$ structures. As a first approximation of structure, the zero levels of any crystal of the mixed metal salts in this series could now be compared to those of the pure end members to determine whether or not the spot pattern matched one or the other. Full data decks were collected on some, but not all, of the mixed salts as a check to make certain that no anomalies occurred in the upper levels. The zero and first levels for two planes were collected on at least three mole fractions of each subseries.

Salts in the series $TMAMCl_3 \cdot 2H_2O$ where M = Mn, Co and Cu have been reported in the literature previously (8-10) and their structures are well documented. Synthesis of the Fe and Ni end members completes the progression across the first row transition metals from configuration $d^5$ to $d^9$ inclusive. Spot patterns on the precession photographs indicate that these two new compounds follow the trend set by the Mn and Co and adopt the orthorhombic structure with space group Pnma. Utilizing the formulas provided by Buerger (21) and Stout and Jensen (22) cell dimensions were calculated for all of the pure compounds from precession data. These values are slightly lower than those reported in the literature for the three compounds on which data is available, but these variations are typical of interlab comparisons. For the data collected in this

work, the Fe and Ni analogs fit the trend developed with decreasing size of the divalent metal cations quite nicely. This correlation between the ionic radii and cell dimensions is illustrated in Table VI.

Table VI

Cell Dimensions for Members of the Series $TMAMCl_3 \cdot 2H_2O$

| Metal | Radius | a | b | c |
|---|---|---|---|---|
| Mn | 0.82 | 16.59 | 7.419 | 8.141 |
| Fe | 0.78 | 16.56 | 7.331 | 8.095 |
| Co | 0.74 | 16.52 | 7.234 | 8.046 |
| Ni | 0.70 | 16.52 | 7.110 | 8.031 |
| Cu* | 0.73 | 7.517 | 7.849 | 16.70 |

* axes change in Cu salt due to different space group

One can also calculate a theoretical value for b based on a square planar arrangement of the chloride anions around the central metal atom and a knowledge of the radii involved for the various ions. Such a calculation using a value of 1.81 Å for the $Cl^-$ radius yields cell dimensions which are in remarkably good agreement with those observed. Table VII contains these values for the $d^5$ through $d^8$ analogs of this series.

Table VII

Theoretical Values of b in Square Planar Arrangement

for $TMAMCl_3 \cdot 2H_2O$ in Pnma

| Metal | Radius | b calc | b found |
|---|---|---|---|
| Mn | 0.82 | 7.467 | 7.419 |
| Fe | 0.78 | 7.326 | 7.331 |
| Co | 0.74 | 7.227 | 7.234 |
| Ni | 0.70 | 7.071 | 7.110 |

## SPECTRA

The final phase of the investigation of the mixed metal series $TMAM_xM'_{1-x}Cl_3 \cdot 2H_2O$ entailed running x-, y- and z-polarized spectra as well as unpolarized spectra of these crystals on the Cary 14. When discussing these spectra, z-polarized light refers to light which has its only allowed vibration direction parallel to the z axis; x, y and z correspond to the a, b and c crystallographic axes in the unit cell. These orientations are depicted in Figure 4.

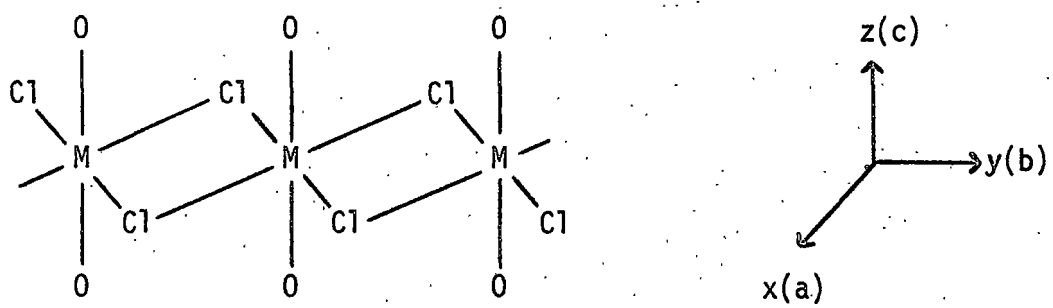


Figure 4

Location of Crystallographic Axes and Polarization Directions

Crystal spectra were taken at room temperature in the near infrared (IR), visible and ultraviolet (UV) regions. In the pure Mn compound three peaks were observed in the UV region, but in all other cases this region yielded very little useful information as charge transfer bands appeared which were off scale. Most of the interesting peaks were observed in the visible and near IR regions.

In order to run spectra on these crystals, specimens at least a

millimeter wide had to be grown, but they could not be so thick as to effectively block all transmitted light. With this particular series such dimensions proved difficult to attain; additionally, the dark colors and intense absorption bands inherent in some of the crystals reduced transmission. Of the pure salts the Mn analog with very weak bands is the most suitable sample on which to take spectra. The pure Co and Cu end members must be cut and ground to get thin enough crystals to produce reasonable spectra. Pure Fe and Ni crystals large enough to record spectra were never obtained. Among the mixed metal compounds, the entire Mn subseries produced crystals which allowed useful spectra to be recorded with a minimum of effort. This translucence was due partly to the habit, but was probably due in larger part to the dilution effect imparted to these salts by the presence of the Mn(II) ion.

Special sample cells had to be improvised to hold the crystal in place while running solid spectra on the Cary 14. Brass plates were cut to fit into the normal cell holder of the instrument and holes a millimeter in diameter were then drilled, positioned in the center of the transmitted beam. The crystals were taped over the hole of the sample plate, oriented with one of the crystallographic axes parallel to the long dimension of the plate. To obtain polarized spectra, strips of Polaroid film were taped over the holes of both reference and sample plates and the orientation and color of the crystal were carefully noted. Many blanks were run with just the plates, the plates with polarized film in place and with different pieces of the film to determine the sort of background to expect. The film has weak bands in the visible and near IR, but they are very small compared to the crystal

scattering and cannot be mistaken for crystal absorption bands in these regions. The film does absorb in the UV region; this, along with the presence of charge transfer bands, made it impossible to get polarized UV spectra.

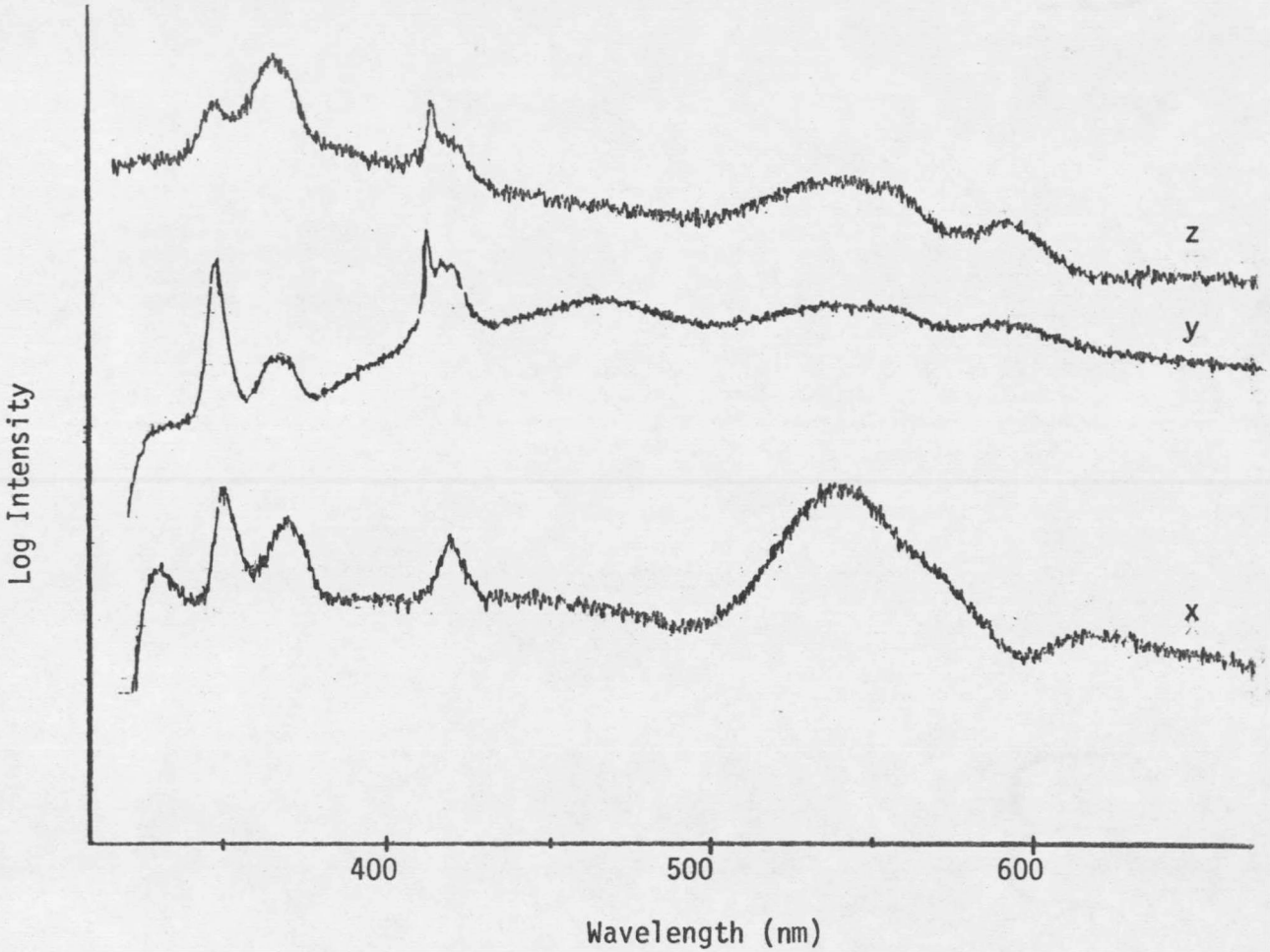


Figure 5 Polarized Crystal Spectra of $TMAMnCl_3 \cdot 2H_2O$

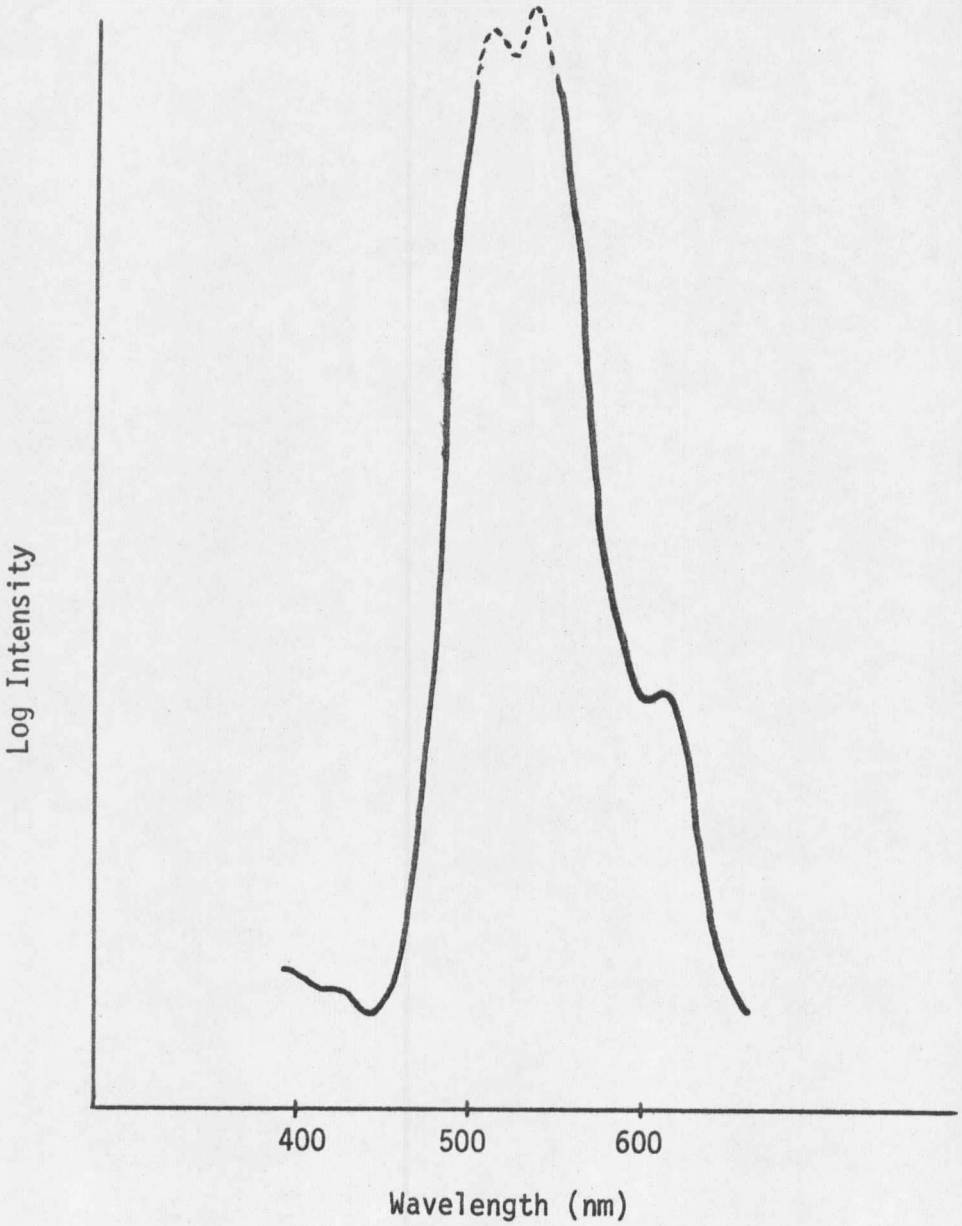


Figure 6

Crystal Spectrum of $TMACoCl_3 \cdot 2H_2O$ in x- or y-Polarized Light

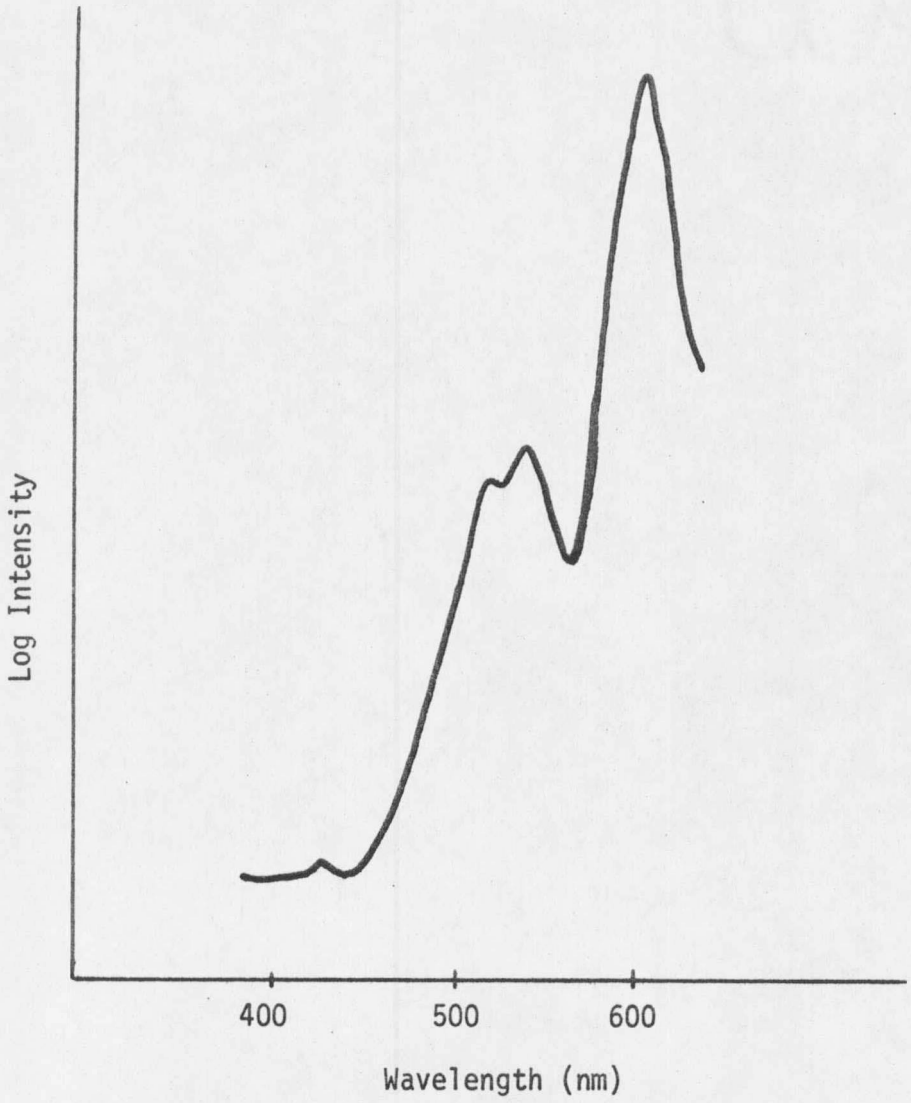


Figure 7

Crystal Spectrum of $TMACoCl_3 \cdot 2H_2O$ in $\underline{z}$-Polarized Light

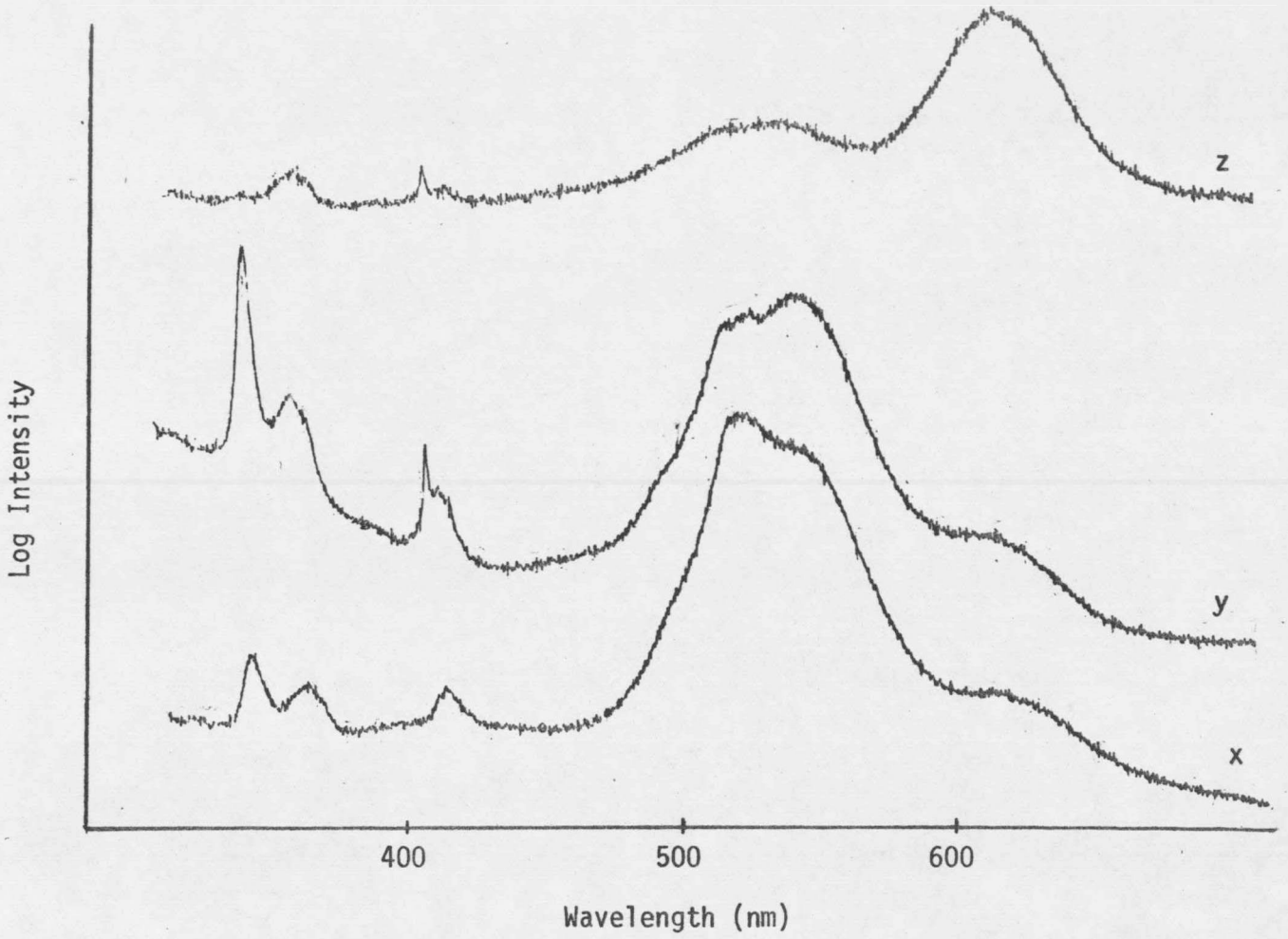


Figure 8 Polarized Crystal Spectra of $TMAMn_xCo_{1-x}Cl_3 \cdot 2H_2O$ (Visible Region)

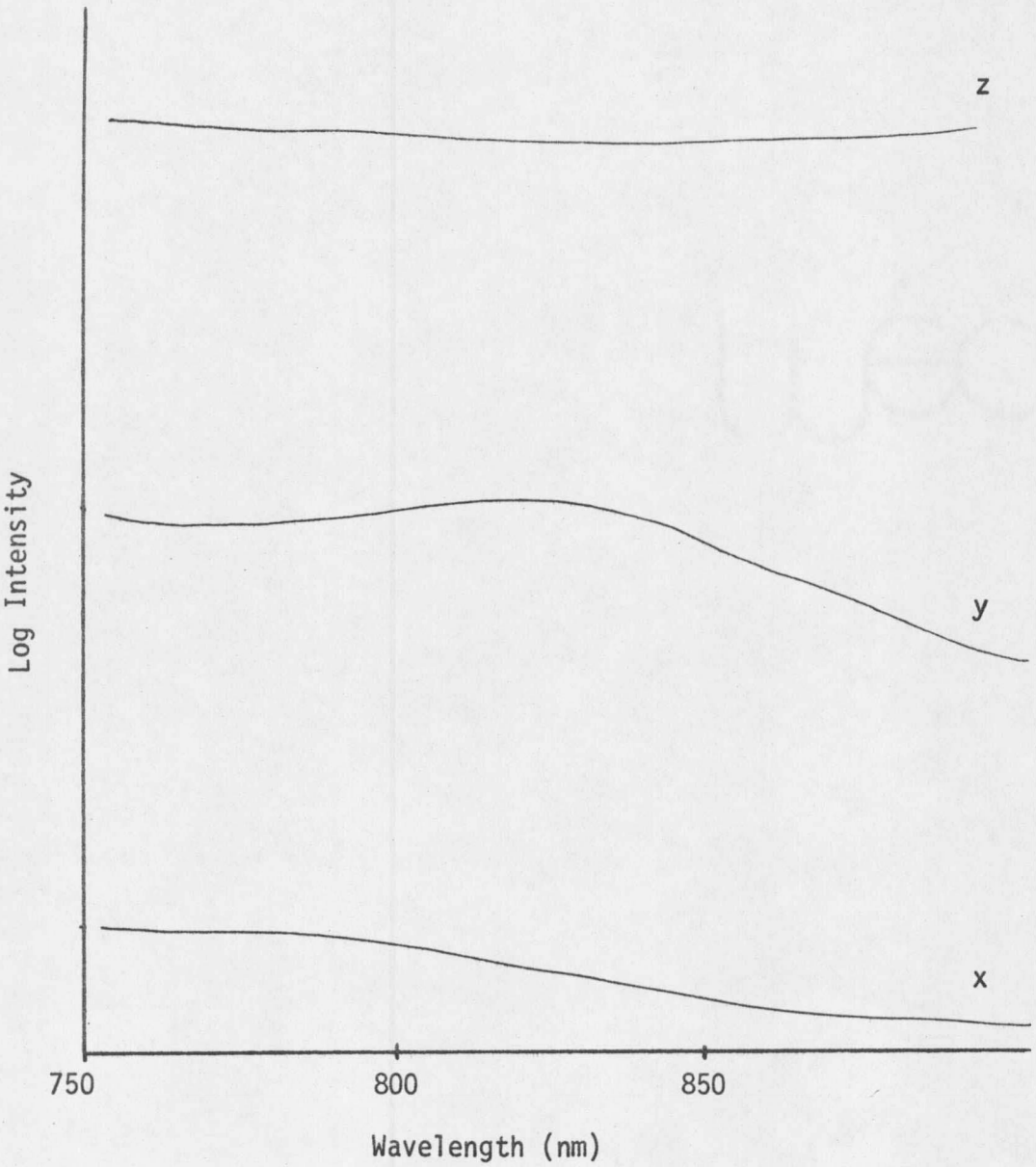


Figure 9 Polarized Crystal Spectra of $TMAMn_xCo_{1-x}Cl_3 \cdot 2H_2O$ or $TMACoCl_3 \cdot 2H_2O$ (IR Region)

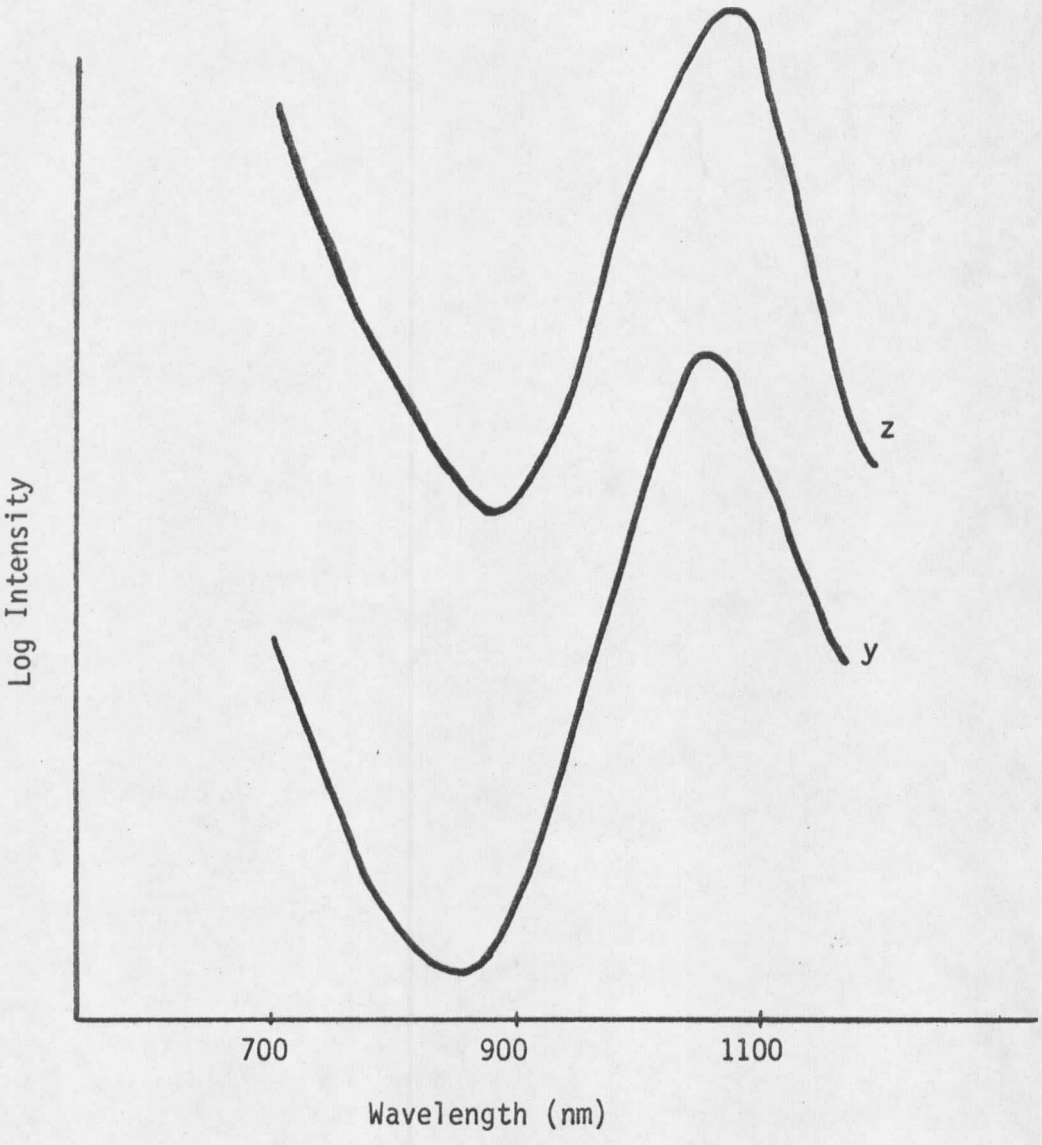


Figure 10 Polarized Crystal Spectra of $TMAMn_xFe_{1-x}Cl_3 \cdot 2H_2O$ (IR)

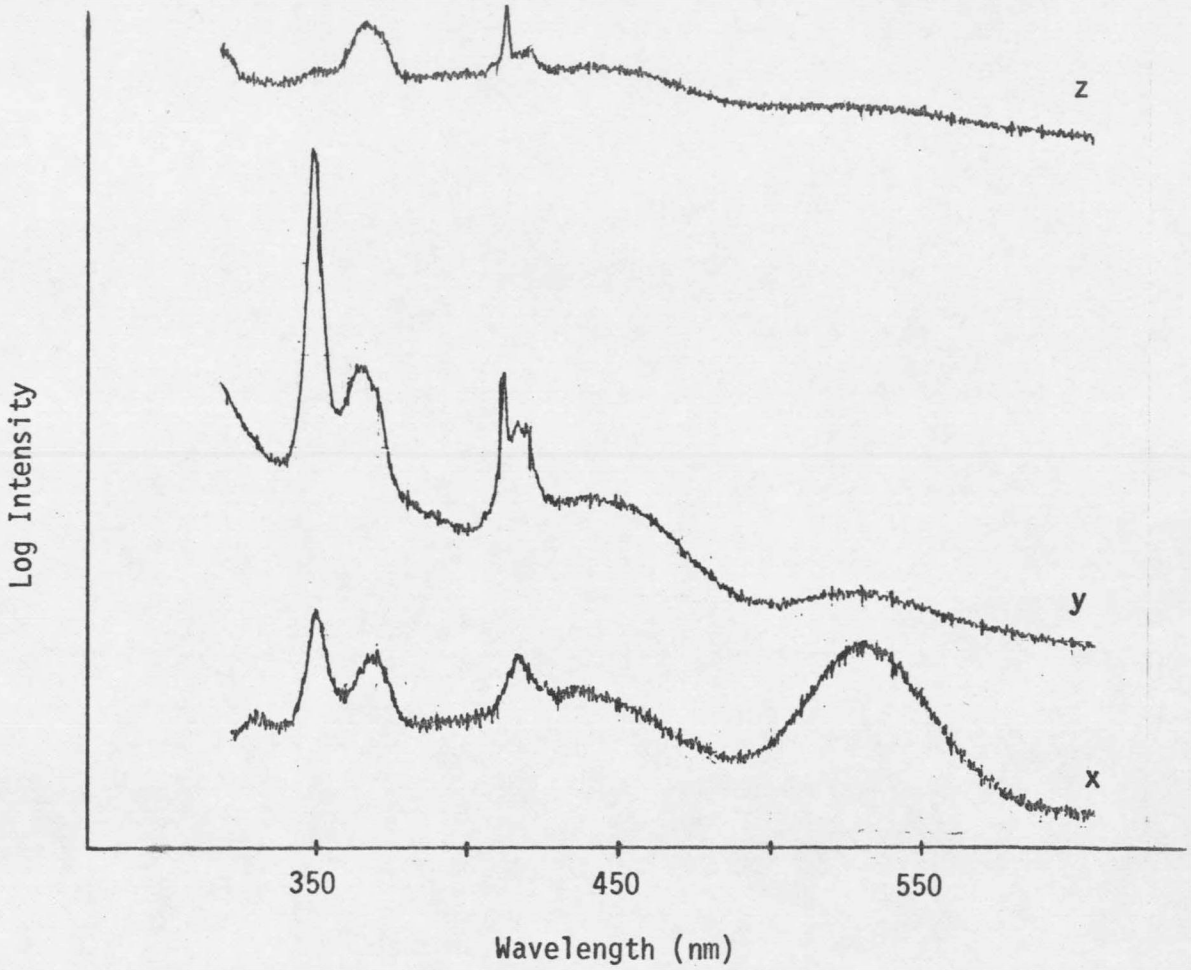


Figure 11 Polarized Crystal Spectra of $TMAMn_xNi_{1-x}Cl_3 \cdot 2H_2O$ (Visible Region)

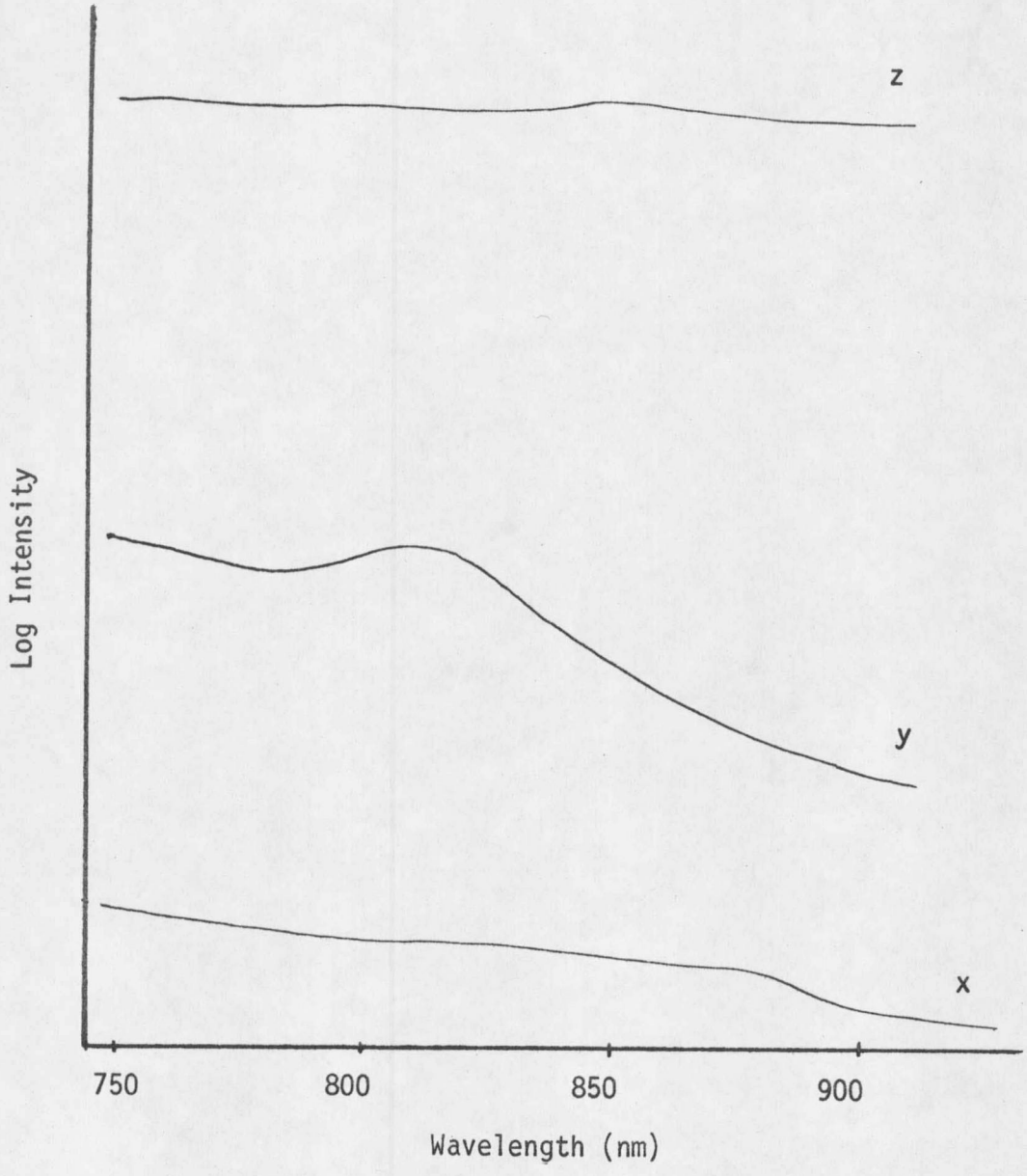


Figure 12 Polarized Crystal Spectra of $TMAMn_xNi_{1-x}Cl_3 \cdot 2H_2O$ (IR)

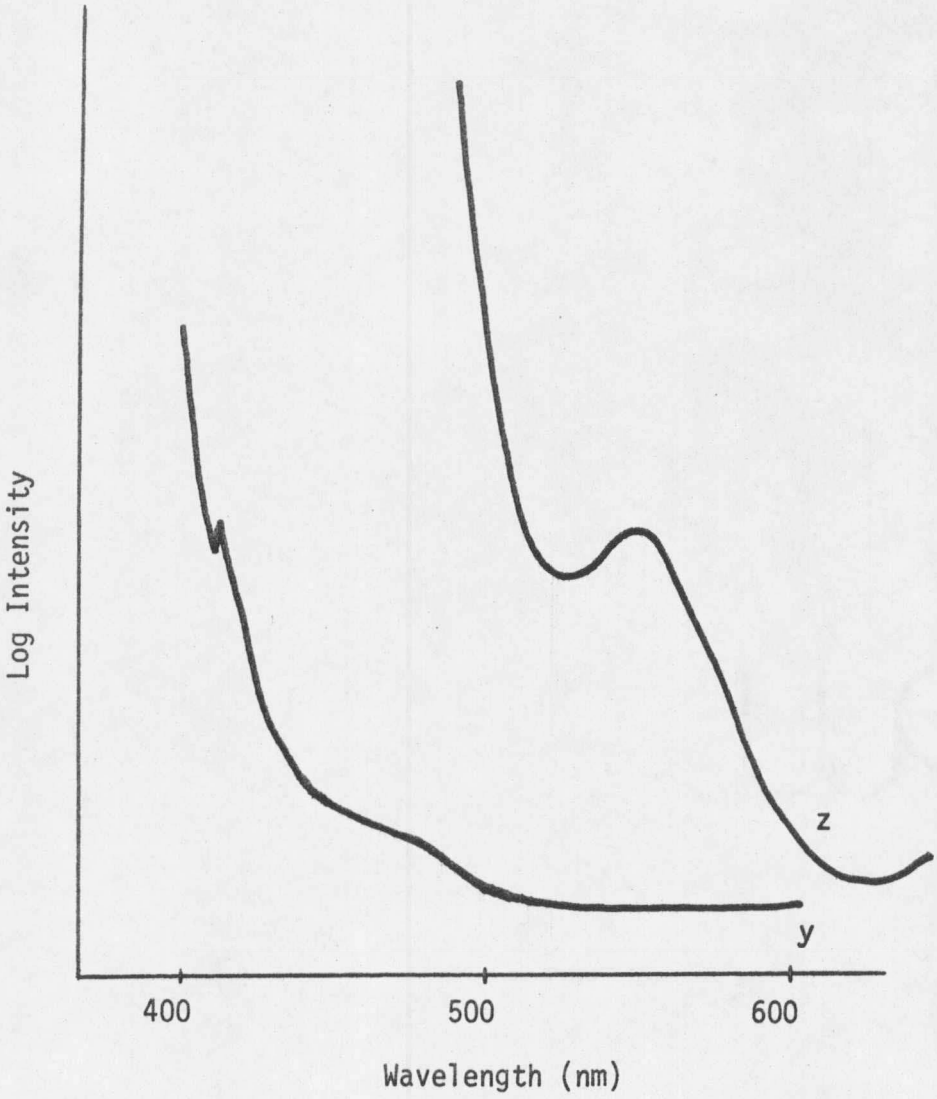


Figure 13

Polarized Crystal Spectra of $TMAMn_xCu_{1-x}Cl_3 \cdot 2H_2O$ (Visible Region)

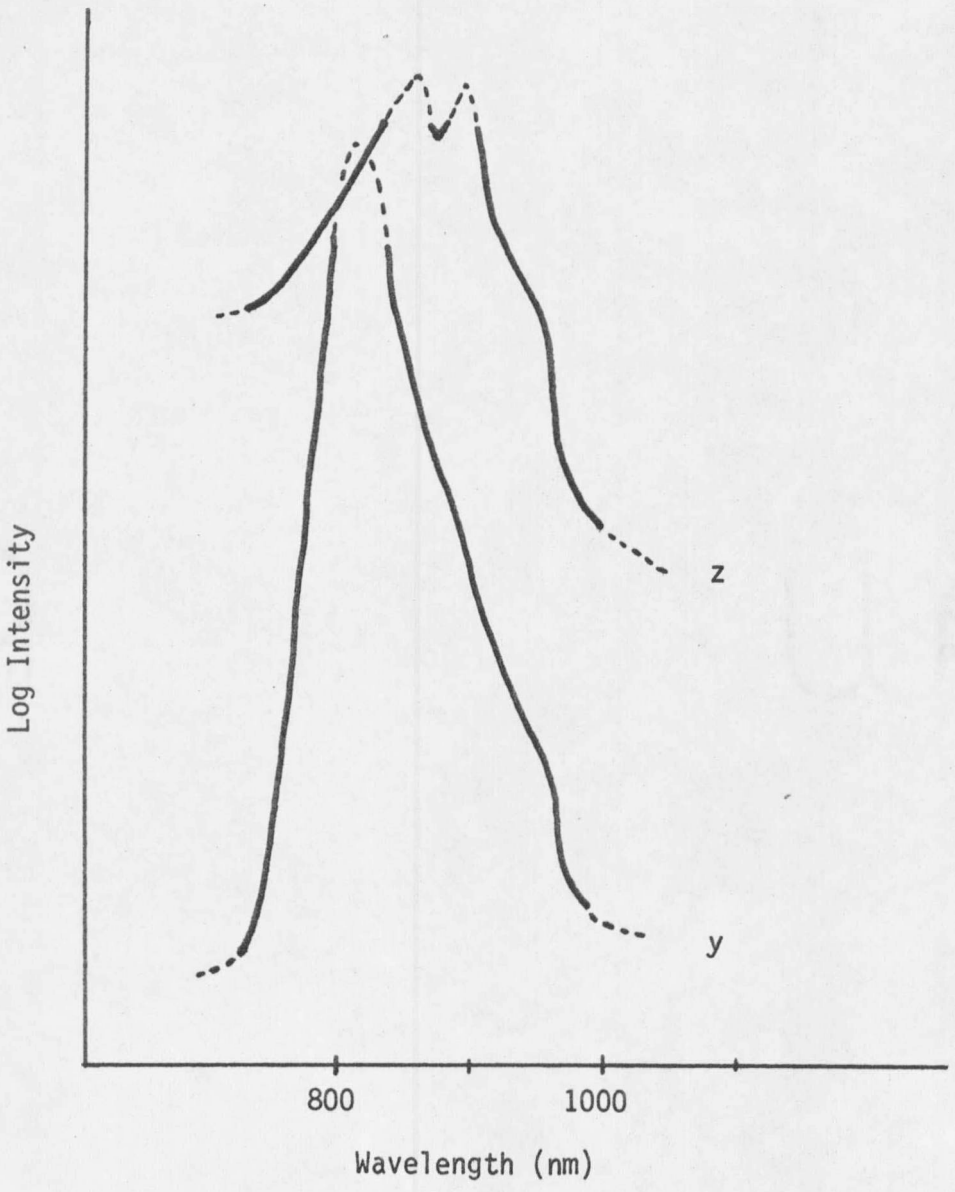


Figure 14

Polarized Crystal Spectra of $TMAMn_xCu_{1-x}Cl_3 \cdot 2H_2O$ (IR Region)

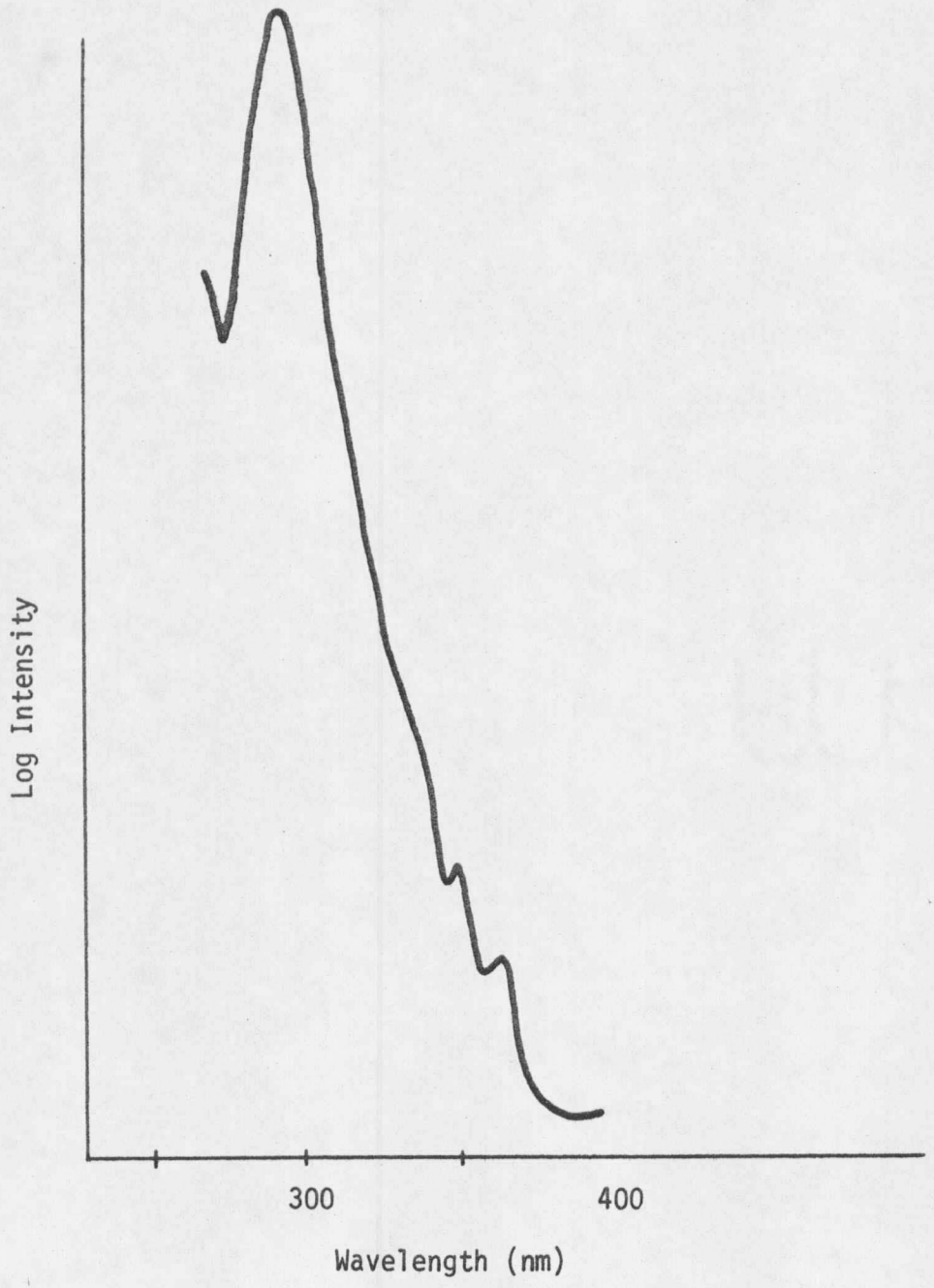


Figure 15

Unpolarized Crystal Spectrum $TMAMn_xFe_{1-x}Cl_3 \cdot 2H_2O$

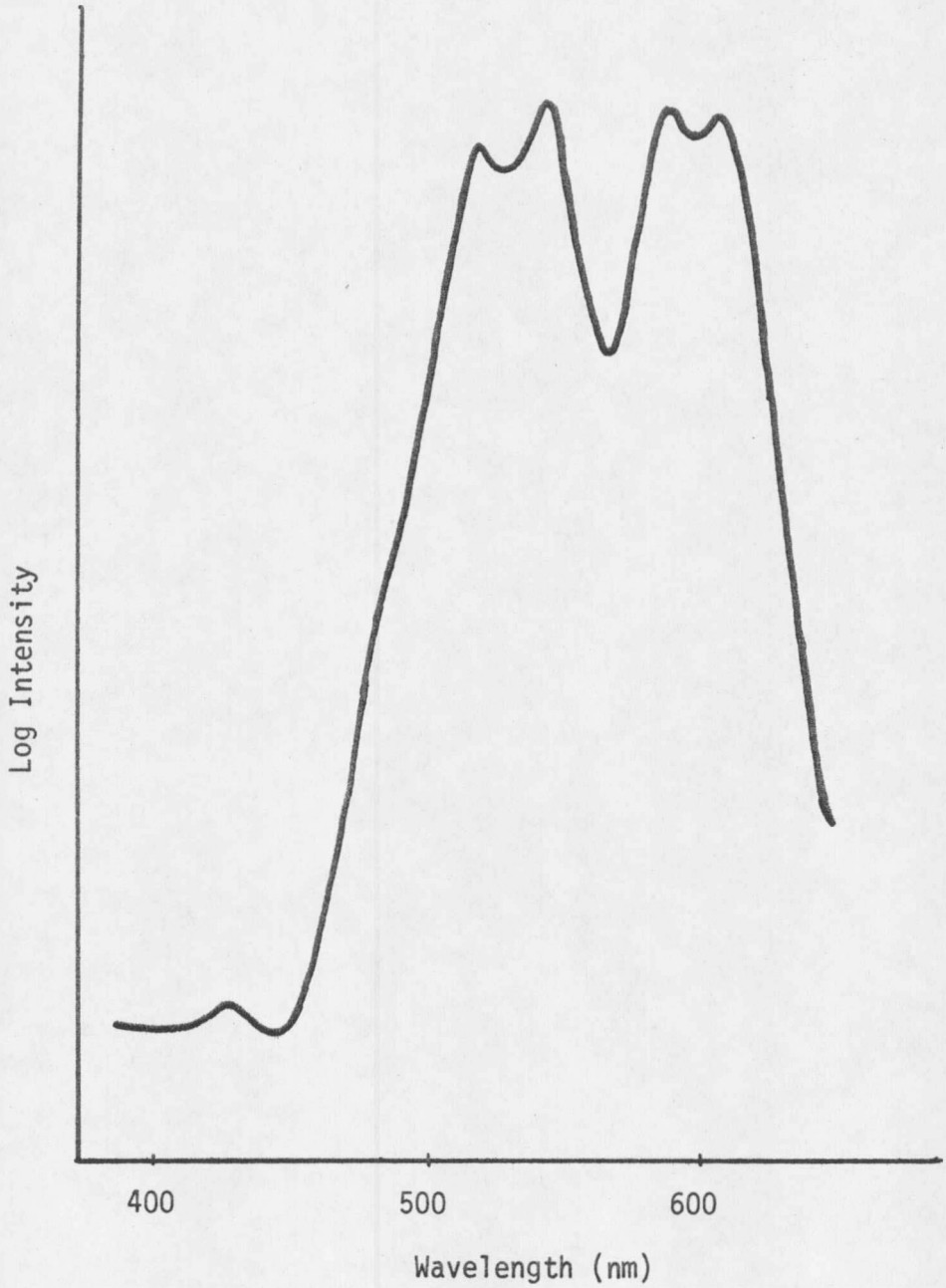


Figure 16

Unpolarized Crystal Spectrum $TMACoCl_3 \cdot 2H_2O$

## DISCUSSION

As mentioned earlier, the original intent of this research was the synthesis of mixed metal crystals of the two-site system $TMA_3M_2Cl_7$ where M and M' were expected to assume their preferred geometries. Preliminary investigation of the crystals grown in this attempt indicated that, although they were not the desired stoichiometry, they were an interesting system in their own right. Crystals of the mixed metal series actually obtained, $TMAM_xM'_{1-x}Cl_3 \cdot 2H_2O$, when observed in the petri dishes in which they were grown, displayed two contrasting colors, making it appear that two different products had formed. Closer examination of individual crystals revealed that both colors were visible in each; subsequently, titration data indicated that a mixed metal product of fairly uniform composition had indeed been prepared. The structure and composition of these mixed metal compounds are now discussed in detail. Dichroism, the visibility of two different colors within a single crystal, is discussed in the following section.

Initial analyses of the crystals prepared from solutions containing equimolar amounts of the two metals, plus a stoichiometric amount of TMA, suggested a 3:1 preference in moles for one metal over the other. The molar ratio of chloride to metal was monitored and X-ray pictures were taken to verify that the mixtures were actually the stoichiometry and structure expected and not double salts or defect structures.

Although there is only one metal site available in the hydrated series, the existence of a reproducible 3:1 metal ratio in the crystals grown from aqueous solutions with a 1:1 metal ratio raised the question as to whether these mixed salts could in fact be stoichiometric. As

the range of mole fractions in the starting solutions was expanded, and the resulting products analyzed, it became evident that this system was actually a solid solution with certain restrictions on the mole fraction of a particular metal which could occupy the metal site of the crystal. In the experimental section on analyses in Tables IV and V the $\chi$ values found in the crystals were compared to those in the starting solutions for various metal pairs. Figures 17-19 are graphic representations of the same data.

These mixed metal compounds are described in terms of solid solutions. One of the pure end members may be designated as the solvent and the remaining transition metal ions are solute particles. If all the metal cations were identical in all of their properties, and their free energies were the same whether in solution or in the crystal site, such a system could be used to represent an ideal solubility curve. In this situation the $\chi$ plot would be a straight line with slope = 1; the crystals grown would have the same composition as the starting solution. The observed deviation from linearity reflects the fact that the ions are not actually identical; they do possess slightly different properties. The nature and extent of the deviation for different metal pairs allows one to compare the relative solubilities of the metal ions in this series.

If the Cu salt is chosen as the solvent, the mole fraction of the solute present in the crystal is represented by:

$$\chi_{M',\,xtal} = \frac{n_{M'}}{n_{M'} + n_{Cu}}$$

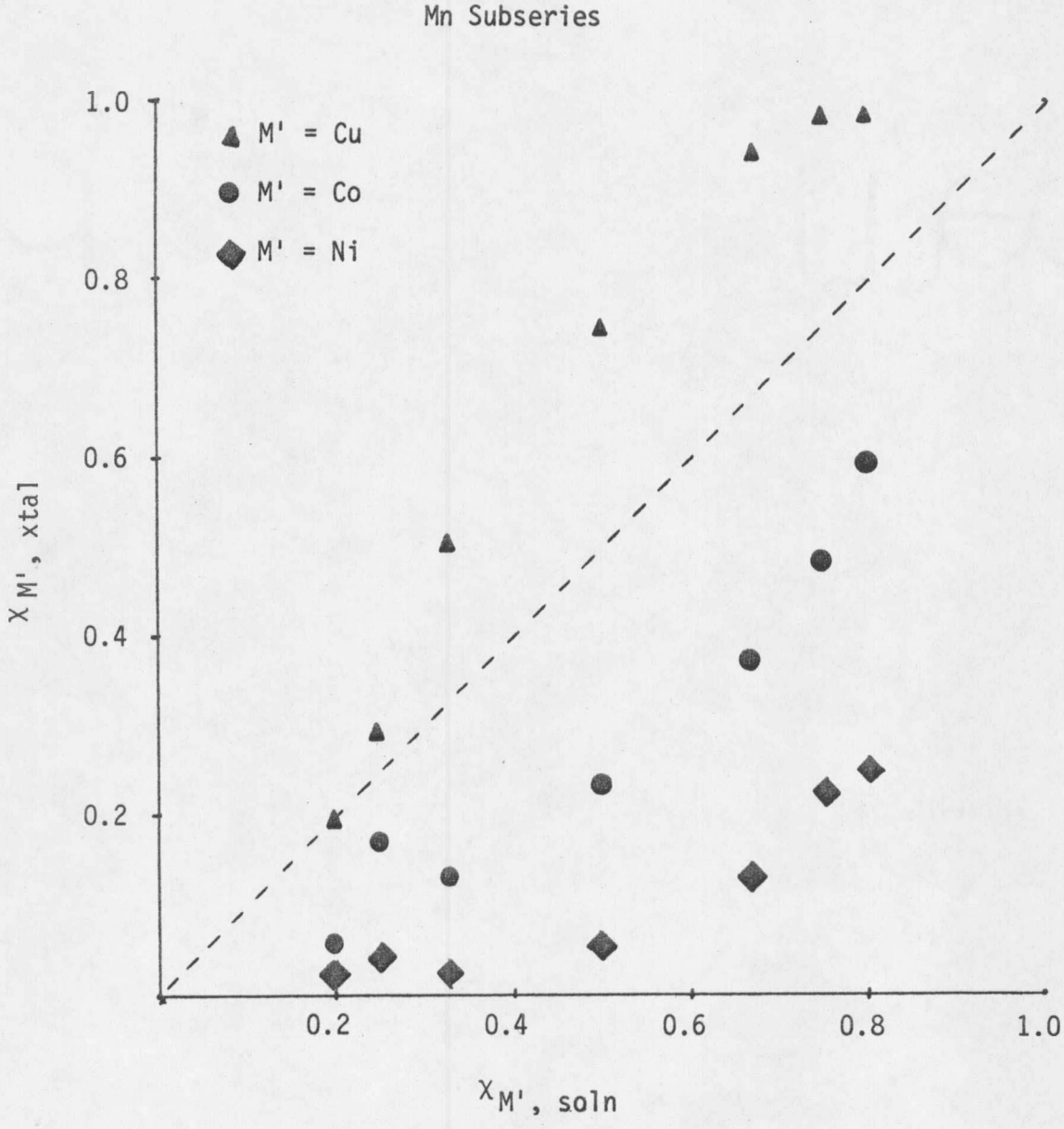


Figure 17 Mole Fraction Plots of $TMAMnM'Cl_3 \cdot 2H_2O$

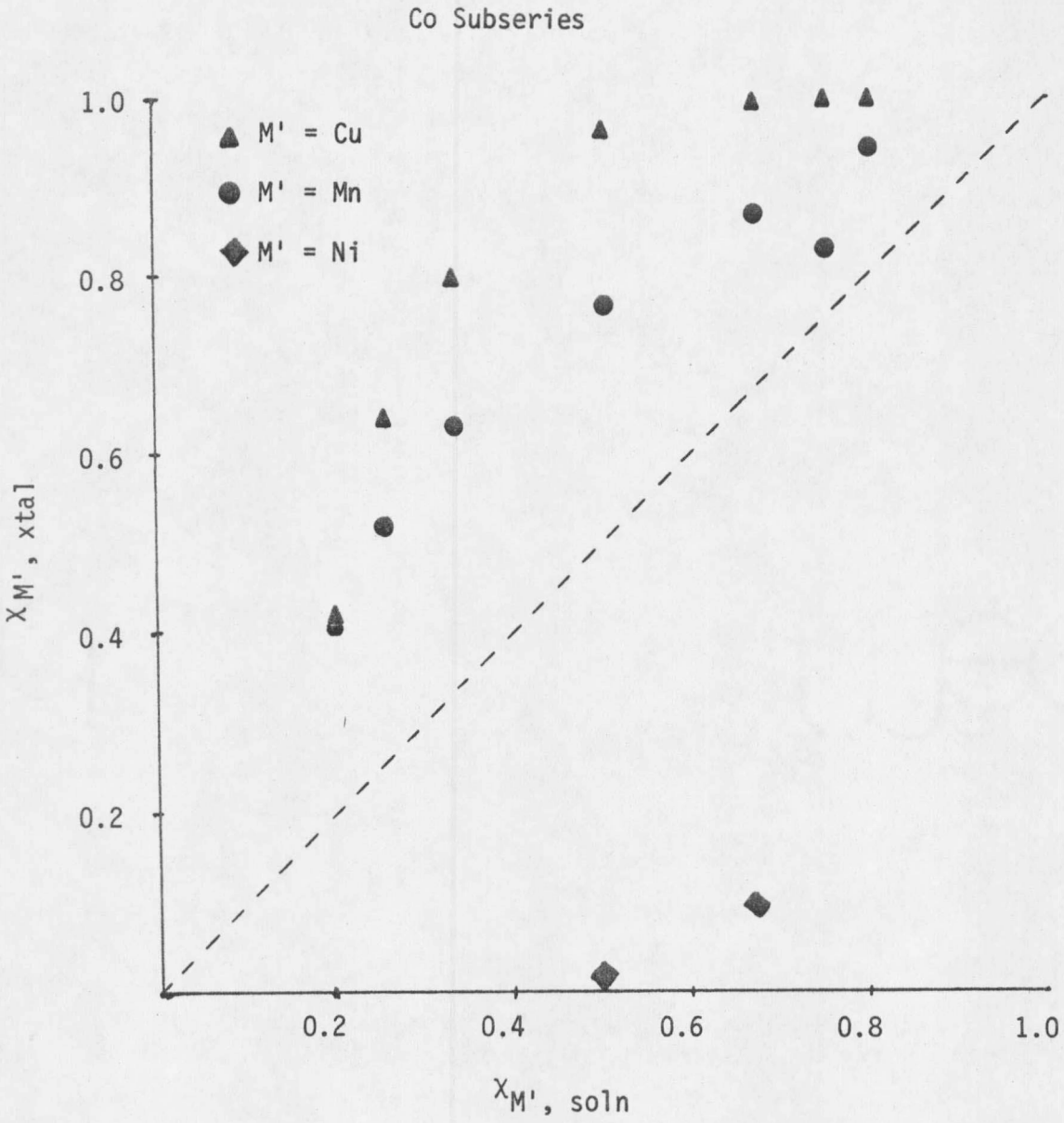


Figure 18 Mole Fraction Plots of $TMACoM'Cl_3 \cdot 2H_2O$

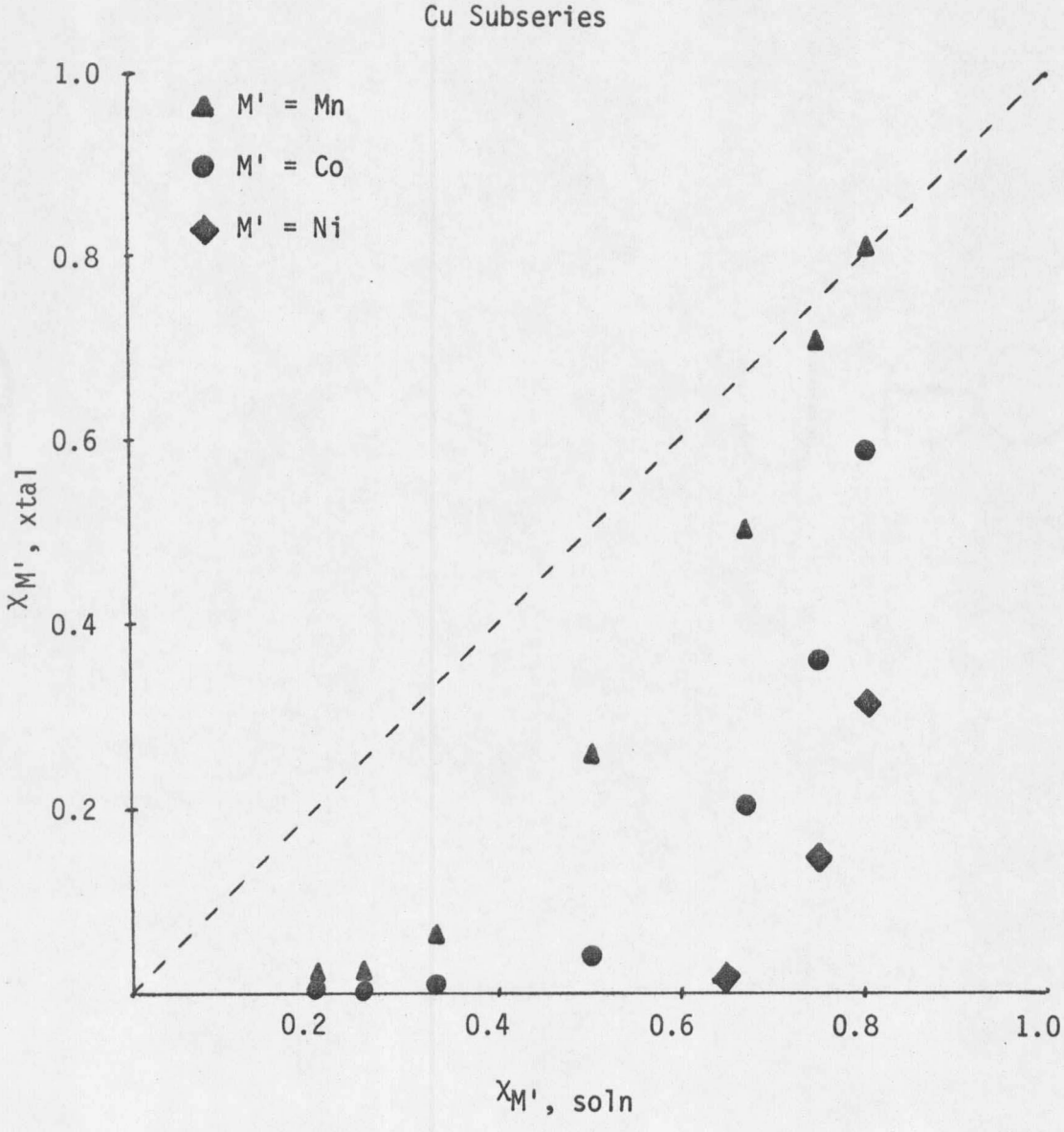


Figure 19 Mole Fraction Plots of $TMACuM'Cl_3 \cdot 2H_2O$

where n refers to the number of moles of the designated metal ion. Figure 19 indicates the relationship between $\chi_{M'}$ in the crystal and that in the solution for the Cu containing subseries. It is noted that all three curves lie below the ideal line; in each case Cu is taken up preferentially in the solid phase. If one examines the Mn-Cu curve, it is seen to possess one point, that for the highest Mn content, which actually does lie on the ideal line. Because all of the pure end members, where $\chi_{M'} = 1$, do exist, all of these curves must approach the ideal case as $\chi_{M'} \rightarrow 1.0$. Thus, even in the real solid solutions, the two end points are fixed; what happens to these curves between the end points is useful in describing the chemistry of this system.

The original aqueous solutions in the Mn-Cu subseries with $\chi_{Mn}$=0.20, 0.25 and 0.33 produce crystals which effectively exclude the solute metal, having mole fractions $\chi_{Mn,xtal} = 0.02$, 0.02 and 0.07 respectively. Structural determinations utilizing data collected with the precession camera indicate that these mixed metal crystals which are nearly all Cu adopt the monoclinic structure of the pure Cu analog. The ions whose pure salts grow in the orthorhombic structure show very little tendency to dope into the monoclinic system of lower symmetry; only trace amounts of Mn, Co or Ni are found in crystals of the $P2_1/c$ space group.

When $\chi_{M'}$ in the crystal reaches a value of about 0.20, the crystal undergoes a structural transition from $P2_1/c$ to Pnma; a different habit characteristic of this region is also exhibited. The habit of the orthorhombic Mn-Cu crystal with the highest Cu content is a distorted octahedron elongated along a, the chain direction in the monoclinic cell, but the direction of van der Waals forces in the orthorhombic cell.

This habit was shown previously in Figure 3. In addition to the change in habit in this transition region, twinning commonly occurs in the Co-Cu and Ni-Cu crystals as well.

It is interesting to note how little of the solute metal is necessary to allow the Pnma structure to predominate. Only 20% of the metal sites in the crystal need be occupied by the solute metal ions to enable the orthorhombic structure to manifest itself. When this structure prevails, the solute metals whose pure salts are orthorhombic enter the crystal site much more readily than they did in the monoclinic case. Their solubility increases sharply following the structural transition and exhibits the order: Cu > Mn > Co > Ni.

The most striking pattern in the observed order is the decrease in the size of the metal cation as the solubility decreases. Although the Cu(II) ion is not the largest cation, it has a $d^9$ electron configuration and displays a Jahn-Teller effect when it occupies the metal site of the crystal; it thus tends to distort the regular octahedral site and appears to have a larger radius than the numbers would indicate. This distortion is sufficient to destroy the Pnma symmetry when more than 80% of the sites are involved. Because of the energy considerations within the crystal, the Mn(II) ion which is the largest of the series, seems to pack better in this environment than the other smaller cations, excluding Cu. Co(II) with a smaller radius would not be expected to substitute for the Cu ion in the lattice sites quite as readily as the Mn; this is indeed what is observed in the Cu subseries. Of all the ions considered, Ni(II) is the most difficult to force into the crystal lattice site; it is also the smallest. The pure Ni end member of this

series tends to form an amorphous powder rather than a crystalline solid, and this effect is observed in the mixed metal salts as well. Ni is by far the least soluble in the solid phase of the transition metals studied in this series.

This effect may be explained by comparing the size of the metal ion to the hole formed by four chloride anions just touching in a square planar arrangement as shown in Figure 20.

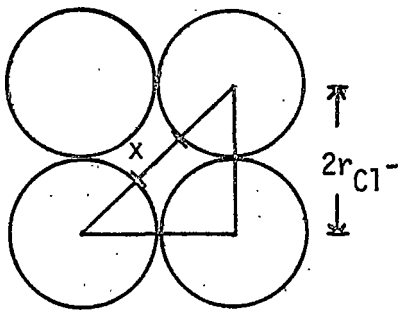


$r_{Cl^-} = 1.81$ Å

$\frac{1}{2}x = r_{hole} = 0.75$ Å

$r_{Ni} = 0.70$ Å

$r_{Co} = 0.74$ Å

Figure 20 Packing Hole Formed by Four Chlorides

In order for the metal cation to touch these chlorides, its ionic radius must be 0.75 Å or larger; Co(II) just fits. Ni(II) with an ionic radius of only 0.70 Å is too small. Since this cation does not fit into the crystal site, growth of the Ni crystal is very difficult to achieve. The larger cations such as Fe and Mn, and Cu as well, tend to push the chloride anions apart when they occupy the site, thus reducing the electrostatic repulsions among the $Cl^-$ ions.

Absolute values for the radii of the ions involved in this exercise are impossible to determine. How well the actual numbers in these

calculations fit the observed solubilities is therefore dependent on the choice of radii one makes. Those calculated by Shannon and Prewitt (11) take into account the spin and coordination number of the metals and were therefore preferred over Pauling's values. As it turned out, these values also indicate quite well that Ni(II) is too small to occupy the crystal site in this series. Regardless of whose radii are chosen, the trend remains the same. Ni(II) is always the smallest and predictably the most difficult to force into the crystal site.

Based on the solubilities observed in the Cu containing subseries and the rationale proposed to account for these observations, one would predict that in the Mn subseries Cu will again be more soluble than Mn, and that Co will dissolve more readily than Ni with the latter two both less soluble than Mn. This is borne out in the $\chi$ plots of these subseries. In the Co subseries both Cu and Mn are more soluble than Co which is indicated by the positive deviations from the ideal line for these curves; Ni has a negative deviation showing that it once again is the least soluble of the transition metal ions in this series.

A spectrophotometric technique (20) was utilized to determine both Co and Ni simultaneously in a single sample; this analytical method was not sensitive enough to detect very low concentrations of Ni, yielding $\chi_{Ni,xtal}$ values of zero for $\chi_{Ni,soln}$ values less than 0.50. This method does indicate at what mole fraction in the aqueous solution appreciable amounts of Ni begin to appear in the resulting crystals. The technique, although not as sensitive as the titration methods, is sufficient to corroborate the existing solubility pattern.

Familiarity with this system allows one to actually rank a group of

crystals from the same subseries according to relative metal content by visual examination alone. Although difficult to describe quantitatively, a gradual, subtle change in color is observed in a group of crystals in the orthorhombic structure as mole fraction changes. One must exercise care in selecting crystals of roughly the same size and quality when doing such a comparison, however. Crystals from solutions which contain progressively more Ni exhibit a gradual, but definite, color change if they are compared to one another, supplying further evidence that more Ni is indeed being dissolved in the solid solution. These qualitative observations on the crystals can be quantified by a nondestructive method, utilizing the precession photographs. As one dissolves more of the solute metal ion into a crystal, not only the color but also the cell dimensions should change gradually as a result of the different sizes of the two ions.

X-ray data indicate that this effect can indeed be seen. For a particular subseries of the mixed metal crystals, the values of a, b and c should vary in a predictable way with the molar ratio of the component metals. A large difference in radii occurs between the Mn(II) and Cu(II) ions; thus, this effect should be noticeable in this subseries. However, a structural transition also occurs in this case which lowers the range of $\chi_{Cu}$ which can be studied. Cell dimensions for orthorhombic crystals of the Mn-Cu subseries with $\chi_{Cu} = 0.20$ and $\chi_{Cu} = 0.75$ are presented in Table VIII on the following page.

The Mn-Co subseries also displays a fairly wide range of mole fractions, $\chi_{Co} = 0.05$ to $\chi_{Co} = 0.60$, and there is no change in structure between end members to complicate matters. Table IX compares the cell

dimensions of the extreme $\chi$ values of the Mn-Co subseries to those of the pure end members.

Table VIII

Cell Dimensions of Some Crystals in the Mn-Cu Subseries

| $\chi_{Cu}$ | Metal | a | b | c |
|---|---|---|---|---|
| 0.00 | Mn | 16.78 | 7.434 | 8.227 |
| 0.20 | Mn-Cu | 16.64 | 7.469 | 8.095 |
| 0.75 | Mn-Cu | 16.59 | 7.419 | 7.828 |
| 1.00 | Cu* | 16.73 | 7.479 | 7.864 |

* Cu axes redefined, a→b, b→c, c→a

Table IX

Cell Dimensions of Some Crystals in the Mn-Co Subseries

| $\chi_{Co}$ | Metal | a | b | c |
|---|---|---|---|---|
| 0.00 | Mn | 16.78 | 7.434 | 8.227 |
| 0.05 | Mn-Co | 16.76 | 7.426 | 8.213 |
| 0.60 | Mn-Co | 16.61 | 7.277 | 8.085 |
| 1.00 | Co | 16.52 | 7.234 | 8.046 |

The Mn-Co crystals seem to fit the expected trend in cell dimensions. The crystal which is nearly pure Mn has values which are very close to those for pure Mn, and the crystal with $\chi_{Co} = 0.60$ has values

which are approaching those for the pure Co end member. In the case of the Mn-Cu crystals, that with a low mole fraction of Cu fits the trend, but the crystal which is predominantly Cu is anomalous. This mole fraction also occurs in the region in which the habit is quite different. The preference for this new habit may be related to some interaction at local sites between the Mn and the Cu cations which could also give rise to the break in the pattern of cell dimensions which is noted in this particular region. An anomaly may well be expected for these crystals in this region of structural and habit transitions. For many of the observed patterns in this work the Cu(II) ion has proven anomalous.

The dichroism exhibited by these crystals has been mentioned earlier, and it is this property above all else which first captures the attention and interest of the observer. One of the special attractions of the mixed metal series is the striking visibility of two and sometimes three different colors within a single crystal. This dichroism may be characterized by visual examination of the crystals, by observation of the crystals with a polarizing microscope, or by comparison of polarized crystal spectra in various orientations. The wavelength at which an absorption maximum occurs has an effect on the value of the refractive index, n, determined for a crystal.

The index of refraction of a substance, defined as the ratio of the velocity of light in a vacuum to that in the substance, is one of the most basic physical properties measured by chemists. The substance of interest is usually a liquid, but may also be a gas or a solid. Measurement of the refractive index of a crystalline solid is of particular interest to the mineralogist (23-25); the physical method used to

determine n is necessarily different for a solid than a fluid. In addition to the problems associated with a more involved procedure, different values may be obtained for n depending on the orientation if the solid exhibits anisotropy. The velocity of light may actually vary depending on what direction it is traveling through the crystal.

Crystals are classified as isotropic or anisotropic. In an isotropic crystal the velocity of light, or the refractive index, is the same in all directions, as is the case for liquids and glasses. If a three-dimensional surface indicating the value of the refractive index, n, in any direction within the crystal were constructed for an isotropic crystal, it would be spherical; such a surface is defined as an indicatrix. Perhaps the most common example of an isotropic crystal is table salt, NaCl. This is a cubic system, the highest possible symmetry class, and is completely described if one cell dimension is known; to use a chemist's expression, it has one degree of freedom. On the basis of the structural symmetry of NaCl, it should not be surprising that a cubic crystal has only one value of n.

In anisotropic crystals the velocity of light varies depending on the orientation of the crystal. Such crystals can be described in terms of their indicatrices as either uniaxial or biaxial. In uniaxial crystals there is one, and only one, axis defined as the optic axis which is perpendicular to a circular or isotropic cross section of the indicatrix; in biaxial crystals there are two such axes. The uniaxial crystal has the higher symmetry and belongs to either the tetragonal, hexagonal or rhombohedral class. Two degrees of freedom must be specified to completely define these systems; two edges, a and c, for the

first two and one edge and one angle for the last one.

In a tetragonal system $\underline{a} = \underline{b}$; thus, symmetry requires a 4-fold principal axis parallel to the $\underline{c}$ axis of the unit cell which will coincide with the optic axis of the indicatrix. The $\underline{c}$ axis may be either longer than or shorter than the $\underline{a}$ and $\underline{b}$ axes. The ellipsoid which represents the indicatrix may also be prolate ($n_\varepsilon > n_o$) or oblate ($n_\varepsilon > n_o$); mineralogists use this distinction to define the sign of a crystal. A tetragonal crystal may be either uniaxial positive, U(+), or negative, U(-), as shown in Figure 21.

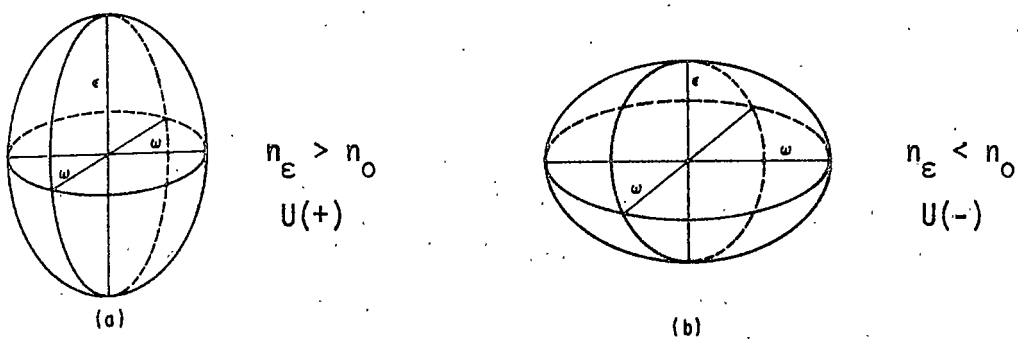


Figure 21 Tetragonal Indicatrices

The sign may actually be determined with a microscope without knowledge of the absolute values of $n_\varepsilon$ and $n_o$. While the cell dimensions define the optic axis, they yield no information on the relative values of n.

The mineralogists's most dramatic example of a uniaxial crystal is Iceland spar, more commonly called calcite. Calcite is calcium carbonate, $CaCO_3$, which falls in the rhombohedral class. It is a transparent crystal which cleaves naturally into rhombs. If one of these rhombs

is placed over a mark on a piece of paper, two marks are visible through the crystal. This is shown in Figure 22.

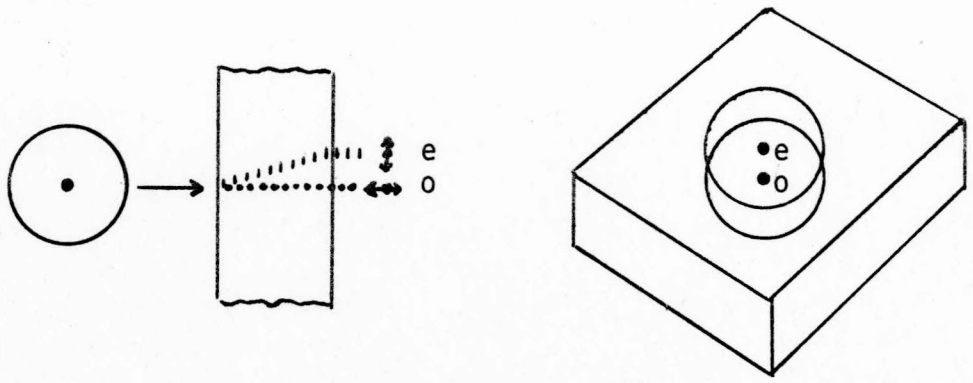


Figure 22 Double Refraction of Iceland Spar

One of the observed images is produced by the ordinary ray, the other by the extraordinary ray. They can be distinguished by rotating the rhomb as it lies on the paper; the ordinary image remains fixed while the extraordinary image rotates with the crystal. A close examination of the two images reveals that both appear higher than the paper which is to be expected due to the difference in refractive index between air and the crystal. However, the image produced by the extraordinary ray appears a little lower than that from the ordinary ray. The different apparent depth is evidence for two refractive indices within a single crystal in this orientation. This illustrates the property of double refraction exhibited by all anisotropic crystals. Mineralogists quantify this property by defining a term, birefringence, which is the difference between the maximum and minimum refractive indices.

The lateral location and rotatory motion of the extraordinary image depends on the wave nature of light and the ability of a crystal to resolve light into two mutually perpendicular vibration directions. Light is electromagnetic radiation; ordinary light has an electric vector, $\vec{E}$, capable of vibration in any direction perpendicular to the propagation direction. In the calcite crystal all of these vibration directions are resolved into two orthogonal directions. The vibration direction which represents $\vec{E}$ normal to the optic axis is that of the ordinary ray. The E vector of the ordinary ray is in the plane of the circular cross section of the indicatrix; this means that the electric field of this ray interacts with that of the electrons in the crystal in the same fashion in any direction within the a-b plane. The ordinary ray propagates through the crystal as if it were isotropic.

The E vector of the extraordinary ray is perpendicular to that of the ordinary ray and in the same plane as the optic axis. By symmetry the atomic arrangement along c is different than that along a or b. The vibrations due to the electrons in this asymmetrical environment interfere with $\vec{E}$ of the extraordinary ray and produce a resultant vector which is no longer exactly perpendicular to the ray direction. However, the propagation direction must still be perpendicular to the E vector; this so-called wave normal no longer coincides with the ray as it does in the ordinary ray. This interaction bends the path of the extraordinary ray slightly; thus, two images appear as light exits the calcite rhomb. The paths of these two rays are shown in Figure 23.

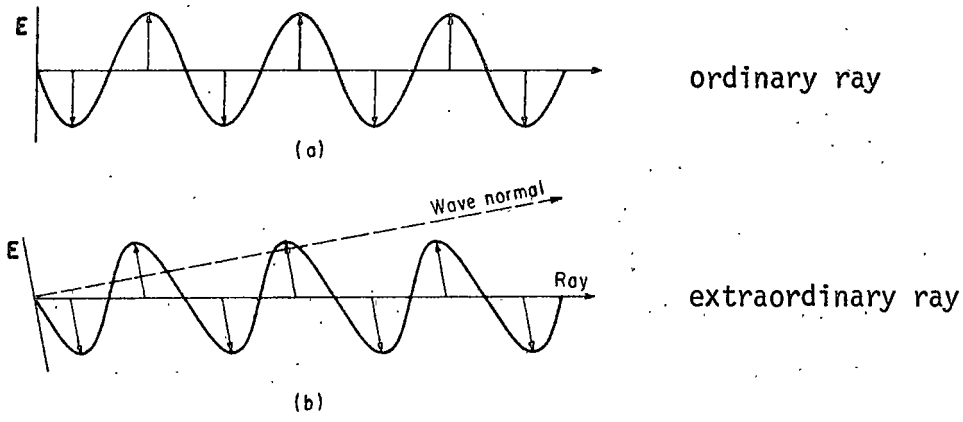


Figure 23 Ray Directions and Wave Normals

The resolution, i.e. the distance between these two images, is directly proportional to the birefringence and to the thickness of the crystal. In calcite light travels faster along the optic axis; in this case, $n_\varepsilon < n_o$. This means that $n_\varepsilon$ is closer to $n_{air}$ than $n_o$ so that the extraordinary image should appear lower than the ordinary one which is indeed the case. A thicker rhomb will cause the two images to appear further apart due to the longer path length the two rays follow. This same process occurs in all anisotropic crystals. Calcite is unusual in that it is transparent and has an extremely high birefringence. Quartz will also form two images, but a crystal 15 times as thick is required to observe the same separation of images.

It is possible to observe anisotropic crystals with light which has only one allowed vibration direction; such light is "polarized." Plane polarized light may be obtained in a number of ways; some

crystals such as biotite or tourmaline naturally polarize light. A Nicol prism often used in polarizing microscopes consists of a calcite crystal which is oriented so that only the crystal's extraordinary ray is allowed to pass through. Large sheets of Polaroid, the substance which was used to obtain the polarized spectra in this work, are made by embedding oriented crystals of herapathite in a plastic sheet. Even light reflected from a bright, nonmetal surface is polarized to some extent.

If the two images produced by calcite are observed through a polarizer as the rhomb is rotated, each one will disappear or extinguish alternately at 90° intervals. The plane of the vibration direction of the ordinary and extraordinary rays can thus be determined. If there is no vector component of the ordinary ray, that image will not be seen; it extinguishes or is at an extinction position. There are two such positions for the extraordinary ray as well, 180° apart and orthogonal to those for the ordinary ray.

All the properties that have been discussed for uniaxial crystals are also present in biaxial crystals, but the latter show other effects as well due to their greater complexity. Crystals which fall into the orthorhombic, monoclinic or triclinic classes are biaxial. For such crystals the indicatrix is a triaxial ellipsoid; each axis has a different value for n. The two extremes are denoted as $n_\alpha$ for the lowest value and $n_\gamma$ for the highest value. The biaxial indicatrix has two optic axes which are normal to circular cross sections whose radii represent $n_\beta$, the intermediate refractive index for biaxial crystals. The location of these indices within the indicatrix is illustrated in

Figure 24.

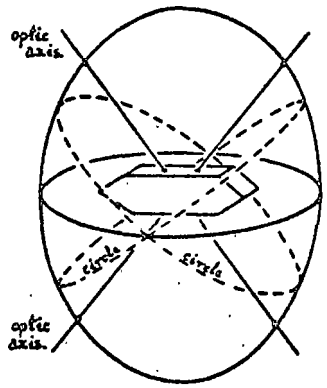


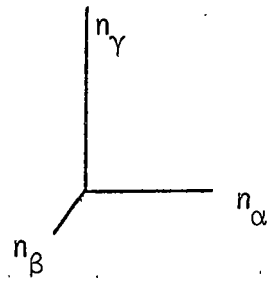


radius of circle = $n_\beta$

Figure 24 Biaxial Indicatrix

In orthorhombic crystals symmetry requires that the three axes of the indicatrix coincide with the three crystallographic axes, but no restrictions are placed on the actual mapping, i.e. the shortest crystallographic axis need not correspond to $n_\alpha$. There are six ways to satisfy this requirement; the correct one for a particular system is found by experiment. In the monoclinic system one of the 2-fold axes of the indicatrix will coincide with the unique axis of the crystal. In the triclinic system any orientation is possible.

The differences in symmetry along the various axes in anisotropic crystals are basically a result of different atomic arrangements. This results in the variable refractive indices observed in such crystals. The interaction of the crystal with light is also what determines the color of a crystal. An anisotropic crystal is therefore capable of displaying different colors depending on the orientation and direction in which it is observed. If all three axes in a biaxial crystal have

a different associated color, the general term for the phenomenon is pleochroism. If only two colors are involved, it is called dichroism. The latter term is often used for all cases, since in any one orientation of the crystal only two colors can be observed.

Tourmaline which grows as elongated prisms is an example of a dichroic crystal; it has been mentioned previously as a source of polarized light. This mineral allows light vibrating parallel to the prism axis to pass through while completely blocking light vibrating normal to the prism axis. Its dichroism may be described as black and white. Two crystals of tourmaline with their prism axes orthogonal will not allow any light to pass.

Most anisotropic crystals are dichroic or pleochroic to some extent, but cases among minerals strong enough to see, particularly with contrasting colors, are very rare. Andalusite, an aluminum silicate, is one such example; some crystals of this mineral which contain a small amount of impurities are yellow, green and red along the principal axes of its indicatrix. When viewed along any principal axis, the color observed is the sum of the colors of the other two axes.

In colored substances such as the dichroic and pleochroic minerals discussed above, the refractive indices have unusually high or low values due to the presence of absorption bands in the visible region. Because the refractive index is a function of wavelength, $\lambda$, values of n are reported with reference to some known wavelength of light used to make the measurement, for example the Na D line. The following equation can be used to describe the relationship between the refractive index, n, and wavelength, $\lambda$ (26):

$$n^2 = 1 + \frac{A_1 \lambda^2}{\lambda^2 - \lambda_1^2} \qquad (1)$$

where $A_1$ is a constant and $\lambda_1$ is an absorbing wavelength. If a substance has more than one absorption band, additional terms involving $\lambda$ are added. There are three cases which can be considered for this equation. If the wavelength used to determine n is much greater than the absorbing wavelength, $\lambda >> \lambda_1$, Equation 1 reduces to:

$$n^2 = 1 + A_1 = k \qquad (2)$$

where k is the dielectric constant. This equation generally holds for gases and dispersion is not usually observed.

If $\lambda > \lambda_1$, but the ratio $\lambda_1/\lambda$ is small, Cauchy's Theorem for dispersion results:

$$n^2 = 1 + A_1 + \frac{A_1 \lambda_1^2}{\lambda^2} \qquad (3)$$

Let $A = 1 + A_1$

$B = A_1\lambda_1^2$

$$n^2 = A + \frac{B}{\lambda^2} \quad \text{which is Cauchy's Theorem.} \qquad (4)$$

If n is plotted against $\lambda$, a normal dispersion curve results from Equation 3 with n increasing gradually as $\lambda$ decreases.

As the wavelength used to measure the refractive index approaches the absorbing wavelength, Equation 1 requires that n become very large, going to infinity at $\lambda = \lambda_1$. Since this cannot actually occur, the expression does not adequately define n at this point. A damping term must be added to the equation in order for it to apply to all values of

λ, including absorption points (27).

The Mn, Fe, Co and Ni salts as well as their mixed metal analogs prepared in this research all crystallize in the orthorhombic class with space group Pnma, and are thus examples of biaxial crystals. Because they are highly colored, they possess visible absorption bands which will give rise to anomalous dispersion curves. These characteristics, lower than cubic symmetry and absorption bands in the visible region, are two requirements a crystal must meet in order to be dichroic. The third and crucial requirement is that the local site symmetry of the chromophore be oriented or aligned in the unit cell so that the dichroic effect is not cancelled in the same way as optical activity in a racemate. The $MCl_4(H_2O)_2$ octahedra in the Pnma structure and in the $P2_1/c$ structure as well also meet this third requirement; therefore, the crystals in the $TMAM_xM'_{1-x}Cl_3 \cdot 2H_2O$ series are dichroic.

The structure and cell dimensions of these compounds have been discussed earlier. To review briefly, the axes and corresponding bonding directions are shown in Figure 25.

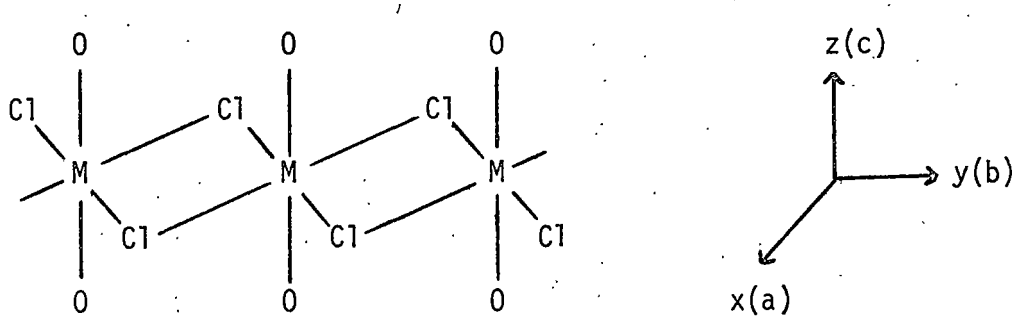


Figure 25 Unit Cell Axes and Bonding Directions

Of the pure orthorhombic salts, the Co analog displays the most readily visible dichroism without the aid of a polarizing microscope, although the crystals must be selected judiciously for the colors to be observed. Literature reports these crystals to be blue in c-polarized light propagating along the a axis; in all other orientations these crystals appear red-violet. These observations have been confirmed in this work. The dichroism of the Mn and Cu analogs has not been reported in the literature previously.

Crystals in the mixed metal subseries containing Co are all strikingly dichroic; Table X summarizes their behavior when observed in polarized and in unpolarized light. Light designated as a-polarized has its allowed vibration direction, which corresponds to $\vec{E}$, parallel to the a crystallographic axis, similarly for the b- and c-polarized light.

If the Co containing compounds were observed only in unpolarized light, these crystals would be classic examples of dichroism and pleochroism. In a crystal of the Mn-Co salt the shorter wavelengths of visible light polarized in the a or b direction are absorbed, and the crystal appears red-violet. When c-polarized light is propagated through the b-c plane of the crystal, the longer wavelengths are absorbed, and the crystal appears blue. The isotropic behavior in the a-b plane can be rationalized on the basis of structure, since the metal ion giving rise to the absorption band is in an essentially square planar environment with the the surrounding $Cl^-$ ions. In the b-c plane, however, the metal is bound to $H_2O$ in one direction and to Cl in the other, quite a different atomic environment and thus a different color may be expected for c-polarized light than for b-polarized light. In

Table X

Colors Exhibited by $TMACo_xM'_{1-x}Cl_3 \cdot 2H_2O$ Crystals

| Crystal | Polarization | a-b Face | b-c Face |
|---|---|---|---|
| pure Co | none | red-violet | blue |
| | a | red-violet | |
| | b | red-violet | red-violet |
| | c | | blue |
| Co-Mn | none | red | blue |
| | a | red | |
| | b | red | red |
| | c | | blue |
| Co-Ni | none | red | blue |
| | a | light red | |
| | b | dark red | dark red |
| | c | | blue |
| Co-Cu | none | dark red | green |
| | a | dark red | |
| | b | dark red | dark red |
| | c | | green |

such a structure dichroism seems to be a logical result. With the aid of an instrument pleochroism can be demonstrated for these salts which are actually orthorhombic in symmetry.

If the polarizer is removed, the color of the b-c face should be red-violet, the resulting combination of red and blue. This is not the case. The b-c planes of the pure Co and the Mn-Co mixed salt are both blue when viewed either in c-polarized light or unpolarized light. This is not normal dichroic behavior. The Cu-Co salt shows the same anomalous persistence of the color green in its b-c plane. In the section on the spectra of these compounds which follows, it is noted that the red absorption bands are indeed present in the unpolarized spectra. It seems that the red color along the b axis is not intense enough to mask or even to mix appreciably with the blue color of the c axis. This problem is discussed in detail below.

The Co-Ni crystals are visibly pleochroic without the aid of an instrument. With polarized light propagating perpendicular to the a-b plane, two shades of red are observed. This is readily apparent if two crystals with this orientation are placed at right angles to one another as in Figure 26. The crystal with its b axis parallel to $\vec{E}$ is dark red whereas the crystal with its a axis parallel to $\vec{E}$ is a much lighter red. In addition, if the polarizer is rotated, one red fades and the other darkens, until at 45° the two shades of red appear identical. This same effect is seen in the b-c face of a crystal with the colors dark red and blue; at 45° both crystals appear purple. With these crystals it is difficult to be certain that the red is actually dark red due to orientation, because the crystals tend to be

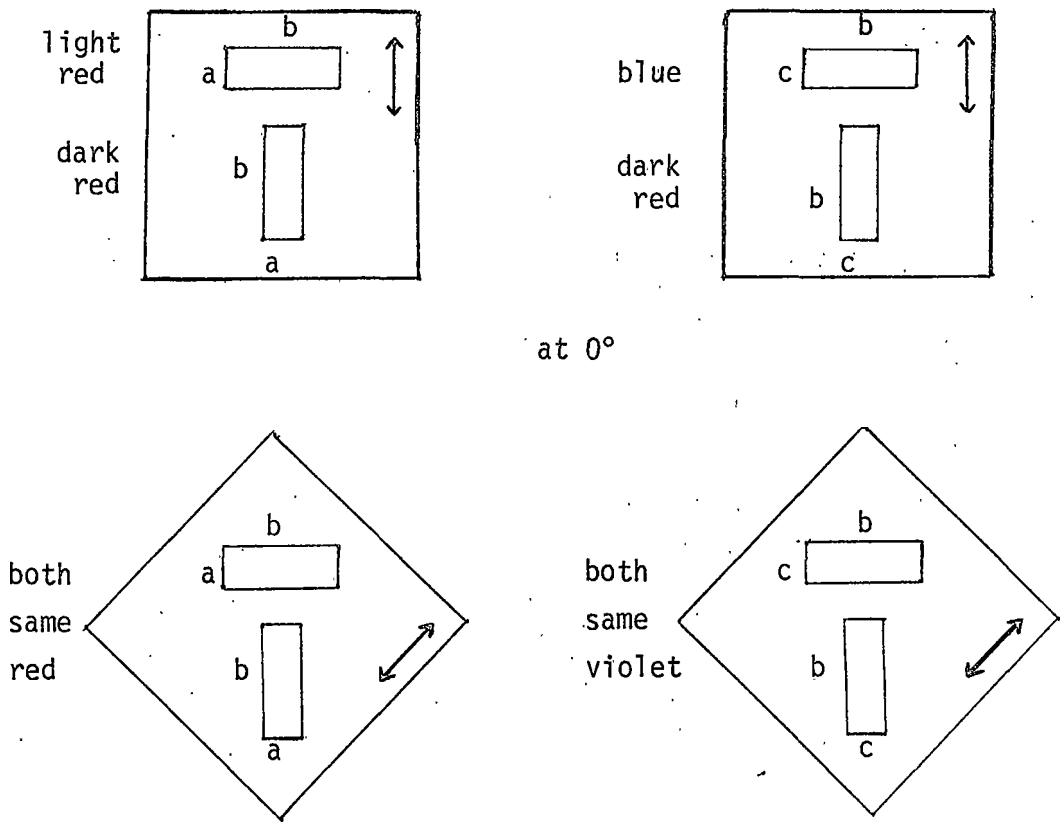


Figure 26 Colors Observed in Co-Ni Crystals in Polarized Light

thicker along c than along a which will also deepen the color observed. However, symmetry requires this red to be the dark red observed in the a-b face. With three different colors visible depending on orientation, this system is a classic case of pleochroism.

In unpolarized light the blue color again persists. Spectral data indicate that two different reds ought to be distinguishable, but unpolarized spectra do not show only blue peaks for the b-c plane.

The subseries containing Mn also exhibits these phenomena; the colors are tabulated in Table XI. Both the Mn and Mn-Ni analogs are pink in a-polarized light and clear in c-polarized light. In b-polarized light the pure Mn crystal remains clear, but the Mn-Ni mixed metal crystal appears yellow. The latter is thus visibly pleochroic as is the Co-Ni analog. However, it is extremely difficult to distinguish between the yellow and clear orientations unless the crystals are about five millimeters thick or there are crystals the same size with which to compare colors. The same technique used to separate the two reds in the Co-Ni case can be applied to this system.

The Mn-Cu analog is dichroic in the true sense of the word as the mineralogist uses the term. Two colors are visible in polarized light; amber in a- or b-polarized light and green in c-polarized light. In unpolarized light the color observed is a mixture of the two seen in the two polarized directions. This may also be true of the Mn and Mn-Ni salts, but it is impossible to tell visually because one of the "colors" involved is transparent.

The optical spectra, particularly in the visible region, of species with transition metal ions are generally described in terms of d-d

Table XI

Colors Exhibited by $TMAMn_xM'_{1-x}Cl_3 \cdot 2H_2O$ Crystals

| Crystal | Polarization | a-b Face | b-c Face |
|---|---|---|---|
| pure Mn | none | pink | clear |
| | a | pink | |
| | b | clear | clear |
| | c | | clear |
| Mn-Fe | none | pink | clear |
| | a | pink | |
| | b | clear | clear |
| | c | | clear |
| Mn-Ni | none | pink | yellow |
| | a | pink | |
| | b | yellow | yellow |
| | c | | clear |
| Mn-Cu | none | amber | amber |
| | a | lt amber | |
| | b | dk amber | dk amber |
| | c | | green |

transitions which have energies on the order of $10^4$ $cm^{-1}$. The intensities of peaks due to d-d transitions are weak as a consequence of their violation of the selection rule, $\Delta l = \pm 1$ ; in complexes which contain high spin Mn(II) these transitions are spin forbidden as well. In the high energy visible and UV regions these d-d peaks may be hidden by the more intense chloride to metal charge transfer bands.

Three different approaches have been utilized to explain the observed spectra of transition metal complexes; these are crystal field theory, CFT, ligand field theory, LFT, and molecular orbital theory, MOT. The first assumes that the central metal ion and all surrounding ions are point charges which undergo purely electrostatic interactions; no overlap of orbitals is allowed to occur. LFT is a refinement on this and allows some interaction or overlapping of orbitals to occur between the metal and neighboring atoms. In the last approach the atomic orbitals of the ligands and the metal interact to form molecular orbitals which may be constructed by group theoretical methods so as to attain maximum overlap.

Because of the nature of the metal ions and ligands involved in this work, CFT was selected as the best approach to explain the observed spectra. Whatever approach is used, the interpretation of the spectra requires some knowledge of the initial and final states of the system. The total energy of a normalized wavefunction is expressed by Equation 5:

$$E = \int \psi^* \hat{H} \psi \, d\tau = \langle \psi | \hat{H} | \psi \rangle \qquad (5)$$

The Hamiltonian operator, $\hat{H}$, for a many electron wavefunction which could be used to describe a transition metal ion is a sum of several

terms:

$$\hat{H} = -\frac{\hbar^2}{2m} \Sigma \nabla_i^2 - \Sigma \frac{Ze^2}{r_i} + \sum_{i>j} \frac{e^2}{r_{ij}} + \Sigma V_i \qquad (6)$$

$$= \hat{H}^\circ + \Sigma V_i \qquad (7)$$

The first three terms are the kinetic energy of the electrons, the coulombic attraction between the nucleus and the electrons and the interelectronic repulsions, respectively. Because these terms are identical for ions with a 3d subshell, they may be collected and defined as $\hat{H}^\circ$. CFT defines $V_i$ as the potential field introduced by a particular environment such as octahedral, $V_{oct}$, or tetragonal, $V_{tet}$. In the metal complexes considered here, $V_i$ is small compared to the electron-electron repulsion term, and may thus be treated as a perturbation of $\hat{H}^\circ$. To determine the relative energy level splitting of the d orbitals in various complexes only the effect of $V_i$ need be considered.

The methods of group theory (28-30) provide a powerful tool in the analysis of spectra without recourse to the tedious computations which solving Equation 5 entails. Symmetry operator commute with the Hamiltonian; if the direct product of the characters of the terms in any integral of the form $\langle\psi|\hat{O}|\psi\rangle$ where $\hat{O}$ is an operator does not contain the totally symmetric representation, the integral has a value of zero. Use of the symmetry of a complex and the character table for its associated point group yields a great deal of information about the possible transitions which may be observed.

The five d orbitals of the transition metal ions may be chosen as a basis set; these are all degenerate in the free ion in spherical symmetry. If the metal ion is surrounded by ligands, the five-fold

degeneracy is removed in a way which depends on the symmetry of the complex. When six identical ligands are coordinated in octahedral symmetry, the point group for the complex is $O_h$. In $O_h$ symmetry the five degenerate d orbitals are split into two energy levels designated $e_g$ and $t_{2g}$ which contain the $z^2$, $x^2-y^2$ and xy, xz, yz d orbitals respectively. If two axial ligands are removed or replaced, the symmetry of the complex is lowered to $D_{4h}$. In this environment all degeneracy is removed from the octahedral $e_g$ level; it splits into an $a_{1g}(d_z2)$ and a $b_{1g}$ $(d_x2-y2)$. The $t_{2g}$ level becomes a $b_{2g}(d_{xy})$ and a doubly degenerate $e_g(d_{xz}$ and $d_{yz})$. If the symmetry is lowered further to the $D_{2h}$ point group, all degeneracy is removed so that each d orbital has its own associated energy level and is described by a one-dimensional representation from this group. These splitting patterns are shown in Figure 27.

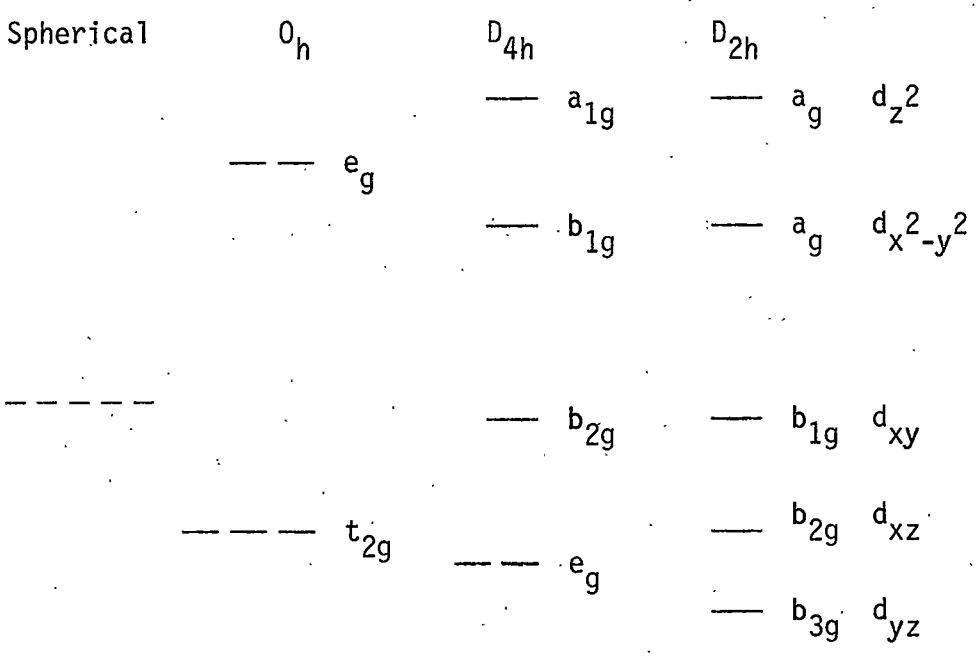


Figure 27 Splitting of the d Orbitals in Various Symmetries

All of the above splitting assignments may be obtained directly from the appropriate point group or can be derived by performing the operations of the point group on the individual d orbitals and comparing the resulting representations with those of the group.

Group theory indicates the possible energy levels, but does not enable one to establish the extent of the splitting and thus the relative energies of the resulting levels. This splitting may be determined without actually solving Equation 5 in part by the location of the ligands with respect to the lobes of the d orbitals, but is also dependent on the nature of the ligands involved. Ligands are described as weak or strong field based on the magnitude of the splitting which they induce between energy levels; the octahedral splitting between $e_g$ and $t_{2g}$ is defined as $\Delta$ or 10Dq. Complexes containing weak field ligands generally possess high spin, because less energy is required to occupy the higher orbital than to pair spins in the lower one.

In the crystals involved in this work the metal ions are octahedrally coordinated, $MCl_4(H_2O)_2$, but with water molecules occupying the axial sites, the local metal ion symmetry is actually $D_{4h}$. Both water and the chloride anion are designated as weak field ligands. This suggests that the splittings which arise due to $D_{4h}$ symmetry are small compared to 10Dq. If this is true, the potential term in the Hamiltonian due to the presence of a tetragonal field, $V_{tet}$, may be treated as a perturbation of the octahedral case. With this assumption one can construct an energy level diagram for a complex in $O_h$ symmetry and subsequently apply group theoretical methods to determine the possible splitting patterns in lower symmetries.

Before transitions can be assigned, the ground and excited states must be described in terms of the possible states for the various symmetries of interest. The ground state for the free metal ions may be determined according to Hund's Rule; in order to find all possible Russell-Saunders(R-S) terms for the excited states, a table of states indicating the number of determinants for each $M_L$-$M_S$ combination must be constructed. As an example, for the $d^2$ or $d^8$ ions in which two electrons or two holes, positrons, respectively, are placed in the five d orbitals with either of two spins, there are $C_{10}^2 = \frac{10!}{2!8!} = 45$ possible states. With the aid of an $M_L$-$M_S$ table these are resolved into five energy levels, the R-S terms $^1G$, $^3F$, $^1D$, $^3P$ and $^1S$. Of these five terms Hund's Rule designates $^3F$ as the ground state. Table XII summarizes the number of states and the term symbols for each configuration of the d orbitals. The ground state is listed first in each case.

By applying the symmetry operations of any point group to an orbital, one can determine its representations in that particular group. The difficulty of the calculation depends upon the orbital involved; operating on the d orbitals is a cumbersome task. Fortunately, there is a method which allows the representation of an orbital to be written knowing the characters of only the rotation symmetry operators. Using the transformation matrix for rotation by an angle, $\alpha$, the trace is given by Equation 8:

$$\chi(\alpha) = \sum_{n=0}^{2l} e^{(l-n)i\alpha} = \frac{\sin (l+\frac{1}{2})\alpha}{\sin \frac{\alpha}{2}} \qquad (8)$$

When $\alpha = 0$, which corresponds to the identity operation, the trace is $2l + 1$. The reducible representation can thus be found in any symmetry

Table XII

Russell-Saunders Term for Free Ions

| Configuration | Term Symbols | Number of States |
|---|---|---|
| $d^1$ ($d^9$) | $^2D$ | 10 |
| $d^2$ ($d^8$) | $^3F$, $^1G$, $^1D$, $^3P$, $^1S$ | 45 |
| $d^3$ ($d^7$) | $^4F$, $^2F$, $^2H$, $^2G$, $^2D$, $^4P$, $^2P$ | 120 |
| $d^4$ ($d^6$) | $^5D$, $^3D$, $2x^1D$, $^1I$, $^3H$, $^3G$, $2x^1G$, $2x^3F$, $^1F$, $2x^3P$, $2x^1S$ | 210 |
| $d^5$ | $^6S$, $^2S$, $^2I$, $^2H$, $^4G$, $2x^2G$, $^4F$, $2x^2F$, $^4D$, $3x^2D$, $^4P$, $^2P$ | 252 |

for any orbital by calculating the character of the various rotations from Equation 8. The states described by the irreducible representations are designated g if they possess a center of inversion, u if they change sign upon inversion.

The matrix above is derived from $e^{im\phi}$, where the quantum number, m, may take on 2l + 1 values for the orbital involved. Similarly, the wavefunction for a R-S term may be expressed as $e^{iM\phi}$, where M may have 2L + 1 values. This correspondence enables one to use the symmetry of the orbitals to define the states into which the analogous R-S terms are

split in various environments. These representations are tabulated for $O_h$, $D_{4h}$ and $D_{2h}$ symmetries in Table XIII.

In the $d^2$ example, which is equivalent to $d^8$, the $^3F$ ground state of the free ion will split into $A_{2g} + B_{1g} + B_{2g} + 2E_g$ in a tetragonal field. Although the f orbitals are antisymmetric, the basis set of d orbitals is symmetric; therefore, regardless of the spin orbit coupling introduced by F, the overall symmetry of the electronic wavefunction must retain its g character for any d configuration. It is again pointed out that group theoretical calculations only indicate which energy levels may be present in a given environment; these predictions reveal nothing about the relative splitting.

As a general rule the R-S terms of excited states are ranked in energy according to angular momentum, L, and spin multiplicity, 2S + 1; the greater the value of L or S, the lower in energy the term. However, there are many exceptions to this rule. The relative energies of the excited states of the free ions may be taken from the ordinate of a Tanabe-Sugano (T-S) diagram. The energy states arising from the splitting of the R-S terms, previously obtained from the character tables by group theory methods, may also be taken directly from T-S diagrams for ions in an octahedral, $O_h$, field. Since both $D_{4h}$ and $D_{2h}$ symmetries are treated as perturbations of the octahedral environment of a metal ion, the weak field splitting of $O_h$ serves as a reasonable starting point in the determination of the possible transitions of these lower symmetries. Reference to appropriate T-S diagrams provides a valuable piece of additional data, the ground state in $O_h$, a result unattainable from group theory alone. If the ground state in $O_h$ is a

Table XIII

Splitting of Russell Saunders Terms in Various Symmetries

| Term | $O_h$ | $D_{4h}$ | $D_{2h}$ |
|---|---|---|---|
| S | $A_{1g}$ | $A_{1g}$ | $A_g$ |
| P | $T_{1u}$ | $A_{2u} + E_u$ | $B_{1u} + B_{2u} + B_{3u}$ |
| D | $E_g + T_{2g}$ | $A_{1g} + B_{1g} + B_{2g} + E_g$ | $2A_g + B_{1g} + B_{2g} + B_{3g}$ |
| F | $A_{2u} + T_{1u} + T_{2u}$ | $A_{2u} + B_{1u} + B_{2u} + 2E_u$ | $A_u + 2B_{1u} + 2B_{2u} + 2B_{3u}$ |
| G | $A_{1g} + E_g + T_{1g} + T_{2g}$ | $2A_{1g} + A_{2g} + B_{1g} + B_{2g} + 2E_g$ | $3A_g + 2B_{1g} + 2B_{2g} + 2B_{3g}$ |
| H | $E_u + 2T_{1u} + T_{2u}$ | $A_{1u} + 2A_{2u} + B_{1u} + B_{2u} + 3E_u$ | $2A_u + 3B_{1u} + 3B_{2u} + 3B_{3u}$ |
| I | $A_{1g} + A_{2g} + E_g + T_{1g} + 2T_{2g}$ | $2A_{1g} + A_{2g} + 2B_{1g} + 2B_{2g} + 3E_g$ | $4A_g + 3B_{1g} + 3B_{2g} + 3B_{3g}$ |

one-dimensional representation, symmetry considerations allow the ground state to be specified in $D_{4h}$ and $D_{2h}$ also. Some ambiguity arises if the octahedral ground state is multi-dimensional. For example, a $T_{1g}$ state splits into an $A_{2g} + E_g$ in $D_{4h}$, either of which may be the new ground state. Table XIV lists the ground states possible for $d^5$ - $d^8$ configurations.

Table XIV

Ground States in Various Symmetries

| | Term | $O_h$ | $D_{4h}$ | $D_{2h}$ |
|---|---|---|---|---|
| $d^5$ | $^6S$ | $A_{1g}$ | $A_{1g}$ | $A_g$ |
| $d^6$ | $^5D$ | $T_{2g}$ | $B_{2g}$ or $E_g$ | $B_{1g}$, $B_{2g}$ or $B_{3g}$ |
| $d^7$ | $^4F$ | $T_{1g}$ | $A_{2g}$ or $E_g$ | $B_{1g}$, $B_{2g}$ or $B_{3g}$ |
| $d^8$ | $^3F$ | $A_{2g}$ | $B_{1g}$ | $A_g$ |

Observed spectral bands for transition metal species in the visible region are generally produced by electric dipole transitions. Whether or not a given transition is allowed in a free ion can be determined by the parity of the integral $\langle\psi_e'|\hat{M}|\psi_e\rangle$ where the symmetries of $\psi_e$ and $\psi_e'$ are those of the ground and excited electronic states. The value of this integral is defined as the transition moment, and $\hat{M}$ is the dipole moment operator.

$$\hat{M} \propto \Sigma e_i \vec{r}_i \tag{9}$$

$$\text{where } r = x\vec{i} + y\vec{j} + z\vec{k} \tag{10}$$

The symmetry of the operator is that of the x, y and z coordinates; the representations for the components of the operator will therefore always be odd. Table XV lists these representations as found in the character tables for $O_h$, $D_{4h}$ and $D_{2h}$. If $\psi_e$ and $\psi_e'$ are both even functions, as they must be arising from d orbitals, this integral will be odd and will vanish. As mentioned earlier, d-d transitions are parity forbidden.

Table XV

Representations of the Dipole Moment Operator

| $O_h$ | $D_{4h}$ | $D_{2h}$ |
|---|---|---|
| $T_{1u}$ (x, y, z) | $E_u$ (x, y) | $B_{1u}$ (z) |
| | $A_{2u}$ (z) | $B_{2u}$ (y) |
| | | $B_{3u}$ (x) |

Magnetic dipole transitions may also be observed, but are usually much less intense than electric dipole transitions. If only the electronic wavefunction is considered, an allowed electric dipole transition is about $10^3$ times as intense as an allowed magnetic dipole transition. The magnetic dipole moment operator has the symmetry of the cross product, $\vec{r} \times \vec{p}$, and transforms as the rotational representations, $R_x$, $R_y$ or $R_z$ of the point group in question. Because these representations possess g symmetry, magnetic dipole transitions are parity allowed for

d-d transitions. The integral which must be considered to determine whether the magnetic dipole transitions are symmetry allowed is $\langle\psi_e'|\hat{R}|\psi_e\rangle$. The direct product is found in the same way as for electric dipole transitions and must still contain the totally symmetric representation for an allowed transition to occur.

Utilization of the symmetry of the electric dipole moment operator to determine whether or not a transition is allowed assumes that the electronic wavefunction, $\psi_e$, is completely independent of the vibrational wavefunction, $\psi_v$. When the ion is in a crystal, vibration of the atoms may momentarily destroy the g character of $\psi_e$ in the local site symmetry. Such interaction between $\psi_e$ and $\psi_v$ is called vibronic coupling. An expanded integral can now be written, $\langle\psi_e'\psi_v'|\hat{M}|\psi_v\psi_e\rangle$, to describe the transition moment. If this integral is nonzero, the transition is vibronically allowed. The spectral bands which arise from such transitions are on the order of $10^3$ times weaker than those which are symmetry and parity allowed for pure electronic transitions.

The introduction of vibronic coupling implies that the direct product of the characters of five representations must be calculated to determine whether or not the integral vanishes. This can be simplified to some extent. Since $\psi_v$ is totally symmetric in the ground state, multiplying by its representation will not change anything, and it need not be considered. Also, any representation multiplied by itself must contain the totally symmetric representation. Therefore, if one of the representations spanned by the direct product of $\psi_e' \hat{M} \psi_e$ is also one of the odd normal modes of vibration of the excited state, $\psi_v^o$, the integral will be nonzero. For all nonlinear complexes, 3N - 6

vibrational modes exist, where N is the number of atoms in the complex; in octahedral coordination N = 7, giving rise to 15 modes. Their representations are determined by assigning normal coordinates to each atom and observing how they transform under the symmetry operations of the point group in question. Each character is a sum of 21 terms, most of which fortunately turn out to be zero. For example, in $D_{2h}$ the first operation other than E is $C_2(z)$. If a $ML_6$ molecule is rotated 180° about the z axis, four atoms change positions, thus contributing nothing to the trace. This rotation is shown in Figure 28 where z is defined by the M-$L_1$ bond.

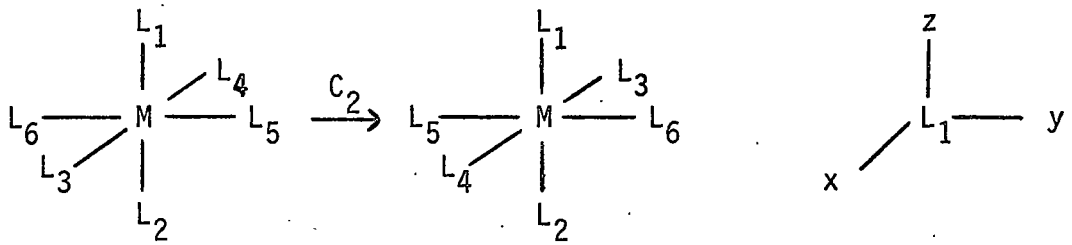


Figure 28 $C_2$ Rotation in Normal Coordinates

The three atoms which lie along the rotation axis do not move; their coordinates transform according to the following matrix. The prime indicates the coordinates after the rotation operation.

| | $X_1$ | $Y_1$ | $Z_1$ |
|---|---|---|---|
| $X_1'$ | -1 | 0 | 0 |
| $Y_1'$ | 0 | -1 | 0 |
| $Z_1'$ | 0 | 0 | 1 |

The coordinate axis, Z, which is also the rotation axis, is unchanged by the operation, but X and Y become -X and -Y. This occurs for three atoms so the trace is -3 for the $C_2(z)$ operation in $D_{2h}$. This process is continued for each operation in the point group. The resulting representation is reduced and the terms due to translation and rotation are removed. The remaining terms are the irreducible representations of the normal modes of vibration of the complex. These are tabulated for $O_h$, $D_{4h}$ and $D_{2h}$ symmetries in Table XVI.

Table XVI

Normal Modes of Vibration

| | |
|---|---|
| $O_h$ | $A_{1g} + E_g + 2T_{1u} + T_{2g} + T_{2u}$ |
| $D_{4h}$ | $2A_{1g} + B_{1g} + B_{2g} + E_g + 2A_{2u} + B_{2u} + 3E_u$ |
| $D_{2h}$ | $3A_g + B_{1g} + B_{2g} + B_{3g} + 3B_{1u} + 3B_{2u} + 3B_{3u}$ |

The transition moment integral will also vanish if the initial and final states do not possess the same spin; this is the selection rule $\Delta S = 0$. The electronic wavefunction may be written as the product of orbital and spin components, $\psi_e = \psi_o\psi_s$. Since the dipole moment operator does not involve spin, the integral may be written:

$$\langle\psi_o'|\hat{M}|\psi_o\rangle \langle\psi_s'|\psi_s\rangle \qquad (11)$$

Orthogonality requires the second integral to be zero, if the spin wavefunctions of the excited and ground states differ.

With the symmetry and splitting information contained in Tables

XII through XVI, one can determine whether a particular transition is allowed or forbidden in the geometry described by a given point group. Ligand coordination for the complexes of the series investigated in this work suggests that $D_{4h}$ is the highest possible symmetry for the local sites. Pleochroism and polarization data indicate that an even lower symmetry, $D_{2h}$, best describes the metal environment. T-S diagrams provide the relative positions of energy levels for regular octahedral complexes only. To construct an energy level diagram for $D_{2h}$ complexes, one may either perform the tedious numerical calculations required to find the sign and magnitude of the splitting, or one may assume that the further splitting of the octahedral levels in lower symmetry is small compared to that which occurs going from spherical to octahedral local site symmetry. Since SCF computations of open shell configurations are beyond the scope of this investigation, the latter assumption is made.

In the complexes in question the transition moment operator, $T_{1u}$ in $O_h$, indicates that all the transitions are allowed. In $D_{4h}$ all of the transitions are allowed in $\underline{x}$- or $\underline{y}$-polarized light, while some are forbidden in $\underline{z}$-polarized light. This pattern allows for dichroism, but not pleochroism. Only in $D_{2h}$ symmetry do the three components of of the transition moment operator transform as three different representations, and thus permit three different spectra.

A large number of workers have published crystal spectra of the divalent ions of Mn, Fe, Co, Ni and Cu in various environments, but very little information correlating polarization and pleochroic effects appears in the literature. In addition most of the spectral

assignments are made utilizing octahedral or square planar symmetry, an assumption which does not allow for the pleochroism so strikingly evident in the mixed metal crystals of the $TMAM_xM'_{1-x}Cl_3 \cdot 2H_2O$ series. Even when polarized spectra were taken in many cases a single crystal face, that produced by the growth habit, was utilized. Crystals which grow with faces aligned along either a vibration direction or a unit cell axis are not common; therefore, many of these polarized crystal spectra remain unresolved. No system reported in the literature offers the simplicity of orthorhombic symmetry coupled with the wide variation in color demonstrated by the metal ions in this series.

Energy level diagrams for the following spectral discussions are based on literature data wherever possible; in most cases the symmetry has been lowered and splitting assignments have been made to best fit the observed polarized spectra. The spectra are discussed in the following order: Mn(II) ion (31-36), Co(II) ion (34-41), Fe(II) ion (42-46), Ni(II) ion (47-51) and Cu(II) ion (52-61).

## MANGANESE SPECTRA

The first spectra to be examined in detail are those of the pure Mn crystal $TMAMnCl_3 \cdot 2H_2O$. For a complex containing high spin Mn(II) all transitions are spin forbidden as well as parity forbidden, if only the electronic wavefunction is considered. The parity restriction may be removed by invoking vibronic coupling, but because these transitions are still spin forbidden, the observed peaks should be narrow and relatively weak in intensity. The ground state, $^6S$ in R-S notation, is a half-filled subshell which transforms as the totally symmetric representation in any point group. The transitions to excited states require the pairing of two electrons; these excited states are the quartet terms G, D, P and F listed in order of increasing energy. This ordering is obtained from the T-S diagram which was constructed by utilizing SCF methods. With reference to a T-S diagram and the information in Table XIII an energy level diagram for the visible spectra of weak field Mn(II) complexes in $D_{2h}$ symmetry may now be constructed. This is shown in Figure 29.

For high spin Mn(II) complexes the ground state is $A_g$ in $D_{2h}$, so only the characters of the operator and the excited electronic state need be considered to determine whether or not a given transition is vibronically allowed. T-S diagrams show that the lowest excited energy level for Mn(II) in $O_h$ symmetry is $T_{1g}$ which splits into $B_{1g} + B_{2g} + B_{3g}$ in $D_{2h}$ as shown in Table XIII. If $\underline{x}$-polarized light is used to excite the complex, the transition moment integrals are $\langle B_{1g}|B_{3u}|A_g\rangle$, $\langle B_{2g}|B_{3u}|A_g\rangle$ and $\langle B_{3g}|B_{3u}|A_g\rangle$ for electric dipole transitions to these excited states. The direct products are $B_{2u}$, $B_{1u}$ and $A_u$ respectively.

Because $A_u$ is not one of the normal modes of vibration in $D_{2h}$, the latter transition is vibronically forbidden. A peak corresponding to this transition and visible in y- or z-polarized light would disappear in x-polarized light. Calculations similar to those above have been performed for the possible transitions in all polarizations which would give rise to peaks in the near IR and visible regions of the spectra for Mn(II) complexes of $D_{2h}$ symmetry. The results indicate one forbidden transition for each polarization direction:

$$A_g \rightarrow B_{3g} \text{ in } x\text{-polarized light}$$
$$A_g \rightarrow B_{2g} \text{ in } y\text{-polarized light}$$
$$A_g \rightarrow B_{1g} \text{ in } z\text{-polarized light}$$

All other transitions are vibronically allowed and should show no polarization effects.

The problem of relative ordering of the energy levels giving rise to these peaks now becomes important. Group theory provides no information on the magnitude of the splitting and SCF methods have not been applied in $D_{2h}$ symmetry for these complexes. The energy levels were therefore ranked arbitrarily so as to yield the best correlation of the observed peaks and their polarizations with the predictions of group theory. For the spectra of the TMA salts which contain Mn(II) it was necessary to invoke rather large splittings in two cases to account for the experimental observations. With this assumption, however, the Mn(II) spectra can be satisfactorily explained with the exception of a very weak band at 460 nm. This band was ultimately assigned as a magnetic dipole transition. The transition assignments for the observed peaks in order of increasing energy are discussed in detail below.

Figures 5-14 display the polarized spectra of the Mn containing crystals; Figure 5 specifically contains the polarized spectra from crystals of the pure salt, $TMAMnCl_3 \cdot 2H_2O$. The following discussion is limited to those peaks due to the Mn(II) ion. The lowest energy peak seen consistently in all crystals occurs as a broad band with a maximum at 530 nm; evidence exists in some crystals of another smaller peak at about 580 nm. The crystals in which this peak appears are of very high quality and thus it is treated here as a real peak. In light of various polarizations the band at 530 nm shows definite changes in shape, the most dramatic of which is a very large decrease in intensity in y-polarized light. In x-polarized light this band is most intense while the band at 580 nm has totally disappeared. Two peaks are observed in both y- and z-polarized light; their intensities are greater in z-polarized light, although not as large as the 530 nm peak in x-polarized light. Inspection of Figure 5 suggests that the relative ordering of these energy levels arising from the octahedral $T_{1g}$ level should be $B_{3g} < B_{1g} < B_{2g}$; this best fits the observed polarization effects as is shown in the energy level diagram for Mn(II) in Figure 29 on the following page. It is logical to assign the $A_g \rightarrow B_{3g}$ transition to the peak at 580 nm which disappears in x-polarized light, as it should based on group theoretical predictions. The band centered around 530 nm can reasonably be $B_{1g} + B_{2g}$ as it has maximum intensity in x-polarized light where both transitions are allowed. The $A_g \rightarrow B_{2g}$ transition seems to be stronger than the $A_g \rightarrow B_{1g}$ transition, because this band is more intense in z-polarized light than in y-polarized light. However, due to variations in crystal thickness and scattering as the

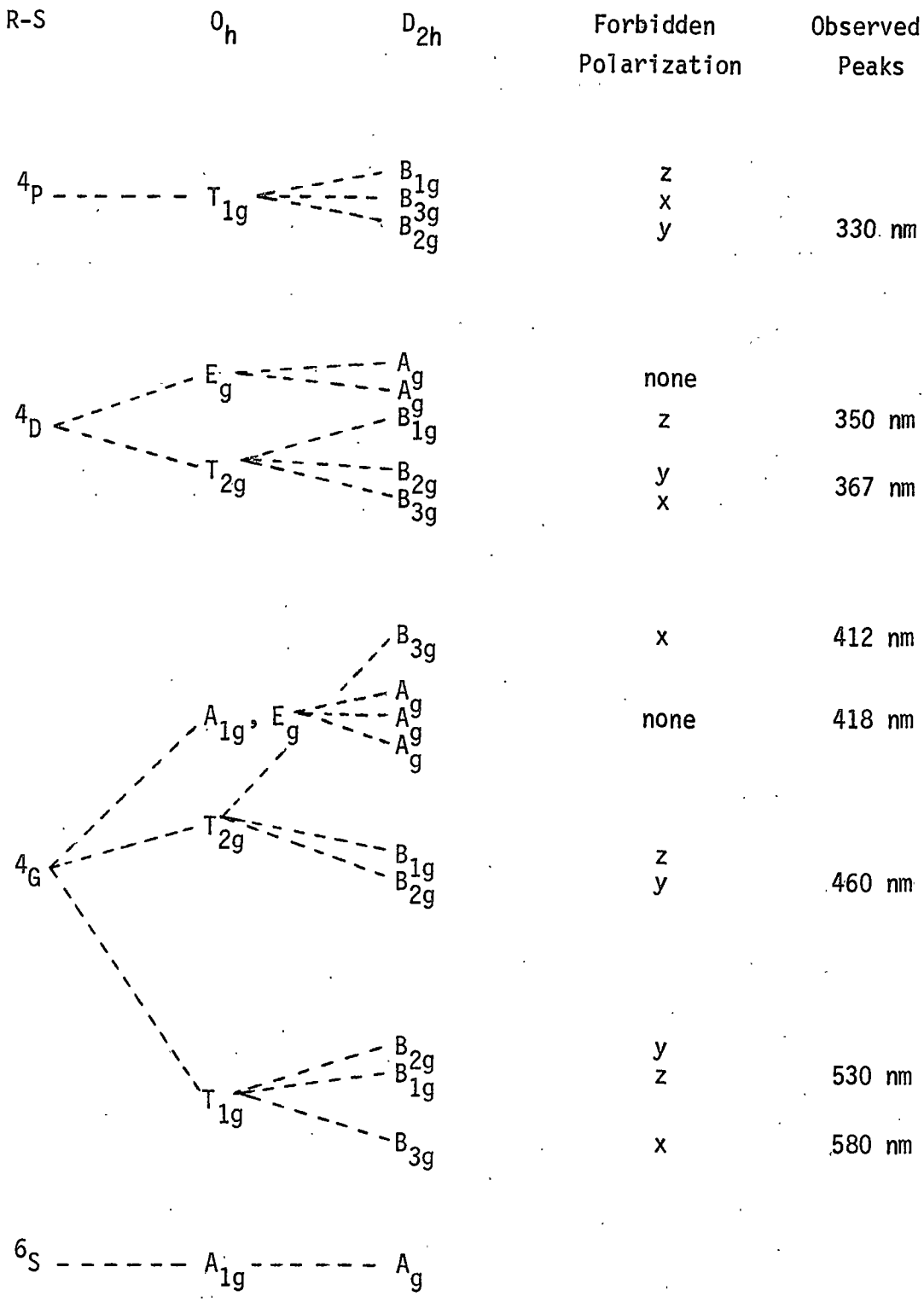


Figure 29 Mn(II) Spectral Transitions

crystal is rotated to obtain all three polarization directions, intensity is not very conclusive evidence for the latter statement.

The peak at 460 nm cannot be assigned solely as an electric dipole transition. It is visible in y-polarized light, disappears in z-polarized light and is barely visible in x-polarized light. There are two transitions which should occur in this region, $A_g \rightarrow B_{1g}$ and $A_g \rightarrow B_{2g}$; the former is forbidden in z-polarized for an electric dipole transition, allowed for a magnetic dipole transition. Since no peak appears in z- polarized light, the weak peak at 460 nm visible in x-polarized light is assigned as the $A_g \rightarrow B_{1g}$ electric dipole transition. This extremely weak transition is lost under the larger peak present in y-polarized light. The behavior of this larger peak suggests that $A_g \rightarrow B_{2g}$ may be a magnetic dipole transition. The operator symmetry for these transitions is even and magnetic dipole transitions are allowed in just those polarizations in which electric dipole transitions are forbidden. This implies that $A_g \rightarrow B_{2g}$ is allowed only in y-polarized light which fits the observed spectra.

Two distinct peaks which behave quite differently in polarized light occur at 412 nm and 418 nm. In x-polarized light the very sharp peak at 412 nm disappears completely; the broader, less intense peak at 418 nm displays no definitive change in any polarization. If a large splitting of the $T_{2g}(^4G)$ energy level occurs, the transition $A_g \rightarrow B_{3g}$ could be the source of the peak at 412 nm; this leaves the $A_g \rightarrow B_{2g}$ transition at lower energy which corresponds with the peak at 460 nm. The three $A_g$ levels arising from $E_g$ and $A_{1g}(^4G)$ could yield the unpolarized peak at 418 nm, and this peak is broad enough to

suggest that there may be more than one transition under the envelope.

A similar large splitting of the $T_{2g}(^4D)$ is required to account for the polarization of the peaks at 367 nm and 350 nm. Again the $A_g$ levels from $E_g(^4D)$ should give rise to an unpolarized peak, but superimposed on this peak at 350 nm is the $A_g \rightarrow B_{1g}$ transition. This peak is drastically reduced in intensity in z-polarized light, but does not completely disappear, presumably because of the presence of the unpolarized $A_g \rightarrow A_g$ transitions.

At about 330 nm the highest energy peak in the spectral region is recorded. The slit on the Cary 14 reaches maximum aperture for useful spectra in this region; thus, this peak could conceivably be an instrument artifact. However, although not visible in all crystals, the peak is consistently at 330 nm when it is seen; it also disappears in y-polarized light. If it is indeed a viable transition, it may be assigned as the $A_g \rightarrow B_{2g}$ transition arising from the octahedral $T_{1g}(^4P)$.

Foster and Gill (31) have published unpolarized crystal spectra for several Mn(II) salts based on octahedral geometry. Although none of the crystals studied by these authors possess the same chromophore as $TMAMnCl_3 \cdot 2H_2O$, the energies reported for the observed peaks in the visible region agree quite well with those found in this work. Dingle, et. al., (33) have examined the polarized crystal spectra at low temperature of $[(CH_3)_4N]MnCl_3$; this hexagonal salt exhibits two different spectra as expected for a uniaxial crystal. Lawson (35) has reported crystal spectra of $MnCl_2 \cdot 2H_2O$. This monoclinic compound contains the same chromophore as the TMA salt. Because the transitions for the Mn(II) ion are spin forbidden, varying the ligand and geometry does not

result in a very large energy shift for the observed peaks. This makes correlation of the spectra a straightforward task. Table XVII lists the $MnCl_2 \cdot 2H_2O$ peaks along with those obtained in this work and also assigns polarizations to the transitions.

Table XVII

Location and Polarization of Mn(II) Peaks

| $MnCl_2 \cdot 2H_2O$ Peaks (nm) | $TMAMnCl_3 \cdot 2H_2O$ Peaks (nm) | Forbidden Polarization |
|---|---|---|
| 325 | 330 | y? |
| 348 | 350 | z |
| 367 | 367 | x, y |
| 373 | | |
| 412 | 412 | x |
| 416 | 418 | none |
| 466 | 460 | x, z |
| 525 | 530 | y, z |
| | 580 | x |

To account for the observed polarization of peaks in the TMA salt, a splitting of the $T_{2g}(^4G)$ energy level large enough to cause overlap with the $E_g(^4G)$ state had to be invoked. This assumption appears to be in accordance with the literature data. The major peaks of the spectra observed in this work are in excellent agreement with those of Lawson recorded for the same chromophore. This close agreement

implies that the original assumption of a small perturbation of the energy levels in octahedral symmetry to account for the splitting in $D_{2h}$ symmetry is a valid one. Although there are more possible transitions due to the decrease in symmetry, the splitting is small and broader peaks are usually seen rather than more peaks. In one instance a sharp new peak is introduced (that at 412 nm) which is a single, nondegenerate polarized transition; Gill has no evidence of this particular transition for the unpolarized spectra in octahedral symmetry. On the whole the predictions of group theory are borne out quite well by the observed polarized crystal spectra of the Mn(II) ion.

## COBALT SPECTRA

Of the first row transition metals utilized in this work, Mn(II) is the only ion for which the transitions are spin forbidden as well as parity forbidden; in the spectra of the Fe, Co, Ni and Cu salts the observed transitions are spin allowed. The peaks for these ions are thus broader and much more intense than those for Mn(II). In addition the near IR region must be scanned for these ions, because some of the lower energy peaks are seen there rather than in the visible region. In order to keep the peaks on scale for spectra of crystals containing the $d^6$ through $d^9$ ions, either very thin crystals or crystals with a very low mole fraction of these ions had to be selected. By grinding an extremely thin cross section of a crystal of $TMACoCl_3 \cdot 2H_2O$, polarized spectra were obtained for this pure salt in the same manner as for the Mn analog. The Mn-Co mixed crystals provided a much less intense spectrum for the Co(II) ion, although it was complicated by the presence of the Mn(II) ion. The higher energy peaks of the Mn spectrum are still visible and virtually unaffected, but the two lowest energy transitions are lost beneath the much larger peaks due to the Co ion.

Comparison of the spectra of the Mn, Mn-Co and Co analogs indicates that there is no interaction between the metal ions in these crystals; the Mn and Co individual spectra are simply additive. There is a marked loss of intensity in Mn and Co individual peaks in the spectra of the mixed metal crystals, but this is to be expected due to lower metal concentrations for both ions. The habit for the mixed metal crystals also made thinner crystals available for these spectra. Nevertheless, there is a good mapping of the Co peaks in the pure salt

to those found in the mixed crystal, if one ignores intensity differences which cannot be avoided. The peaks due to the $d^5$ ion also map, except for the two which are lost beneath the intense transitions of the Co ion. Because of the intensity differences between a spin allowed and spin forbidden transition, it is assumed that any polarization effects for the peaks in this region are due solely to the Co(II) ion.

The R-S ground state for Co(II), a $d^7$ ion, is $^4F$; in an octahedral field this splits into $A_{2g} + T_{2g} + T_{1g}$, the latter of which is the ground state as seen in T-S diagrams. When the degeneracy of the $T_{1g}$ level is removed by lowering the symmetry to $D_{2h}$, three new energy levels arise, $B_{1g} + B_{2g} + B_{3g}$, any of which could be the new ground state. Without access to SCF methods the actual ground state may be assigned by correlating the predicted transitions with the observed polarization data; for each ground state nine spin allowed transitions which may yield peaks in the visible or near IR regions must be considered. Group theoretical evaluation of the transition moment integrals and comparison with the polarized spectra in Figures 6-9 eliminate $B_{2g}$ as the ground state. Both $B_{1g}$ and $B_{3g}$ fit portions of the Co(II) spectra, but neither is satisfactory for the entire IR-visible range. Because identification of the ground state is crucial to the discussion of the $TMACoCl_3 \cdot 2H_2O$ spectra, previously published spectra of other Co(II) crystals were examined to establish a valid framework upon which to base transition assignments.

Several articles appear in the literature (34-41) which contain polarized crystal spectra of the Co(II) ion in an environment similar to

that found in the TMA salt. Ferguson and Wood have published low temperature data for $CoCl_2 \cdot 6H_2O$ (38) and $CoCl_2 \cdot 2H_2O$ (39). The dihydrate is of particular interest, because the chromophore in this compound, $CoCl_4(H_2O)_2$, is the same as that found in the TMA salt. An energy level diagram has been constructed for $D_{4h}$ symmetry based on the data for the hexahydrate which contains $Co(H_2O)_4Cl_2$ octahedra. However, neither the spectra of $CoCl_2 \cdot 2H_2O$ nor $TMACoCl_3 \cdot 2H_2O$ allows a reasonable interpretation of the polarization patterns in tetragonal symmetry. Ferguson and Wood have attempted to explain the IR spectra of the dihydrate as magnetic dipole transitions in $C_{2h}$ symmetry. Choice of ground state is again ambiguous, and regardless of the choice made, all of the observed peaks cannot be assigned.

For the TMA salts the electric dipole moment operator was originally chosen to describe the spectra because most peaks persisted in two polarizations; such behavior is typical of d-d vibronic transitions. In the Mn salt only one peak appeared which could not be assigned as an electric dipole transition. In the Co analog many of the peaks decrease in intensity in two polarizations, behavior indicative of magnetic dipole transitions. Another problem encountered in dealing with the Co(II) spectra is that not all of the possible transitions are seen in the TMA salt, making assignment of peaks a tentative process.

Because neither electric nor magnetic dipole transitions alone can account for the Co(II) spectra of these dihydrates, the question as to whether both could be present must be raised. The intensity of a symmetry allowed magnetic dipole transition is much weaker than that of a symmetry allowed electric dipole transition. However, in the solid

state where thermal vibrations are much weaker, one can imagine that an electric dipole transition which is parity forbidden and can be explained only by vibronic coupling, might actually be of the same order of intensity as the parity and symmetry allowed magnetic dipole transition. Thus, in these crystals one might reasonably expect a magnetic dipole transition to appear at room temperature and an electric dipole transition to persist at very low temperature. Work done in this lab at room temperature on several crystals containing Co(II) has yielded consistent spectra with well-defined peaks in the visible region, but good IR spectra have proven difficult to attain. Lacking low temperature data for the TMA salts, there is no evidence to distinguish between the two types of spectra in this work.

The argument presented above can be tested on spectra taken from the literature such as those reported by Ferguson and Wood (38,39). The energy level diagram for Co(II) in $D_{4h}$ symmetry is presented in Figure 30 along with possible splitting patterns if the symmetry is lowered to $D_{2h}$. Also included in this figure are the locations of peaks in the $CoCl_2 \cdot 2H_2O$ spectra and the polarizations calculated assuming that electric dipole transitions are involved. The relative ordering of the $D_{4h}$ energy levels, which establishes $A_{2g}$ as the ground state, is based on the spectral data of Ferguson and Wood for the hexahydrate, $CoCl_2 \cdot 6H_2O$. Explanation of the spectra of the dihydrate, $CoCl_2 \cdot 2H_2O$, requires a lower symmetry. The spectral measurements for the latter salt were made on crystals which were oriented with orthogonal axes, a', b and c where a' and b were defined by extinction directions. These axes correspond to a, c and b respectively in the

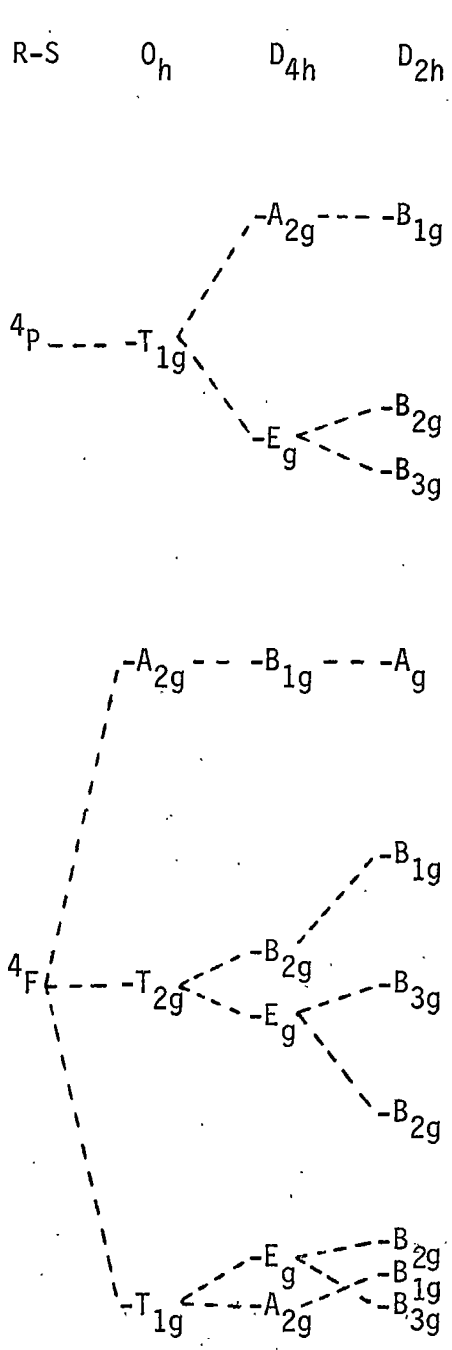


| Forbidden Polarization Calculated | $CoCl_2 \cdot 2H_2O$ Peaks (Ref. 39) | Forbidden Polarization Observed |
|---|---|---|
| y | 395 nm CT | y,z |
| z | 505 nm | z |
| none | | |
| x | 610 nm | x,y |
| y | 830 nm | y,x? |
| none | 1200 nm | none |
| z | 1630 nm | z |

Figure 30 Possible Energy Level Diagram for Co(II)

orthorhombic TMA salt. Careful comparison of actual polarization directions with respect to the Co octahedra indicates that, although $CoCl_2 \cdot 2H_2O$ is monoclinic, the visible spectra in all polarizations at 10 K are very similar to those in $TMACoCl_3 \cdot 2H_2O$ at room temperature; these compounds possess the same chromophore. The highest energy peak in the near IR also exhibits the same behavior in both salts. Such agreement demonstrates the validity of the assumption that the spectra of these two hydrates arise from the same energy level diagram. The near IR spectra obtained by Ferguson and Wood cannot be satisfactorily explained utilizing magnetic dipole transitions in $C_{2h}$ symmetry; in $\underline{x}$- and $\underline{y}$-polarized light two peaks are always visible in the observed spectra whereas only one is allowed based on group theoretical predictions.

In the IR spectra all of the peaks can be explained if they are assigned as electric dipole transitions utilizing $B_{3g}$ as the ground state in $D_{2h}$ symmetry. Unfortunately, this requires a rather arbitrary splitting of the $E_g$ energy level which arises from the $T_{2g}(^4F)$ term as can be seen in Figure 30. The transitions from $B_{3g}$ to $B_{1g}$ and $B_{2g}$ which arise from the same $T_{1g}$ term occur at such low energy that they are not seen in the near IR region. The lowest energy peak appears at 1630 nm in Ferguson's spectra and may be assigned as the transition $B_{3g} \rightarrow B_{2g}$ which disappears in $\underline{z}$-polarized light. The peak at 1200 nm which shows no polarization effects is assigned as the $B_{3g} \rightarrow B_{3g}$ transition. The remaining peak at 830 nm corresponds to the $B_{3g} \rightarrow B_{1g}$ transition which is forbidden in $\underline{y}$-polarized light, but this is an extremely weak transition in the $CoCl_2 \cdot 2H_2O$ spectra. In addition to the

unsatisfactory splitting of the $E_g$ and $B_{2g}$ levels from $D_{4h}$, this model suffers due to the total inapplicability of $B_{3g}$ as the ground state for any of the peaks in the visible region.

Selection of $B_{1g}$ as the ground state in $D_{2h}$ yields a more reasonable splitting arrangement as shown in Figure 31, but leaves the peak at 1630 nm which should be the $B_{1g} \rightarrow B_{2g}$ transition unexplained either as a magnetic or electric dipole transition. The $B_{1g} \rightarrow B_{1g}$ transition at 1200 nm is allowed in all polarizations as an electric dipole transition; it is forbidden in all polarizations as a magnetic dipole transition. The peak at 830 nm can be assigned as the $B_{1g} \rightarrow B_{3g}$ electric dipole transition which is forbidden in y-polarized light. It can also be assigned as a magnetic dipole transition, if one assumes that this peak has disappeared in the x-polarized spectrum. There is some justification for both of these arguments.

This second model has another advantage in that the $B_{1g}$ ground state can be used to interpret the polarization patterns of the peaks in the visible region as well. If splitting is small as symmetry is lowered from $D_{4h}$ to $D_{2h}$, one would expect $B_{1g}$ as the new ground state, because $A_{2g}$ transforms as $B_{1g}$. Although this is conjecture since the $E_g$ and $A_{2g}$ energy levels from $T_{1g}(^4F)$ cannot be located, it lends some additional credibility to the assignment of $B_{1g}$ as the ground state.

The disadvantage of the energy level diagram presented in Figure 31 is that the peaks in the spectra of the TMA salt must be described as magnetic dipole transitions. Explanation of the visible spectra also requires a transition, a broad band between 500 and 550 nm, which is very intense in x- and y-polarized light, but weak in z-polarized

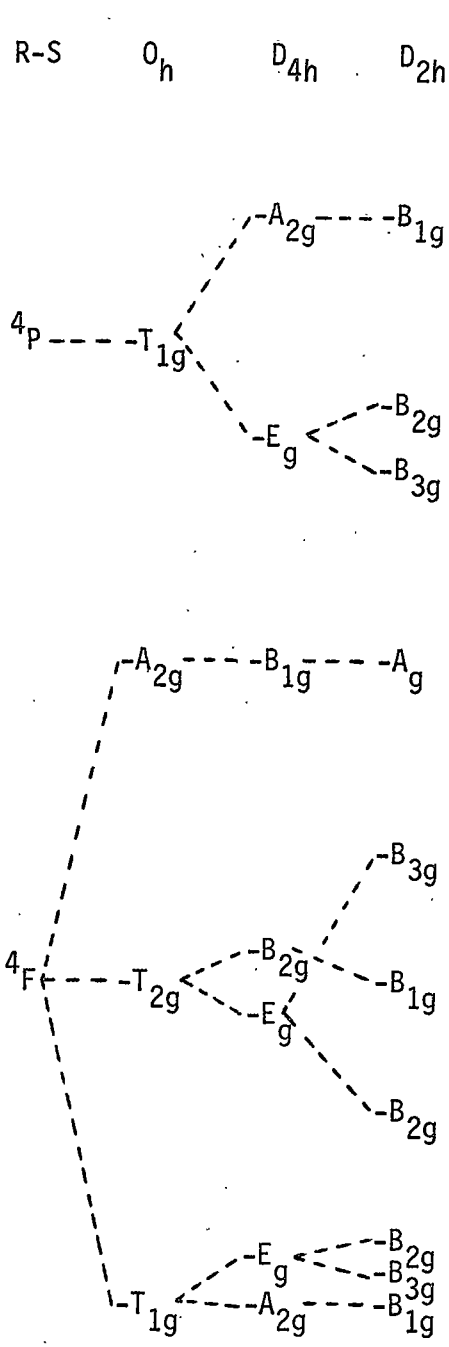


| Forbidden Polarization Calculated | $TMACoCl_3 \cdot 2H_2O$ Peaks | Forbidden Polarization Observed |
|---|---|---|
| none | 425 nm | ? |
| x | 515 nm | y,z |
| y | 545 nm | x,z |
| z | 610 nm | x,y |
| y | 830 nm | x,z |
| none | | |
| x | | |

Figure 31 Preferred Energy Level Diagram for Co(II)

light. Ferguson and Wood have designated this peak as an "anomalous" band; it will be discussed separately below.

On top of this broad band are two peaks which are assigned as magnetic dipole transitions; these two peaks at 515 and 545 nm represent the $B_{1g} \rightarrow B_{2g}$ and $B_{1g} \rightarrow B_{3g}$ transitions, respectively. The peak at 515 nm is allowed only in x-polarized light; that at 545 nm is allowed only in y-polarized light.

The peak at 610 nm is the lowest energy transition in the visible region; it is assigned as the $B_{1g} \rightarrow A_g$ transition allowed only in z-polarized light. This peak is located at the same wavelength and is polarized in the same way in both $TMACoCl_3 \cdot 2H_2O$ and $CoCl_2 \cdot 2H_2O$; the latter displays better resolution due to lower temperature.

The highest energy peak in the near IR occurs at 830 nm for both of these complexes as well and also behaves similarly in polarized light. In the $TMACoCl_3 \cdot 2H_2O$ this peak is seen only in y-polarized light; this corresponds to the $B_{1g} \rightarrow B_{3g}$ magnetic dipole moment transition. The remaining two IR peaks were never seen in the spectra of the TMA salt which were taken at room temperature.

The highest energy spin allowed magnetic dipole transition, $B_{1g} \rightarrow B_{1g}(^4P)$ is forbidden in all polarizations; such a peak does not appear in any of the Co(II) spectra. Ferguson and Wood report a charge transfer band at 395 nm which increases in intensity as temperature decreases; it is polarized perpendicular to the chain direction. This particular peak is not seen in the spectra of the TMA salt, but absorption is increasing as the slit opens beyond useful aperture in this region. A very weak peak appears at 425 nm in the $TMACoCl_3 \cdot 2H_2O$

spectra which is not seen in the $CoCl_2 \cdot 2H_2O$ spectra. Although it is most intense in z-polarized light, it is visible in x- and y-polarized light as well. This is the only peak which is not clearly visible in both the pure Co and the mixed Mn-Co spectra. Because of its low intensity in the pure salt, its absence in the mixed Mn-Co crystal would not be surprising. Nevertheless, if one examines the Mn-Co spectra carefully, there is some evidence of a shoulder on the Mn(II) 418 nm peak which may be this transition. This peak may be explained in two ways: as the $B_{1g} \rightarrow B_{1g}$ electric dipole transition or as a spin forbidden transition to one of the energy levels arising from the $^2G$ term which falls in this range as seen on the T-S diagrams. The intensity is very low for an electric dipole transition; thus, the latter interpretation is preferred.

Description of the Co(II) spectra in the TMA salt as magnetic dipole transitions leaves only one peak unexplained. This broad, intense band present in x- and y-polarized light almost completely disappears in z-polarized light. Although one would expect it to be an electric dipole transition, since it is present in two polarizations, no choice of ground state in either $D_{2h}$ or $D_{4h}$ symmetry can account for its polarization. Ferguson and Wood have described this peak as an "anomalous" crystal field band utilizing water vibrations to induce intensity for some of the doublet terms which are spin forbidden. Because of its intensity, it is difficult to accept this peak as a spin forbidden transition. The peak is well documented, appearing in all Co(II) spectra, but only in symmetry as low as $D_{2h}$ does its interpretation become a problem. It has always been described as the $T_{1g}(^4F)$ to

$T_{1g}(^4P)$ transition in octahedral geometry or the $A_{2g}$ to $E_g$ electric dipole transition in tetragonal geometry; without polarization data no conflict arises in terms of the energy level diagram. More spectral work needs to be done utilizing polarized light in complexes of lower symmetry in order to fully explain the origin of this peak.

## IRON SPECTRA

Crystals of the pure Fe and the pure Ni salts were never grown large enough for spectra to be recorded from them. However, precession photographs of these needle-like crystals indicate that they are also orthorhombic, isomorphic with the Mn analog. This information, coupled with the fact that the Mn-Co mixed metal spectra are simply the sum of the spectra of the individual pure salts, leads one to assume that the Fe(II) and Ni(II) spectra may also be extracted from the spectra of the corresponding mixed metal analogs. Crystals of the mixed Mn-Fe and Mn-Ni salts which are suitable for collection of spectral data are obtained fairly readily. Even though spin allowed transitions exist for these two ions, their spectra should be relatively simple, because there are fewer possible transitions.

The energy level diagram for Fe(II) is presented in Figure 32. The R-S ground state, $^5D$, splits into $E_g + T_{2g}$ in octahedral symmetry; the $T_{2g}$ level is the $O_h$ ground state. As in the case of the Co(II) ion, there is some ambiguity in designation of the ground state when the symmetry is lowered to $D_{2h}$; any of the three levels which arise from $T_{2g}$ may be the $D_{2h}$ ground state. The number of peaks observed in the polarized spectra of the Fe(II) salt depends a great deal upon the magnitude of the splitting of the energy levels in orthorhombic symmetry. If the splitting is small, only one peak may be visible. If the splitting of the energy levels from $E_g$ is large, one would expect two peaks, both ground state to $A_g$ transitions. If the splitting of the $T_{2g}$ level is also large, one could expect a maximum of four spin allowed transitions in the Fe(II) spectra. As in the Co(II) spectra,

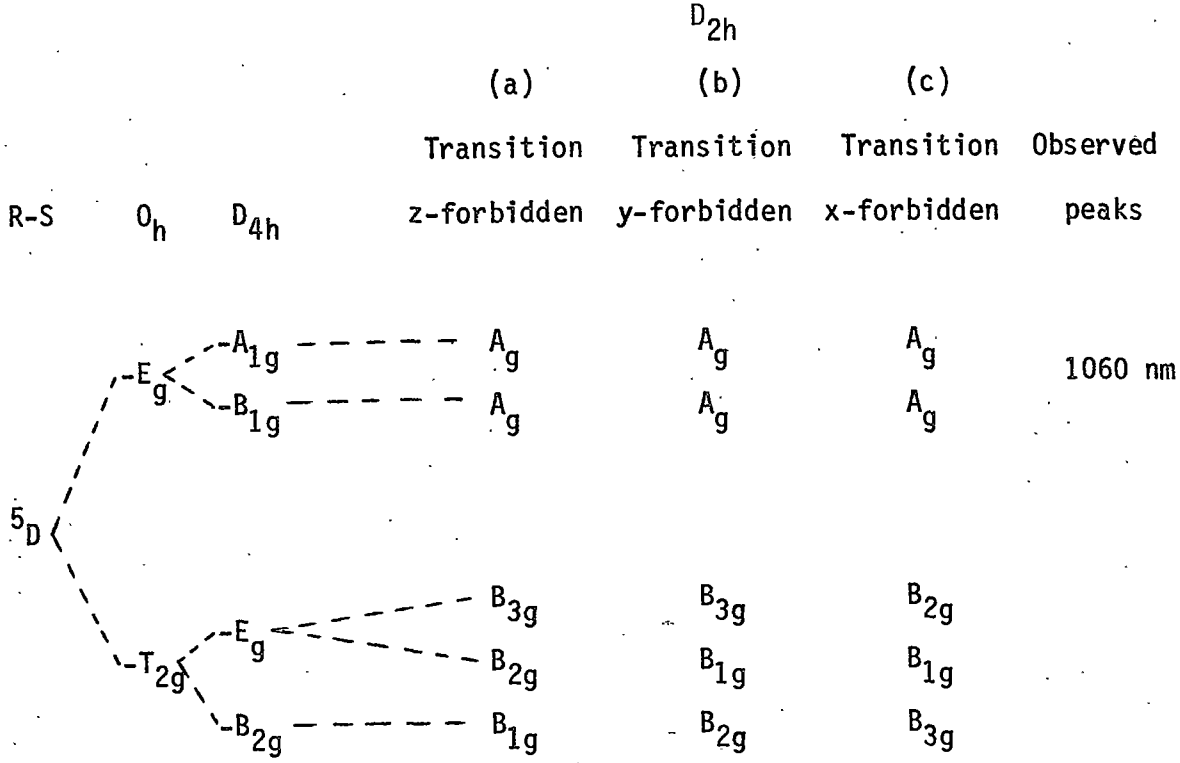


Figure 32 Possible Energy Level Diagrams for Fe(II)

the peaks due to transitions among the energy levels from splitting of the $T_{2g}$ term are not considered, as they are so low in energy that they are unlikely to be observed. Three possible ground states must be considered: $B_{1g}$, $B_{2g}$ and $B_{3g}$. One or perhaps two peaks ought to occur in the near IR.

A cleavage fragment, a clear crystal containing the b-c cross section, was utilized to collect the observed polarized spectra of the Mn-Fe salt. No peaks appear in the visible region other than those ascribed to the Mn(II) ion. One large peak appears in the near IR at 1060 nm and is identical in shape and in intensity in both y- and z-polarized light. Unfortunately, due to the habit of the Mn-Fe crystal, the spectrum in x-polarized light could not be obtained. Based on the evidence available, the assignment for this peak implies a $B_{3g}$ ground state for the Fe(II) ion in $D_{2h}$ symmetry. However, lacking the x-polarized spectrum, this assumption cannot be verified.

The optical and near IR spectrum for $Fe(C_4O_4)(H_2O)_2$ in unpolarized light has been determined by Long (42); no peaks show in the visible region and two broad bands appear at 930 and 1180 nm. Long assumes tetragonal symmetry and assigns these as transitions from an undetermined ground state to $A_{1g}$ and $B_{1g}$ respectively. The resolution between these two peaks is not good; if they were not resolved, the maximum would occur at 1055 nm which is very close to the value observed for the single peak in the TMA salt. It may be that the two energy levels are not split very much in the TMA salt, and thus remain unresolved.

Putnik, et. al., (43) have examined polarized crystal spectra of

$RbFeCl_3$ and $CsFeCl_3$ at 4.2 K. These compounds crystallize in the $P6_3/mmc$ space group and exhibit two colors in polarized light, red and yellow. However, the broad band at about 1330 nm which these authors identify as the $T_{2g} \rightarrow E_g$ transition remains unchanged in a- or c-polarized light. The color change in this compound appears to be due to polarization of the spin forbidden transitions to triplet states. It is interesting to note that this compound has hexagonal symmetry as did the $[(CH_3)_4N]MnCl_3$ discussed earlier (33) and is therefore uniaxial; two different spectra are again predicted.

Polarized spectra of minerals which contain Fe(II) such as gillespite, fayalite and almandine also show a peak in the near IR at about 1000 nm (44). Other workers have found similar peaks (45,46). Thus the observed spectra of the Fe(II) TMA salt corresponds to those found in the literature for Fe(II) compounds. Unfortunately, without the x-polarized spectrum, the ground state cannot be proven to be $B_{3g}$.

## NICKEL SPECTRA

The transitions involved for the Ni(II) ion are illustrated in Figure 33. The ground state in $O_h$ symmetry, $A_{2g}$, is already a one-dimensional representation so in this case there is no problem assigning the ground state in $D_{2h}$ symmetry; $A_{2g}$ transforms as $A_g$. The two triplets, $T_{1g}$ and $T_{2g}$, which arise from the $^3F$ term are each split into $B_{1g} + B_{2g} + B_{3g}$ in any order; the lower energy term, $T_{2g}$, probably involves a transition low enough in energy to be located in the near IR. There is also a $T_{1g}$ in octahedral symmetry which arises from a $^3P$ term; this yields a third band composed of $B_{1g} + B_{2g} + B_{3g}$. The latter is the highest energy spin allowed transition and should appear in the visible region.

The Mn-Ni crystals large enough to be utilized for spectral measurements contained very low mole fractions of Ni(II); this ion is the least soluble in the Mn(II) lattice site. The z-polarized spectrum taken on a thin crystal yields peaks of extremely low intensity. Attempts to increase the intensity of the observed peaks by using larger crystals resulted in so much scatter that peaks could no longer be identified.

In the Mn-Ni polarized spectra a broad band appears in the near IR at 825 nm which is visible in y-polarized light. If it is actually present in x-polarized light, it is a very weak transition. It does not show in z-polarized light, but this may be due to the thinness of the crystal and low Ni(II) concentration rather than to polarization effects. In the visible region there is a peak at 440 nm; this is superimposed on the Mn(II) 460 nm peak which makes sorting out the

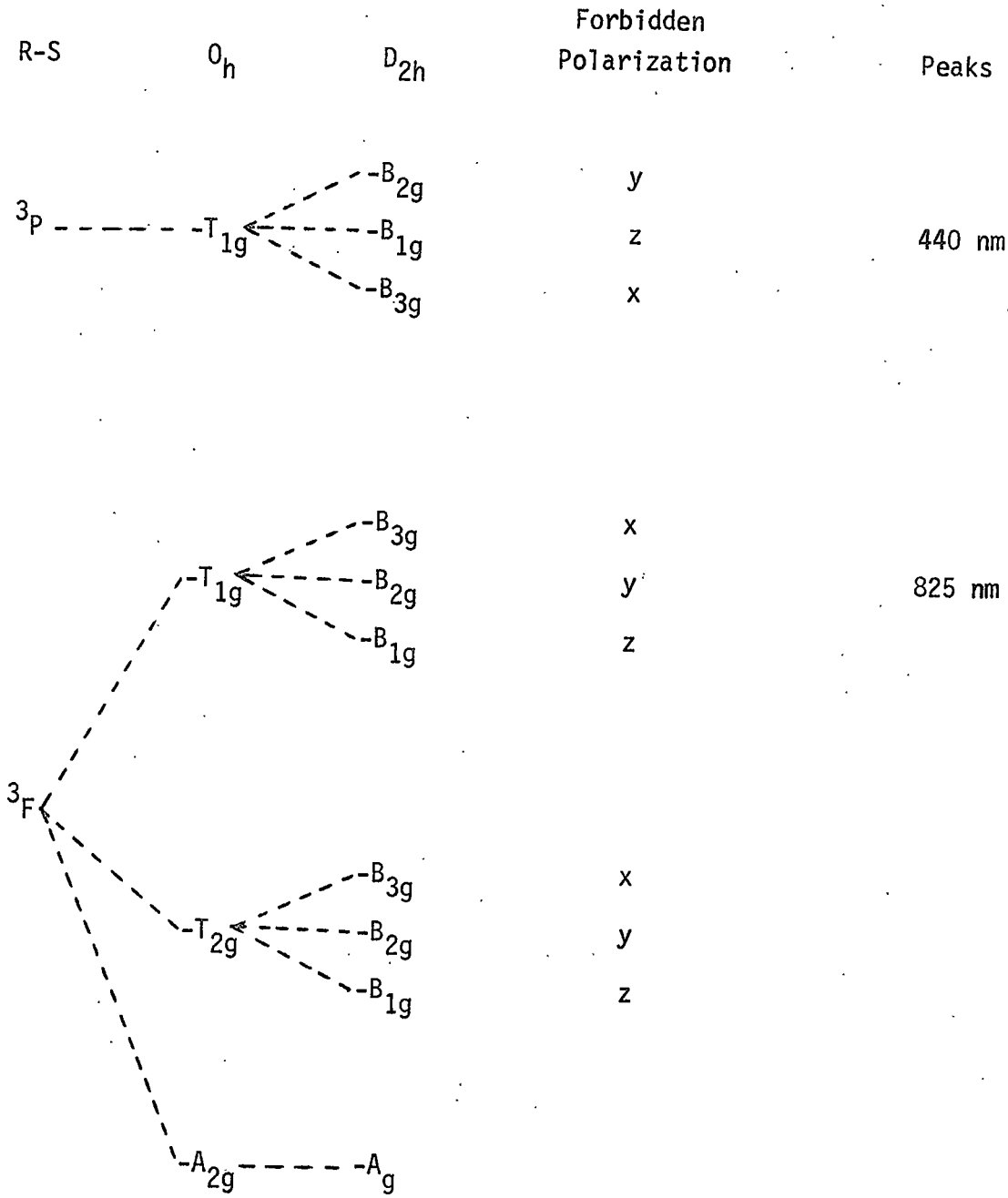


Figure 33 Energy Level Diagram for Ni(II)

polarization effects difficult. As the polarization direction is changed, this peak does indeed shift location and change in shape slightly. This indicates that it could be the high energy visible transition predicted by group theory, the electric dipole transition from $A_g$ to the three closely spaced levels, $B_{1g} + B_{2g} + B_{3g}$, arising from $T_{1g}(^3P)$. Examination of the polarization effects suggests the splitting $B_{3g}$ lower than $B_{1g}$ lower than $B_{2g}$. .

The literature on Ni(II) salts deals primarily with low temperature investigations of magnetic chains of the type $AMX_3$. The Ni(II) compounds $RbNiCl_3$, $CsNiCl_3$ and $[(CH_3)_4N]NiCl_3$ (47,49) belong to the same general category as the Fe(II) compounds (43) which were discussed in the preceding section. The Ni(II) ion can also be doped into the salts $KMgCl_3$ (48) and $CsMgCl_3$ (49). All of the above compounds belong to the $P6_3/mmc$ space group except $[(CH_3)_4N]NiCl_3$ which crystallizes in $P6_3/m$. Such crystals are uniaxial with the possibility of dichroism. These workers have obtained polarized spectra; however, they again describe the transitions in terms of octahedral symmetry. Many peaks are present in the spectra of these compounds which are not seen in the TMA salt; spin forbidden as well as spin allowed transitions appear in the low temperature spectra. The spin allowed transitions from $A_{2g}$ to $T_{2g}(^3F)$, $T_{1g}(^3F)$ and $T_{1g}(^3P)$ are located at 1430 nm, 850 nm and 460 nm, respectively. The location of the two higher energy peaks correlates quite well with those observed in the Mn-Ni TMA salt at 825 nm and 440 nm. Resolution of the 440 nm peak allows assignment of the relative order of the $B_{1g} + B_{2g} + B_{3g}$ levels and its location is supported by the literature data. However, the peak in the near IR at 825 nm cannot

be split based on the polarization data with any degree of certainty. The lowest energy spin allowed transition is not seen at all in the spectra of the TMA salt taken at room temperature.

## COPPER SPECTRA

Several serious problems were encountered trying to obtain crystal spectra for the Cu(II) ion. Due to the Jahn-Teller distortion exhibited by the $d^9$ ion, the pure Cu salt crystallizes in a monoclinic rather than an orthorhombic space group. This makes orientation of the principal vibration directions a more difficult problem than for the orthorhombic crystals. As has been mentioned previously, the unit cell axes in the pure Cu salt are redefined as compared to the orthorhombic unit cell; by crystallographic convention the unique axis in the monoclinic cell is defined as b. In the Cu salt this b axis happens to correspond to the direction of hydrogen bonding; the chain axis is along a. The a-b cross section of the pure Cu unit cell therefore corresponds to the orthorhombic b-c cross section. In the $d^9$ ion the $x^2-y^2$ and $z^2$ orbitals split so that the lone electron occupies the higher energy orbital. This, the Jahn-Teller effect, causes distortion of the square planar $CuCl_4^=$ arrangement with two of the Cu-Cl bonds lengthening, two shortening. The overall result is that the c axis of the unit cell is no longer perpendicular to the needle axis, a; the cell is now monoclinic. However, even though the unit cell axes are no longer orthogonal, the three principal vibration directions remain so. The unique axis may define one vibrational direction within the monoclinic indicatrix, but there are no restrictions on the location of the remaining two. Location of these vibration directions with respect to the unit cell axes is necessary if unambiguous spectra are desired. Examination of a $TMACuCl_3 \cdot 2H_2O$ crystal mounted and oriented on a goniometer head fixed to a graduated stage and

between crossed polarizers indicated parallel extinction in the a-b plane and an extinction angle of approximately 30° from the a axis in the a-c plane. With respect to the chromophore these extinction directions are identical to those found by Ferguson and Wood in the dihydrate $CoCl_2 \cdot 2H_2O$ (39).

Extremely thin plates of the pure Cu salt are easily grown, yielding samples for spectra of the a-b cross section. Large crystals are also readily obtained which may be sliced in the proper orientation to give access to the remaining direction necessary for a complete set of polarized spectra. Thus, it is theoretically possible to solve the problem presented by the monoclinic structure of the pure Cu salt. However, decomposition of the pure Cu crystal when exposed to the IR source made it impossible to obtain the desired polarization data.

In the Cary 14 the IR source, a high intensity tungsten lamp, is located in the compartment adjacent to the sample cell. The extreme sensitivity of the Cu TMA crystals to the IR source may be explained by this proximity, coupled with the fact that the sample is irradiated by the entire output of the source throughout the scan.

There are several possible explanations for this decomposition: one is loss of water which seems to be a problem for this hydrated salt even at room temperature. Previous work done in this lab (52) offers another explanation: a photochemical redox reaction may take place between the Cu(II) and the chloride ions. Either or both of the above may occur during a scan, rendering the resulting spectrum unusable.

Mixed metal crystals containing Cu can be grown in either the orthorhombic or monoclinic space group; thus, the structure problem can

be circumvented by selecting a mixed metal crystal with a low mole fraction of Cu for spectral work. The Mn-Cu crystal with the least Cu was chosen both because of its lath-like habit for easy orientation and its lack of interfering peaks due to the presence of the Mn(II) ion. The mixed metal crystals proved more durable than the pure Cu salt, but they were also susceptible to damage by the IR source. Despite all the precautions taken, information on the Cu(II) polarized spectra gained from the Mn-Cu crystals is not as complete as that for some of the other ions studied. Even though the crystal remained intact during a scan, the intensity of transitions due to the $d^9$ ion drove the peaks off scale. As the crystals were ground thinner, decomposition once again occurred. Low temperature spectra would have been helpful, but this capability was unavailable on the Cary 14. This problem with intensity of the chlorocuprate spectra has been observed by other workers as well.

There is a great deal of literature data concerning Cu(II) spectra, but few workers have looked at this ion in $D_{2h}$ symmetry (53-55). Hitchman and Cassidy have studied two salts in which the planar $CuCl_4^=$ unit is present; these are (methylphenethylammonium)$_2CuCl_4$ (54) and (creatinium)$_2CuCl_4$ (55) hereafter designated as $A_2CuCl_4$ and $A'_2CuCl_4$. There is no axial ligation in these compounds, the nearest axial atom lying more than 3.0 Å distant from the central Cu atom; there are two slightly different Cu-Cl bond lengths, 2.23 Å and 2.27 Å in $A'_2CuCl_4$ and 2.25 Å and 2.28 Å in $A_2CuCl_4$, making the local site symmetry for these complexes $D_{2h}$. Hitchman and Cassidy have assigned transitions for the $d^9$ ion from which the relative splitting of the d orbitals can be determined. This is presented in Figure 34; they noted that the

$d_z2$ orbital was lowered in energy much more than was expected. The energy level diagram based on symmetry representations along with polarization data is shown in Figure 35.

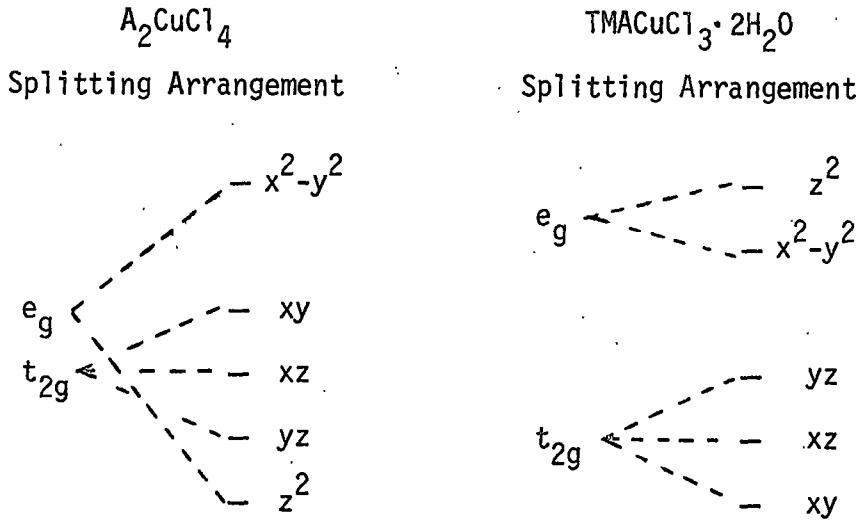


Figure 34 Splitting of the d Orbitals in $D_{2h}$

Although the orbital splitting pattern proposed by Hitchman and Cassidy (54) fits the spectra for the two planar complexes, it cannot explain that of the TMA salt. Only low temperature data were reported for $A_2CuCl_4$, but the room temperature spectra of $A'_2CuCl_4$ in one polarization is virtually identical to one of the polarized spectra of the TMA salt. However, the polarization effects predicted by group theory do not match even when the cell axes are compared with respect to the chromophore orientation. Therefore, one must assume that a different splitting arrangement is responsible for the Cu(II) spectra

| Representation in $O_h$ | Representation in $D_{2h}$ | Forbidden Polarization Calculated | Observed Peaks | Forbidden Polarization Observed |
|---|---|---|---|---|
| | $-A_g$ | none | 588 | none |
| | $-B_{3g}$ | x | 692 | x |
| $T_{2g}$ | $-B_{2g}$ | y | 712 | y |
| $E_g$ | $-B_{1g}$ | z | 800 | z |
| | $-A_g$ | | | |

Figure 35 Energy Level Diagram for $A_2CuCl_4$ in $D_{2h}$

| Representation in $O_h$ | Representation in $D_{2h}$ | Forbidden Polarization Calculated | Observed Peaks | Forbidden Polarization Observed |
|---|---|---|---|---|
| | $-B_{1g}$ | z | 805 | z |
| $T_{2g}$ | $-B_{2g}$ | y | 860 | y |
| | $-B_{3g}$ | x | 895 | y? |
| | $-A_g$ | none | 960 | none |
| $E_g$ | $-A_g$ | | | |

Figure 36 Energy Level Diagram for $TMACuCl_3 \cdot 2H_2O$ in $D_{2h}$

in the TMA salt.

There is axial ligation in $TMACuCl_3 \cdot 2H_2O$; the Cu-O bond length is about 2.0 Å and the two Cu-Cl bond lengths are 2.3 Å and 2.8 Å. Another difference between the dihydrate and Hitchman's salts is the extent of the distortion within the $CuCl_4^=$ plane. The Cu-Cl distances differ by only 0.04 Å in $A_2CuCl_4$ whereas in the TMA salt they differ by 0.5 Å. These differences in geometry seem to favor a different orbital splitting pattern in $TMACuCl_3 \cdot 2H_2O$. To compound the problem the Cu(II) ion has been doped into an orthorhombic site dominated by the Mn(II) ion. In $TMAMnCl_3 \cdot 2H_2O$ the Mn-O bond distance is 2.2 Å; the Mn-Cl bond distances are 2.5 Å and 2.6 Å. This suggests that the $d^9$ ion is forced into an octahedral structure where the axial bond lengths are shorter than the equatorial bond lengths, although the actual environment is probably somewhere between that of the two pure end members of the TMA series.

Several possible splitting arrangements exist for the d orbitals; the one proposed in Figure 34 can be used to construct an energy level diagram suitable for the explanation of the observed polarized spectra of the Mn-Cu TMA salt. Symmetry representations based on this splitting arrangement are shown in Figure 36.

There are only five possible electron configurations for the $d^9$ ion. Placing nine electrons in the d orbitals results in the same symmetry as placing one hole in these five orbitals. Therefore, the symmetry of the orbital occupied by the unpaired electron will be the symmetry of the state. The d orbital splitting pattern proposed for the TMA salt in $D_{2h}$ is reasonable in that the Cu-O bond which defines

the z axis is the shortest bond; the most repulsion will be along z, making the $z^2$ orbital the highest energy level. The x and y axes lie within the $CuCl_4^=$ plane; the Cu-Cl bonds are longer than the Cu-O bond, so there is least repulsion along x and y. Presence of the Cu(II) ion distorts the nearly square planar $CuCl_4^=$ arrangement; this will remove the degeneracy of the xz and yz orbitals. The $t_{2g}$ triplet is split so that the xy orbital has the lowest energy, the xz orbital is slightly higher and the yz orbital is the highest in energy of these three.

If nine electrons are to occupy the d orbitals as split in Figure 34, the ground state has the symmetry of the $d_z2$ orbital, $A_g$ in $D_{2h}$. The lowest energy excited state is found by promoting an electron from the $x^2-y^2$ orbital to the $z^2$ orbital; the symmetry of this excited state is also $A_g$. Transferral of an electron from the yz, xz or xy orbitals yields excited states with representations $B_{3g}$, $B_{2g}$ and $B_{1g}$, respectively. This gives rise to the energy level diagram presented in Figure 36.

Spectra were taken of the b-c cross section of the Mn-Cu crystals; in y-polarized light these crystals are dark amber, in z-polarized light they are light green. Four peaks can be identified in the near IR for the Cu(II) spectra obtained, but only one remains on scale. Due to the habit of the Mn-Cu crystals only the y- and z-polarized directions were accessible. A large peak, the top of which is off scale, appears in the near IR in y-polarized light; interpolation indicates that the top of this peak lies at 805 nm. In z-polarized light a broader double peak appears; the tops of both are off scale,

but interpolation suggests peak maxima at 860 and 895 nm. In both of these polarized spectra a well-defined shoulder is evident at 960 nm.

The peak at 960 nm is assigned as the $A_g \rightarrow A_g$ transition which is unpolarized. The peak at 895 nm is the only one which does not fit as an electric dipole transition; this IR peak seems to disappear in y-polarized light whereas it should only disappear in x-polarized light. Because the IR region was scanned rapidly to preserve the crystal, this peak may be hidden under the large peak seen at 805 nm. There is some slight evidence of a shoulder in the proper region, if one examines the spectrum closely. The peak at 860 nm is assigned as the $A_g \rightarrow B_{2g}$ transition; it is visible in z-polarized light and vanishes in y-polarized light. The highest energy peak in the IR region occurs at 805 nm and is assigned as the $A_g \rightarrow B_{1g}$ transition which is forbidden in z-polarized light. The x-polarized spectrum would have provided valuable additional data, but could not be obtained due to the habit of these crystals.

In the visible portion of the Mn-Cu spectrum a peak appears at 548 nm in y-polarized light; it is not present in z-polarized light. This peak is tentatively assigned as a charge transfer band occurring at relatively low energy; this band is presumably the origin of the amber color of the crystal in this orientation. The peaks due to the Mn(II) ion can be seen in the z-polarized spectrum, but the intensity goes off scale soon after the observed peak in the y-polarized spectrum.

Crystals of $(CH_3NH_3)_2MnCl_4$ and $(enH_2)MnCl_4$ when doped with small amounts of Cu(II) are deep red; Willett has reported a polarized peak at 480 nm in these crystals which is responsible for the color (58).

The chromophore for this peak is $CuCl_6$ whereas the chromophore for the peak seen in the TMA salt is $CuCl_4(H_2O)_2$. The Cu-Cl bonds are longer in the latter, and two chlorides have been replaced by water, which should weaken the crystal field interactions. Thus, these two peaks may have similar origins.

One other system has been reported in the literature which contains a Mn-Cu mixture; dimers of $Cu(C_5H_5NO)Cl_2 \cdot H_2O$ and $Cu(C_5H_5NO)_2Cl_2$ have been studied (59). The doped crystals also exhibit a color change from the pure compounds (60).

Willett, et. al., (58) worked with a very small range of mole fractions, claiming that the Cu(II) ion cannot be forced to occupy the Mn(II) site, even though the space groups are identical for both end members. Work done by Campana at this campus (61) indicates that the entire range is possible for $(CH_3NH_3)_2Mn_xCu_{1-x}Cl_4$. There also seems to be no problem getting any mole fraction in the TMA series although a structural change occurs as $\chi_{Cu} \rightarrow 1$.

The existence of a different color in mixed metal substances containing Mn and Cu than is present in either pure end member is well documented. The source for the peak in the visible region which causes this color change has been postulated to be an electron transfer of some sort, either $\pi_{Cl}$ to Cu or Mn to Cu. If an electron transfer oc curs between Mn and Cu, this peak should be seen in all Mn-Cu systems; this has not been obs ved. Therefore, the charge transfer from Cl to Cu induced by local site interactions seems more probable.

## CONCLUSION

Orthorhombic crystals of $TMAM_xM'_{1-x}Cl_3 \cdot 2H_2O$ where M and M' represent the divalent transition metal ions Mn, Fe, Co, Ni and Cu were found to exist as solid solutions. The ease with which these ions are incorporated into the lattice sites was established: Ni < Co < Mn < Cu. Solubility increases as the size of the ion increases; Cu is unusually soluble because Jahn-Teller distortion increases the effective size of this ion. Cell parameters were determined for the mixed metal salts and also for the previously unpublished pure Fe and Ni analogs. These values fit the trend expected, i.e. longer cell dimensions for the larger cations.

Because these highly colored crystals are orthorhombic, their unit cell axes are easily oriented with respect to the electric vector, $\vec{E}$, of polarized light. Utilizing $D_{2h}$ symmetry to account for the pleochroism exhibited by these crystals, energy level diagrams were constructed to fit the observed polarized spectra. In the Mn(II) spectra one peak appears which must be assigned as a magnetic dipole transition; the remainder were assigned as electric dipole transitions. In the Co(II) spectra all of the observed peaks must be assigned as magnetic dipole transitions. One peak remained unexplained as either a magnetic or an electric dipole transition; this "anomalous" band needs further study before its origin can be fully understood. In the Fe(II) and Ni(II) spectra insufficient polarization data was obtained to establish and adequately support the relative splitting pattern in a $D_{2h}$ energy level diagram. In the Cu(II) spectra the peaks were assigned solely as electric dipole transitions with a charge transfer band appearing in

the visible region. In all cases the observed spectral data correlate well with those in the literature for ions in similar environments.

Crystals with lower Cu(II) concentrations and higher Ni(II) concentrations are necessary to verify the exact splitting pattern in $D_{2h}$ symmetry for these ions. Low temperature spectra of these crystals would provide a means to distinguish between magnetic and electric dipole transitions experimentally rather than solely by group theoretical predictions.

## LITERATURE CITED


1. P. Groth, Chemische Kristallographie, (Wilhelm Engleman, Leipzig, 1908), Vol. I, p. 375.
2. H. Remy and G. Laves, Ber., 66, 401 (1933).
3. J. H. Day, Chem. Rev., 68, 649 (1968).
4. R. D. Willett, et. al., Inorg. Chem., 13, 2510 (1974).
5. S. A. Roberts, et. al., J. Am. Chem. Soc., 103, 2603 (1981).
6. R. E. Caputo, et. al., Inorg. Chem., 15, 820 (1976).
7. R. M. Clay, J. Murray-Rust and P. Murray-Rust, J. Chem. Soc., Dalton, 595 (1973).
8. D. B. Losee, et. al., Phys. Rev. B, 4342 (1972).
9. D. B. Losee, et. al., Phys. Rev. B. 2185 (1973).
10. R. E. Caputo, R. D. Willett and J. A. Muir, Acta. Cryst., B32, 2639 (1976).
11. R. D. Shannon and C. T. Prewitt, Acta. Cryst., B26, 1046 (1970).
12. I. M. Kolthoff and E. B. Sandell, Textbook of Quantitative Inorganic Analyses, (Third Ed., Macmillan Co., N. Y., 1952), p. 543
13. F. J. Welcher, The Analytical Uses of Ethylenediaminetetraacetic Acid, (D. van Nostrand Co., Inc., Princeton, N. J., 1958).
14. I. I. M. Elbeih, Chem. Anal., 45, 75 (1956).
15. C. C. Houk, Doctor's Thesis, (Montana State University, 1966).
16. D. N. Grindley, An Advanced Course in Practical Inorganic Chemistry, (Butterworths, London, 1964), p. 24.
17. E. H. Swift, A System of Chemical Analysis for the Common Elements, (Prentice-Hall, Inc., 1939).
18. R. Pribil and Z. Roubal, Chem. Listy, 48, 818 (1954); C. A. 48, 13524 (1954).
19. H. Flaschka, Chem. Anal., 42, 56 (1953).
20. W. E. Harris and B. Kratochvil, Chemical Separations and Measurements, (W. B. Saunders Co., Philadelphia, 1974), p. 141.
21. M. J. Buerger, Crystal Structure Analysis, (John Wiley and Sons, Inc., N. Y., 1960).
22. G. H. Stout and L. H. Jensen, X-Ray Structure Determination, (Macmillan Co., N. Y., 1968).
23. E. A. Wood, Crystals and Light, (D. van Nostrand Co., Inc., Princeton, N. J., 1964).
24. C. Bunn, Crystals: Their Role in Nature and Science, (Academic Press, N. Y., 1964).
25. P. F. Kerr, Optical Mineralogy, (Third Ed., McGraw-Hill Book Co., Inc., N. Y., 1959).
26. J. K. Robertson, Introduction to Physical Optics, (D. van Nostrand Co., Inc., N. Y., 1937), p. 352.
27. R. W. Wood, Physical Optics, (Macmillan Co., N. Y., 1934), p. 487.
28. F. A. Cotton, Chemical Applications of Group Theory, (Interscience Publishers, N. Y., 1967).
29. C. J. Ballhausen, Introduction to Ligand Field Theory, (McGraw-Hill Co., N. Y., 1962).
30. D. S. McClure, Electronic Spectra of Molecules and Ions in Crystals, (Academic Press, N. Y., 1959).

31. J. J. Foster and N. S. Gill, J. Chem. Soc. (A), 2625 (1968).
32. L. L. Lohr and D. S. McClure, J. Chem. Phys., 49, 3516 (1968).
33. R. Dingle, M. E. Lines and S. L. Holt, Phys. Rev., 187, 643 (1969).
34. O. G. Holmes and D. S. McClure, J. Chem. Phys., 26, 1686 (1957).
35. K. E. Lawson, J. Chem. Phys., 44, 4159 (1966).
36. D. R. Rosseinsky and I. A. Dorrity, Coord. Chem. Rev., 21, 31 (1978).
37. J. Ferguson, D. L. Wood and K. Knox, J. Chem. Phys., 39, 881 (1963).
38. J. Ferguson and T. E. Wood, Inorg. Chem., 14, 184 (1975).
39. J. Ferguson and T. E. Wood, Inorg. Chem., 14, 190 (1975).
40. B. Morosin and E. J. Graeber, Acta. Cryst., 16, 1176 (1963).
41. L. G. Vanquickenborne and E. Verdonck, Inorg. Chem., 15, 454 (1976).
42. G. J. Long, Inorg. Chem., 17, 2702 (1978).
43. C. F. Putnik, et. al., Inorg. Chem., 15, 826 (1976).
44. R. G. Burns, Mineralogical Applications of Crystal Field Theory. (Cambridge University Press, 1970).
45. G. D. Jones, Phys. Rev., 155, 259 (1967).
46. F. A. Cotton and M. D. Myers, J. Am. Chem. Soc., 82, 5023 (1960).
47. G. L. McPherson and G. D. Stucky, J. Chem. Phys., 57, 3781 (1972).
48. J. Brynestad, H. L. Yakel and G. P. Smith, J. Chem. Phys., 45, 4652 (1966).
49. J. Ackerman, E. M. Holt and S. L. Holt, J. Solid State Chem., 9, 279 (1974).
50. J. D. Lebedda and R. A. Palmer, Inorg. Chem., 11, 484 (1972).
51. M. Habenschuss and B. C. Gerstein, J. Chem. Phys., 61, 852 (1974).
52. K. D. Mannila, Master's Thesis, (Montana State University, 1969).
53. D. W. Smith, Coord. Chem. Rev., 21, 93 (1976).
54. M. A. Hitchman and P. Cassidy, Inorg. Chem., 18, 745 (1979).
55. M. A. Hitchman, J. Chem. Soc., Chem. Comm., 973 (1979).
56. M. R. Udopa and B. Krebs, Inorg. Chim. Acta, 33, 241 (1979).
57. R. L. Harlow, et. al., Inorg. Chem., 13, 2106 (1974).
58. U. Schmid, H. Gudel and R. Willett, Inorg. Chem., 21, 2977 (1982).
59. D. A. Krost and G. L. McPherson, J. Am. Chem. Soc., 100, 987 (1978).
60. K. Emerson, Personal communication.
61. K. Emerson, Personal communication.